Design and Testing of a Laboratory Ultrasonic Data Acquisition System for Tomography

By

Wesley Byron Johnson

Thesis submitted to the faculty of the Virginia Polytechnic Institute and State University in partial fulfillment of the requirements for the degree of

Master of Science

In

Mining and Minerals Engineering

Committee Members:

Dr. Erik Westman, Chair

Dr. Thomas Novak

Dr. Mario Karfakis

December 2, 2004

Blacksburg, VA

Keywords: Tomography, Ultrasonic, Rock Mechanics, Data Acquisition

DESIGN AND TESTING OF A LABORATORY ULTRASONIC DATA ACQUISITION SYSTEM FOR TOMOGRAPHY

Wesley Byron Johnson

(ABSTRACT)

Geophysical tomography allows for the measurement of stress-induced density changes inside of a rock mass or sample by non-invasive means. Tomography is a non-destructive testing method by which sensors are placed around a sample and energy is introduced into the sample at one sensor while the other sensors receive the energy. This process is repeated around the sample to obtain the desired resolution. The received information is converted by a mathematical transform to obtain a tomogram. This tomogram shows a pixelated distribution of the density within the sample. Each pixel represents an average value at that point.

The project discussed in this paper takes the principle of ultrasonic tomography and applies it to geomechanics. A new instrumentation system was designed to allow rapid data collection through varying sample geometries and rock types with a low initial investment. The system is composed of sensors, an ultrasonic pulser, a source switchbox, and analog to digital converters; it is tied together using a LabVIEW virtual instrument.

LabVIEW is a graphical development environment for creating test, measurement, and other control applications. Using LabVIEW, virtual instruments (VIs) are created to control or measure a process. In this application LabVIEW was used to create a virtual instrument that was automated to collect the data required to construct a tomogram.

Experiments were conducted to calibrate and validate the system for ultrasonic velocity determination and stress redistribution tomography. Calibration was conducted using polymethylmethacrylate (PMMA or Plexiglas) plates. Uniaxial loads were placed on limestone and sandstone samples. The stress-induced density contrasts were then

imaged using the acquisition system. The resolution and accuracy of the system is described.

The acquisition system presented is a low-cost solution to laboratory geophysical tomography. The ultimate goal of the project is to further the ability to non-invasively image relative stress redistribution in a rock mass, thereby improving the engineer's ability to predict failure.

ACKNOWLEDGEMENTS

I would like to thank the Virginia Tech Mining and Minerals Engineering Department and the National Science Foundation for the opportunity to contribute to this project. I am thankful for the educational and financial support that was extended to me for this project.

I would like to thank my advisor Dr. Erik Westman for his guidance and support throughout this project and throughout my academic career. I would also like to thank my other major advisors to this project, Dr. Mario Karfakis, and Dr. Thomas Novak. I am thankful for my committee's patience and support in mentoring me on this project.

To my wife Laura, I am grateful for her love and sacrifice to see me finish this project. In addition I would like to thank my parents and family for their support and love.

TABLE OF CONTENTS

LIST OF FIGURES ..... **VII**

LIST OF TABLES ..... **X**

CHAPTER 1: INTRODUCTION **1**

CHAPTER 2: LITERATURE REVIEW **4**

2.1 ULTRASONIC WAVE PROPAGATION 4

2.1.1 ULTRASONIC SENSORS *7*

2.2 DATA ACQUISITION 10

2.2.1 SAMPLING *11*

2.3 LABVIEW PROGRAMMING 13

2.4 TOMOGRAPHY 15

2.4.1 APPLICATIONS OF TOMOGRAPHY *17*

CHAPTER 3: ULTRASONIC DATA ACQUISITION SYSTEM: HARDWARE DESIGN **20**

3.1 SENSOR SELECTION 21

3.2 SENSOR MOUNTING 22

3.3 ULTRASONIC PULSER 24

3.4 ULTRASONIC SWITCHBOX 25

3.5 DATA ACQUISITION INSTRUMENTATION 28

3.6 LABVIEW PROCESSING 31

3.7 LABVIEW PROGRAM FOR ULTRASONIC DATA ACQUISITION 31

CHAPTER 4: ULTRASONIC DATA ACQUISITION SYSTEM: CALIBRATION AND TESTING **35**

4.1 CALIBRATION TESTING 35

4.2 APPLICATION TESTING 41

4.2.1 Berea Sandstone Experiment *42*

4.2.2 Five Oaks Limestone Experiment *50*

CHAPTER 5: SUMMARY AND CONCLUSIONS **63**

REFERENCES **66**

APPENDIX: A **70**

A.1 PLEXIGLAS TOMOGRAMS 71

A.2 BEREA SANDSTONE TOMOGRAMS 71

A.3 FIVE OAKS LIMESTONE TOMOGRAMS 73

APPENDIX: B 78

B.1 MAIN APPLICATION CONTROL 79
B.2 SETUP PROGRAM 81
B.3 SIMULTANEOUS ACQUISITION PROGRAM 88
B.4 PAIRED ACQUISITION PROGRAM 90
B.5 ARRIVAL TIME CORRELATION PROGRAM 92

APPENDIX: C 95

LIST OF FIGURES

CHAPTER 1: INTRODUCTION 1

CHAPTER 2: LITERATURE REVIEW 4

FIGURE 2.1: ILLUSTRATION OF SNELL'S LAW, ACOUSTIC WAVE REFRACTION AND REFLECTION AT A INTERFACE WITH DIFFERENT ACOUSTIC VELOCITIES 7

FIGURE 2.2: SIGNAL ALIASING IN THE TIME DOMAIN 11

FIGURE 2.3: LABVIEW VIRTUAL INSTRUMENT FRONT PANEL 13

FIGURE 2.4: LABVIEW VIRTUAL INSTRUMENT BLOCK DIAGRAM 14

CHAPTER 3: ULTRASONIC DATA ACQUISITION SYSTEM: HARDWARE DESIGN 20

FIGURE 3.1: ULTRASONIC DATA ACQUISITION SYSTEM HARDWARE FLOWCHART 21

FIGURE 3.2: BEESWAX COUPLANT APPLICATION 22

FIGURE 3.3: PANAMETRICS 5077PR ULTRASONIC SQUARE WAVE PULSER 24

FIGURE 3.4: ESG ULTRASONIC SWITCHBOX PULSER 26

FIGURE 3.5: (A) DIGITAL INPUT/OUTPUT CONNECTOR BLOCK, (B) NI PCI-6503 DIGITAL INPUT/OUTPUT DATA ACQUISITION CARD 26

FIGURE 3.6: ULTRASONIC SWITCHBOX CONTROLLER HARDWARE CONNECTIONS 27

FIGURE 3.7: PXI 1006 CHASSIS WITH PXI 5102 DIGITAL OSCILLOSCOPES 28

FIGURE 3.8: PXI 5102 DIGITAL OSCILLOSCOPE 29

FIGURE 3.9: (A) BREADBOARD VOLTAGE DIVIDER CIRCUIT, (B) VOLTAGE DIVIDER CIRCUIT SCHEMATIC 30

FIGURE 3.10: HARDWARE FLOWCHART 32

FIGURE 3.11: LABVIEW PROGRAM FLOWCHART 33

CHAPTER 4: ULTRASONIC DATA ACQUISITION SYSTEM: CALIBRATION AND TESTING 35

FIGURE 4.1: SCALED IMAGE OF THE PLEXIGLAS PLATE WITH A HOLE (PLATE 2) 36

FIGURE 4.2: PLEXIGLAS PLATE TOMOGRAPHIC SETUP 36

FIGURE 4.3: SENSORS MOUNTED TO PLEXIGLAS (A) SOLID PLATE 1 AND (B) PLATE 2 WITH A HOLE USING BEESWAX 37

FIGURE 4.4: PLATE 1 TIME VS. DISTANCE PLOT 37

FIGURE 4.5: PLATE 2 TIME VS. DISTANCE PLOT 38

FIGURE 4.6: VIRGINIA TECH ROCK MECHANICS LABORATORY ULTRASONIC VELOCITY VIEWER 38

FIGURE 4.7A: TOMOGRAM OF THE SOLID PLEXIGLAS CALIBRATION PLATE 40

FIGURE 4.7B: TOMOGRAM OF THE PLEXIGLAS CALIBRATION PLATE WITH A HOLE 41

FIGURE 4.8: BEREA SANDSTONE TOMOGRAPHIC SETUP 43

FIGURE 4.9: BEREA SANDSTONE TEST SAMPLE (A) PRIOR AND (B) POST FAILURE 44
FIGURE 4.10A: BEREA SANDSTONE TIME VS. DISTANCE PLOT AT LOAD 1, 0 MPA LOAD 44
FIGURE 4.10B: BEREA SANDSTONE TIME VS. DISTANCE PLOT AT LOAD 2, 17.24 MPA LOAD 45
FIGURE 4.10C: BEREA SANDSTONE TIME VS. DISTANCE PLOT AT LOAD 3, 24.82 MPA LOAD 45
FIGURE 4.10D: BEREA SANDSTONE TIME VS. DISTANCE PLOT AT LOAD 4, 34.47 MPA LOAD 45
FIGURE 4.10E: BEREA SANDSTONE TIME VS. DISTANCE PLOT AT LOAD 5, 46.54 MPA LOAD 46
FIGURE 4.11A: BEREA SANDSTONE TOMOGRAM AT INITIAL STATE, 0 MPA 48
FIGURE 4.11B: BEREA SANDSTONE TOMOGRAM AT LOAD 1, 17.24 MPA 48
FIGURE 4.11C: BEREA SANDSTONE TOMOGRAM AT LOAD 2, 24.82 MPA 49
FIGURE 4.11D: BEREA SANDSTONE TOMOGRAM AT LOAD 3, 34 MPA 49
FIGURE 4.11E: BEREA SANDSTONE TOMOGRAM AT LOAD 4, 46 MPA 50
FIGURE 4.12: FIVE OAKS LIMESTONE TOMOGRAPHIC SETUP 52
FIGURE 4.13A: FIVE OAKS LIMESTONE TIME VS. DISTANCE PLOT AT INITIAL STATE, 0 MPA 53
FIGURE 4.13B: FIVE OAKS LIMESTONE TIME VS. DISTANCE PLOT AT LOAD 1, 17.24 MPA 53
FIGURE 4.13C: FIVE OAKS LIMESTONE TIME VS. DISTANCE PLOT AT LOAD 2, 34.47 MPA 54
FIGURE 4.13D: FIVE OAKS LIMESTONE TIME VS. DISTANCE PLOT AT LOAD 3, 51.71 MPA 54
FIGURE 4.13E: FIVE OAKS LIMESTONE TIME VS. DISTANCE PLOT AT LOAD 4, 68.95 MPA 55
FIGURE 4.13F: FIVE OAKS LIMESTONE TIME VS. DISTANCE PLOT AT LOAD 5, 86.18 MPA 55
FIGURE 4.13G: FIVE OAKS LIMESTONE TIME VS. DISTANCE PLOT AT LOAD 6, 103.42 MPA 56
FIGURE 4.13H: FIVE OAKS LIMESTONE TIME VS. DISTANCE PLOT AT POST FAILURE, 0 MPA 56
FIGURE 4.14: FIVE OAKS LIMESTONE TEST BLOCK (A) PRIOR AND (B) POST FAILURE 57
FIGURE 4.15A: FIVE OAKS LIMESTONE TOMOGRAM PRIOR TO LOADING, 0 MPA (UNITS – FT/SEC) 58
FIGURE 4.15B: FIVE OAKS LIMESTONE TOMOGRAM AT 17.24 MPA (UNITS – FT/SEC) 58
FIGURE 4.15C: FIVE OAKS LIMESTONE TOMOGRAM AT 34.47 MPA (UNITS – FT/SEC) 59
FIGURE 4.15D: FIVE OAKS LIMESTONE TOMOGRAM AT 51.71 MPA (UNITS – FT/SEC) 59
FIGURE 4.15E: FIVE OAKS LIMESTONE TOMOGRAM AT 68.95 MPA (UNITS – FT/SEC) 60
FIGURE 4.15F: FIVE OAKS LIMESTONE TOMOGRAM AT 86.18 MPA (UNITS – FT/SEC) 60
FIGURE 4.15G: FIVE OAKS LIMESTONE TOMOGRAM AT 103.42 MPA (UNITS – FT/SEC) 61
FIGURE 4.15H: FIVE OAKS LIMESTONE TOMOGRAM POST FAILURE, 0 MPA (UNITS – FT/SEC) 61

CHAPTER 5: SUMMARY AND CONCLUSIONS 63

REFERENCES 66

APPENDIX: A 70

FIGURE A.1A: TOMOGRAM OF THE SOLID PLEXIGLAS CALIBRATION PLATE 71
FIGURE A.1B: TOMOGRAM OF THE PLEXIGLAS CALIBRATION PLATE WITH A HOLE 71
FIGURE A.2A: BEREA SANDSTONE TOMOGRAM AT INITIAL STATE, 0 MPA 71
FIGURE A.2B: BEREA SANDSTONE TOMOGRAM AT LOAD 1, 17.24 MPA 72

FIGURE A.2C: BEREA SANDSTONE TOMOGRAM AT LOAD 2, 24.82 MPA 72
FIGURE A.2D: BEREA SANDSTONE TOMOGRAM AT LOAD 3, 34 MPA 72
FIGURE A.2E: BEREA SANDSTONE TOMOGRAM AT LOAD 4, 46 MPA 73
FIGURE A.3A: FIVE OAKS LIMESTONE TOMOGRAM PRIOR TO LOADING, 0 MPA (UNITS – FT/SEC) 73
FIGURE A.3B: FIVE OAKS LIMESTONE TOMOGRAM AT 17.24 MPA (UNITS – FT/SEC) 74
FIGURE A.3C: FIVE OAKS LIMESTONE TOMOGRAM AT 34.47 MPA (UNITS – FT/SEC) 74
FIGURE A.3D: FIVE OAKS LIMESTONE TOMOGRAM AT 51.71 MPA (UNITS – FT/SEC) 75
FIGURE A.3E: FIVE OAKS LIMESTONE TOMOGRAM AT 68.95 MPA (UNITS – FT/SEC) 75
FIGURE A.3F: FIVE OAKS LIMESTONE TOMOGRAM AT 86.18 MPA (UNITS – FT/SEC) 76
FIGURE A.3G: FIVE OAKS LIMESTONE TOMOGRAM AT 103.42 MPA (UNITS – FT/SEC) 76
FIGURE A.3H: FIVE OAKS LIMESTONE TOMOGRAM POST FAILURE, 0 MPA (UNITS – FT/SEC) 77

APPENDIX: B 78

FIGURE B.1: UDAQ LABVIEW PROGRAM ARCHITECTURE 80
FIGURE B.2: MAIN APPLICATION CONTROL FRONT PANEL 81
FIGURE B.3: GET SR FRONT PANEL 82
FIGURE B.4: SENSOR CALCULATION UTILITY FRONT PANEL 83
FIGURE B.5: GET SR:BLOCK DIAGRAM – DRAW EVENT 85
FIGURE B.6: GET SR:BLOCK DIAGRAM – PICTURE EVENT 86
FIGURE B.7: GET SR:BLOCK DIAGRAM – OUTPUT EVENT 87
FIGURE B.8: GET SR:BLOCK DIAGRAM – DRAW RAYPATHS EVENT 88
FIGURE B.9: SIMULTANEOUS ACQUISITION FRONT PANEL 89
FIGURE B.10: SIMULTANEOUS ACQUISITION BLOCK DIAGRAM 90
FIGURE B.11: PAIRED ACQUISITION FRONT PANEL 91
FIGURE B.12: ARRIVAL TIME FRONT PANEL 92
FIGURE B.13: GEOTOM FORMAT FRONT PANEL 93

APPENDIX: C 95

FIGURE C.1: ULTRASONIC DATA ACQUISITION SYSTEM HARDWARE WIRING FLOWCHART 96

LIST OF TABLES

CHAPTER 1: INTRODUCTION **1**

CHAPTER 2: LITERATURE REVIEW **4**

CHAPTER 3: ULTRASONIC DATA ACQUISITION SYSTEM: HARDWARE DESIGN **20**

TABLE 3.1: PHYSICAL ACOUSTICS MICRO-80 AE SENSOR PROPERTIES 23

TABLE 3.2: PANAMETRICS 5077PR ULTRASONIC SQUARE WAVE PULSER SPECIFICATIONS 25

TABLE 3.3: PXI 5102 SPECIFICATIONS 29

CHAPTER 4: ULTRASONIC DATA ACQUISITION SYSTEM: CALIBRATION AND TESTING **35**

TABLE 4.1: ULTRASONIC DATA ACQUISITION SYSTEM VELOCITY CALIBRATION MEASUREMENTS 39

TABLE 4.2: BEREA SANDSTONE INDEX PROPERTIES 43

TABLE 4.3: SANDSTONE VELOCITY SUMMARY 46

TABLE 4.4: FIVE OAKS LIMESTONE INDEX PROPERTIES 51

TABLE 4.5: LOAD CONDITIONS FOR TOMOGRAPHIC DATA COLLECTION 52

CHAPTER 5: SUMMARY AND CONCLUSIONS **63**

TABLE 5.1: SYSTEM COST 64

REFERENCES **66**

APPENDIX: A **70**

APPENDIX: B **78**

APPENDIX: C **95**

TABLE C.1: HARDWARE DESCRIPTIONS 97

CHAPTER 1: INTRODUCTION

Roof falls and pillar failures are common workplace hazards in underground mining. The cause of these geologic hazards can be a result of a number of geologic factors including stress redistribution resulting from mining. Monitoring of geologic hazards to predict failure within mine workings has been conducted with minimal success. Microseismic and acoustic emission monitoring methods have been used to collect acoustic signals through the roof/back or the floor, thereby assessing the stress state in those structures. The results from these mine-wide monitoring systems have been inconclusive in determining the direct result of stress redistribution to the prediction of geologic failure. The phenomenon of stress redistribution must be understood before field predictions can be made. Ultrasonic investigations used in the petroleum industry show promise in imaging stress redistribution.

Ultrasonic investigations in rock mechanics have been historically used to determine the index properties of rock. By determining the pressure and shear wave velocities, dynamic properties such as the modulus of elasticity can be computed. New technology allows ultrasonic investigations to go beyond index properties and infer the stress state within the rock. When a mechanical stress is applied to a material that behaves according to Hooke's Law [3] (stress increases with strain), the sound velocity increases with increasing stress. This is known as the acoustoelastic effect. This effect makes ultrasonic stress redistribution studies possible. Because rock is not a uniform material, differences in the internal velocity of the rock exist due to the presence of fissures, discontinuities, changing mineralogy, and other geologic factors.

Ultrasonic tomography allows for a cross sectional image of ultrasonic velocities to be created. Tomography is derived from the Greek word *tomos*, meaning section. Tomography uses the principals of the Radon Transform to invert ultrasonic data creating an image of the velocity within a cross section of rock. Ultrasonic data is acquired by transmitting an ultrasonic pulse through a rock and then measuring the velocity along the raypath of the ultrasonic wave. The captured velocity data can then be processed using an inversion algorithm to produce a tomogram. From the velocity tomogram an inference of the stress state within the rock can be inferred. By comparing different velocity

tomograms obtained at different stress states patterns of stress movement can be identified and studied. This imaging method has been used in mining and tunneling operations to monitor and map the movement of stress within a rock mass. By moving ultrasonic tomography into the laboratory, stress redistribution studies can be conducted in a controlled environment through tomographic image collection and interpretation.

Tomography is an essential tool for stress redistribution studies in active mine workings. The mapping of stress around underground openings helps identify hazards within the mine. Tomography can also be used to identify geologic structures, abandoned mine workings, and other interfaces within a rock mass. The data collected from these investigations are often very hard to interpret due to factors such as groundwater, complex geology, faults and fissures, poor ultrasonic reception, and background noise. Some of these factors can be minimized in the laboratory, reducing errors that influence tomographic results.

The Mine Safety and Health Administration (MSHA) Accident, Injury, Illness Database shows in the past four years (2000-2003) 11.8% of fatal incidences were a result of the failure of a geologic structure (roof, rib, pillar, etc) in a surface or underground mine. This statistic could be lowered by monitoring the stress states inside of these dangerous places. Non-fatal incidences resulting in man hours lost totaled 83,213 man hours in the past four years. In underground coal mining the number of man hours lost totaled 70,963 hours. Labor statistics show that the average tons per man hour in underground coal mines equals 4.05 tons. With an estimated market value of $40 per ton over the last four years, this equates to 11.5 million dollars in lost production due to geologic failure in underground coal mines. This statistic does not take into account down time for production equipment directly resulting from geologic failures inside of a mine. To reduce the human and economic cost that mines face due to geologic failures, monitoring must be conducted. The laboratory provides a controlled environment where it is possible to explore what ultrasonic tomographic data is implying about rock samples.

The study presented in this report describes a new laboratory ultrasonic data acquisition system for acquiring and processing ultrasonic tomograms. This system uses National Instrument's LabVIEW programming to control the acquisition of ultrasonic waves from a rock sample under uniaxial compression. Tomograms were collected

during uniaxial compression of Five Oaks Limestone and Berea Sandstone. The limestone samples were collected from the Kimballton Limestone Quarry which is owned and operated by Chemical Lime Corporation. The sandstone samples were obtained from Cleveland Quarries in Amherst, Ohio. The data acquisition system designed in this study is adaptable to be used with different rock types as well as adapting to image different cross sectional planes. This study details the development and tomographic testing of a data acquisition system as well as recommendations for other ultrasonic investigations that are capable with this system.

CHAPTER 2: LITERATURE REVIEW

2.1 ULTRASONIC WAVE PROPAGATION

Ultrasonic sound waves are classified as waves that have frequencies higher than what can be heard by the human ear. These mechanical waves have a frequency range above 20 kHz. These waves can only exist in a material medium, such as air, water, rock [1]. These Ultrasonic waves travel in two modes, longitudinal and transverse. A longitudinal ultrasonic wave is also known as a pressure wave or P-wave. This type of wave is the fastest moving ultrasonic wave. The wave propagates along a straight line due to particles on the molecular level oscillating parallel to the direction of propagation. A transverse wave is also known as a shear wave or S-wave. This wave propagates perpendicular to the direction of travel due to a shear oscillation on the molecular level. The S-wave is slower than the P-wave due to the mode of oscillation.
To completely describe an ultrasonic wave a function can be formed that describes the shape of the wave. This function is described in Equation 2.1 [1].

$$y = h(x,t) \qquad (2.1)$$

The variable y represents transverse displacement of an element in the function h at the time t and in the position of x. The amplitude of y is the magnitude of the displacement of the wave. The phase of the function refers to the angular motion with respect to the position x. The phase changes linearly with time [1]. Repetitions of the pattern or shape of the function can be measured to determine the wavelength of the wave. A wavelength is the linear distance the wave travels in one cycle of the wave's function. For example, a sine function begins to repeat itself when its angle is increased by 2π, so the distance traveled over the angular change from 0 to 2π is the wavelength [1].

The onset of the wave across a material marks the arrival time of the wave. The time it takes to travel across the sample Δt is divided from the distance traveled, Δx, to determine the speed of the wave. This relationship is also equal to the product of the wavelength and the frequency of the wave. This is shown in Equation 2.2.

$$V = \frac{\Delta x}{\Delta t} = \lambda f \qquad (2.2)$$

where: V = sound velocity

λ = wavelength

f = frequency

Δx = change in position

Δt = change in time

Ultrasonic waves depend on the elastic properties of a material. Equation 2.3 shows how density and the bulk modulus are related to the speed of sound through a material.

$$V = \sqrt{\frac{C}{\rho}} \qquad (2.3)$$

where: C = elastic constant

ρ = density

$$K = -\frac{\Delta p}{\nu} \qquad (2.4a)$$

$$K = \frac{E}{3(1-2\nu)} \qquad (2.4b)$$

$$K = \rho\left[V_p^2 - \frac{4}{3}V_s^2\right] \qquad (2.4c)$$

where: K = Bulk Modulus

E = Elastic Modulus

ν = Poison's Ratio

Δp = change in pressure

V_p = P-wave Velocity

V_s = S-wave Velocity

$$E = \frac{\sigma}{\varepsilon} \qquad (2.5)$$

where: σ = stress

ε = strain

Elastic constants such as, the bulk modulus, K, and the Young's Modulus, E, are found experimentally. These index values can be used to characterize a rock sample, as Equation 2.3 shows, to find the theoretical material velocity. The equations for these moduli are shown in Equations 2.4(a-c) and 2.5 [5]. The theoretical value of velocity may not be the same as the measured value due to the presence of discontinuities within the rock sample.

Ultrasonic waves can travel through any natural material, as explained above. The resonant frequency of a material is an important property to note when attempting to pass ultrasonic waves through the material. In rock this value is usually nonlinear. The resonant frequency of a rock can change with saturation or stress. Matching the resonant frequency of the rock to the transmitted ultrasonic signal will maximize the amount of the wave's energy that is passed through the rock. The resistance to the flow of sound wave through the rock is known as acoustic impedance (Z). The equation for acoustic impedance is shown in Equation 2.6.

$$Z = \rho V \qquad (2.6)$$

where: Z = Acoustic Impedance

ρ = material density

V = material velocity

Frequency matching is a common way to maximize the signal strength and minimize acoustic impedance.

Refraction is another concern when passing an ultrasonic signal through a rock. Refraction is the incomplete transmission of a wave through an interface. When a wave interacts with two materials that are not the same (i.e. mineralization, faults, or bedding planes inside of a rock) the wave is split in two and is said to be refracted [1, 2]. Part of this refracted wave is reflected and the other part is transmitted at a different angle. This angle of refraction is influenced by the angle of wave incidence.

$$\sin\theta_2 = \frac{n_1}{n_2}\sin\theta_1 \qquad (2.7)$$

where: θ_1 = angle of incidence

θ_2 = angle of refraction

V_1 = velocity of material 1

V_2 = velocity of material 2

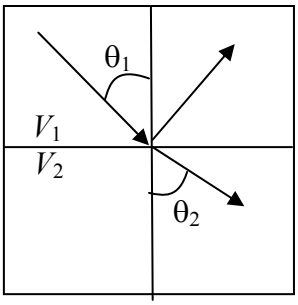

FIGURE 2.1: ILLUSTRATION OF SNELL'S LAW, ACOUSTIC WAVE REFRACTION AND REFLECTION AT A INTERFACE WITH DIFFERENT ACOUSTIC VELOCITIES

The equation for Snell's Law is shown in Equation 2.7 and is illustrated in Figure 2.1 [1, 2].

2.1.1 ULTRASONIC SENSORS

When selecting a transducer it is important to understand how an ultrasonic wave enters a material and how it travels through the material to the place of reception. There are two methods of transmitting and receiving commonly used in ultrasonic applications. These methods are the Pulse-Echo and Through Transmission techniques. The Pulse-Echo technique uses one transducer that switches from active to passive to measure reflections within a material. This method is commonly used in flaw detection to determine the depth to a flaw when the transmission length and material velocity are known. The Through Transmission technique uses two transducers with one actively transmitting a wave and the other passively receiving the wave. This method is used to determine material velocity through a cross section of the material. Reflections can be measured using this technique to locate flaws. When using either method it is important to know how a transducer will transmit and receive the wave. When transmitting a wave

it is important to match the impedance of the transducer to that of the rock to maximize the energy transmitted, it is also important to know the mineralology of the sample being tested to know if refraction will be an issue. These concepts were discussed above.

At the reception point other factors such as sensor sensitivity, reflections, sensor directionality, and the sound field become important. Sensor sensitivity and directionality are properties of the sensor. The sensor sensitivity is the sensor's ability to detect a signal. Sensitivity is commonly associated with the ability to detect a weak signal. A sensor can be damped to improve sensitivity. By damping the sensor is tuned to resonate at a distinct frequency. The sensor then becomes very sensitive to this frequency but not to others. An undamped sensor is not sensitive but will have a wide frequency reception bandwidth. Directionality refers to the angular reception and transmission range of a sensor, for example; a point source would have an angular transmission of 360° whereas a planar source would have a directionality of 0°.

The sound field consists of a near field and far field. These fields are similar to the focal length of a lens, where within the near field the image is unfocused but beyond that region the image becomes clear. The near sound field, *N*, is the area in front of the transducer where a signal is hard to measure due to multiple waves from all parts of the transducer. The distance of this area can be found using Equation 2.8.

$$N = \frac{d^2}{4\lambda} \qquad (2.8)$$

Where: d = transducer diameter

λ = wavelength

The far sound field is the region outside of the near field where the transducer waves coalesce to produce a plane wave whose on-axis intensity decreases inversely with distance [3]. From Equation 2.8 it is seen that the diameter of the transducer influences the length of the near field. The advantage of a small diameter transducer is that it can measure thin materials; the disadvantage is that the intensity of the wave rapidly decreases with distance. In contrast to a small diameter transducer, a large diameter

transducer will have a larger near field but the intensity of the wave does not diminish as quickly.

2.2 DATA ACQUISITION

Data acquisition (DAQ) is the process of collecting data in a digital or analog format to describe a physical occurrence. The components included in a data acquisition system consist of a sensing device, a signal conditioning device, and analog to digital conversion.

The resolution of a DAQ system is relative to the resolution of the sensing device and of the A/D converter. The sensing device used in most applications of ultrasonic testing is a piezoelectric transducer (PZT). These sensors consist of a piezoelectric crystal that is damped to produce a sensor that resonates at a specific frequency. The orientation of the crystal determines whether the sensor will detect compressional or shear wave types. To create a sensor that is highly sensitive, a small amount of dampening is used. To create a sensor that is selective, a larger amount of dampening is used to allow the sensor to resonate at a specific frequency. The size of the sensor determines the length of the near field and the resonating frequency determines the minimum wavelength that can be resolved by the sensor. To maximize the resolution of a sensor applied to geophysical monitoring, the frequency of the rock type that is being measured must be known. Most rock types will only transmit ultrasonic frequencies in the range of 200 kHz to 1 MHz. Therefore, a sensor with a wide bandwidth at a lower frequency range would be preferable for measuring ultrasonic waves in rock.

The resolution of an analog to digital (A/D) conversion device is determined by its quantization. The quantization of an A/D device is defines its digital resolution. The resolution is determined by the number of quantization steps. This is commonly reported by the bit resolution of the A/D device [32]. A bit consists of 2^n steps, where n is the number of bits. The digital encoding of an A/D device takes an analog value and assigns it to the nearest digital step within the digital range being measured. The range of encoding is important to the final resolution of the digitized wave. If the range is too wide, the waveform will become pixilated, and if the range is too narrow, the waveform will be clipped. It is important to know the properties of the wave being measured and the properties of the sensing device before assigning a digitizing range.

Analyzing an acquired waveform using digital signal processing (DSP) can remove unwanted frequencies which will improve the signal of interest. LabVIEW has built in DSP functions that allow for a waveform to be filtered, transformed, and otherwise manipulated digitally to better resolve a noisy or incomplete waveform. These methods are useful when post processing data, but can create false data points by over smoothing or interpolating the waveform.

2.2.1 SAMPLING

The information contained within an analog waveform can be captured by sampling the waveform. Continuous analog data are sampled at discrete intervals. The sampling interval must be chosen carefully to insure an accurate representation of the original signal. Faster sampling of a continuous signal will allow for a more accurate picture due to the abundance of sampling points, but if fewer samples are taken a point is reached where information about the signal can be lost. This point is defined by Nyquist's criteria [32]. The Nyquist criteria requires that the sampling frequency, f_s, be at least twice the signal bandwidth, f_a, or information about the signal will be lost. The loss in information will result in what is known as aliasing. An example of aliasing is shown in Figure 2.2.

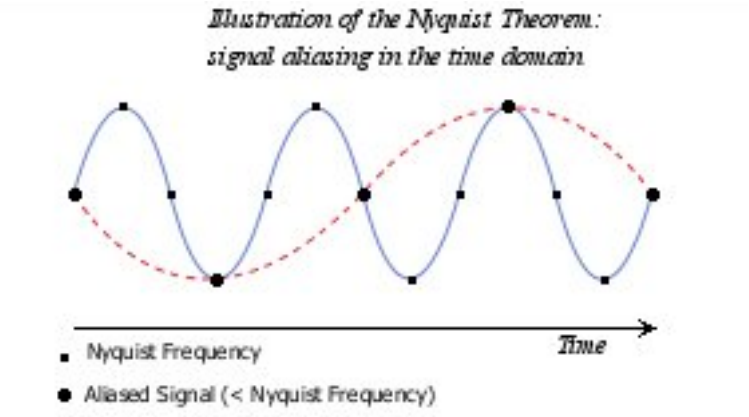

FIGURE 2.2: SIGNAL ALIASING IN THE TIME DOMAIN

Proper sampling rates must be used to prevent aliasing. Sampling rates higher than the required rate (determined by the Nyquist theorem) improve the resolution of the first break of the waveform, allowing for more accurate arrival time picking.

2.3 LABVIEW PROGRAMMING

Laboratory Virtual Instrumentation Engineer's Workbench (LabVIEW) is a graphical programming language developed by National Instruments. This program was developed for instrument control and data collection. Virtual Instruments (VIs) are made to collect data from measurement devices, control or manipulate instrumentation, and process data. A VI consists of a front panel and a block diagram. The front panel is a VI's control panel while the program is executing. On this screen graphs, knobs, buttons, and other objects can be manipulated by the user. An example of a VI front panel is shown in Figure 2.3.

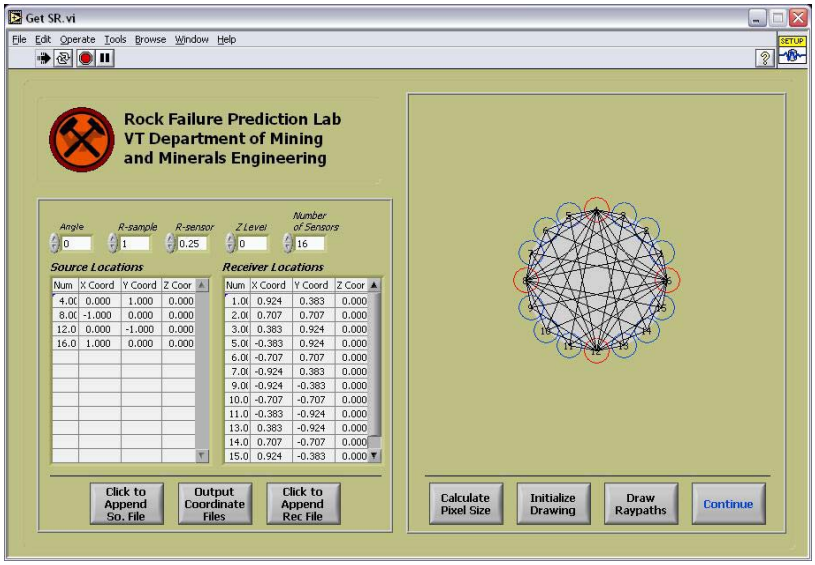

FIGURE 2.3: LABVIEW VIRTUAL INSTRUMENT FRONT PANEL

The block diagram is where the front panel objects are 'wired' together, similar to an electrical schematic. An example of a VI block diagram is shown in Figure 2.4.

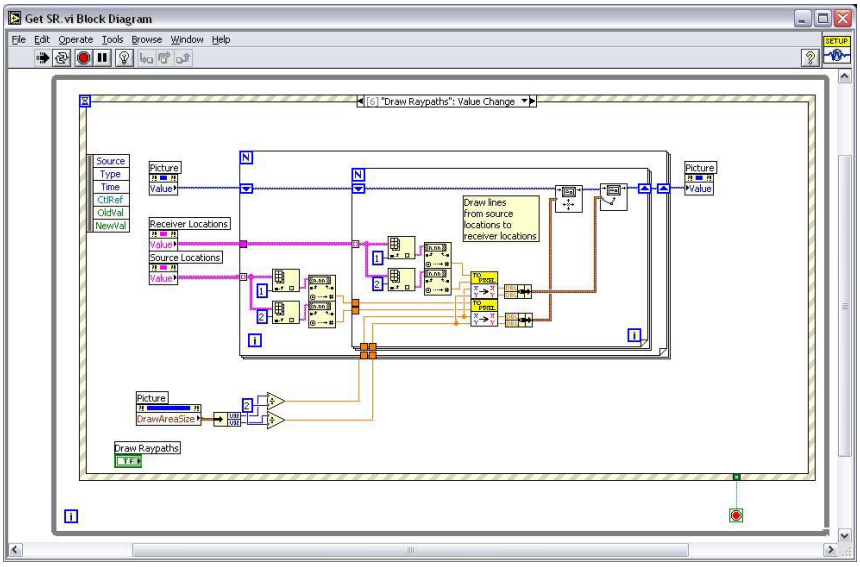

FIGURE 2.4: LABVIEW VIRTUAL INSTRUMENT BLOCK DIAGRAM

The wires connect to executable icons called nodes. The wires represent the flow of data from one function block to another [4].

LabVIEW was created to interact with data acquisition cards and instrument controllers. Using LabVIEW a custom measurement instrument can be made for a data acquisition system. To acquire data a virtual measurement channel is created to represent the input for data acquisition. Once a signal is digitized it can then be processed within LabVIEW using digital signal processing. Instrument control can also be conducted within LabVIEW. A custom instrument control panel can be created in a VI for a specific application.

2.4 TOMOGRAPHY

Tomography (derived from the Greek word *tomos*, meaning section) is an application of nondestructive testing to view the interior of a body without penetrating its surface by physical means. In tomography, radiation is either passed through a material or reflected inside a material along a straight line. The radiation carries information about the physical properties in the transmitted medium [6]. This process is repeated with different locations of transmitting and receiving radiation to achieve the desired resolution. This method of imaging is used widely in the medical field using X-Rays to create a cross-sectional image. The data is then inverted using a transform. Tomographic inversion techniques are derived from the Radon Transform. The transform is named after Radon (1917) who first derived an inverse transform. The Radon Transform is described in depth by Nolet [5]. The focus of this study is on geophysical applications of tomography. This area of study was pioneered by Dines and Lytle in 1979 [9].

Geophysical tomography can utilize different radiation sources such as X-Ray, electrical resistivity, reflection, seismic and ultrasonic. The radiated energy is passed through a medium and measured in slightly different ways, producing transforms that display different physical information in the cross-section. In X-Ray tomography the cross sectional image is of the boundaries within a medium such as cracks in rock. In electrical resistivity tomography the tomograph shows the resistivity through the medium [8]. Reflection tomography measures reflected ultrasonic waves as they bounce off of interfaces within a body. This method can be used to locate geologic structures or old mine workings [24]. Seismic tomography is very similar to ultrasonic tomography. The difference between these two methods of tomographic imaging is the frequency ranges used. Seismic tomography utilizes low frequency waves to measure structures within the earth. The low frequencies correspond to long wavelengths which are capable of traveling long distances. Ultrasonic tomography is used more for laboratory and mine-wide monitoring systems. Ultrasonic waves have small wavelengths which can resolve small structures; however ultrasonic waves attenuate quickly and can therefore only be transmitted over short distances. Ultrasonic tomography can be used to measure the

slowness of the P or S wave across the sample as well as amplitude variations across the sample.

This study involves ultrasonic P-wave velocity tomography. This type of tomography produces a cross-sectional image of velocity across a body. Rocks behave according to Hooke's Law, where stress and strain are related. When the rock is under a load it reaches an equilibrium point where the rock will change in length (strain) to accommodate a change in the load across the area of the rock (stress). This is known as elastic loading. As a rock is mechanically loaded the acoustic velocity through the rock will increase proportionally with stress. This is known as the acousto-elastic effect. A tomographic survey which is conducted at a stress state within the acousto-elastic region will show a cross sectional picture of the relative internal stress. To observe this, the velocity within the material is first found by collecting an ultrasonic waveform by transmitting an ultrasonic wave through the material, and the arrival time of the wave is found. There are different methods of automatically finding the arrival time of the waveform. In seismology, automatic P-wave arrival picking is very important and many studies have been done to make this process more robust. The main difference between laboratory applications of arrival time picking and seismic applications is the difference in the signal to noise ratio (SNR). The SNR for laboratory testing normally is very high; this is not the case for seismic testing. Therefore, the algorithms used for arrival time picking are complex for seismic data to account for the poor SNR. The methods of fuzzy logic and wavelet transforms are too complex for the application in this study and will not be discussed.

The direct correlation method of arrival time picking is used in the laboratory and in the field. This method uses statistics to determine the arrival time of the waveform. It is a simple method in which a portion of a waveform is compared to a reference waveform and the correlation between the two plots is compared. A high correlation indicates a high probability that the sections of the waveforms are the same. This method of arrival time picking is explored in depth by Molyneux and Schmitt [11]. Once the arrival time is picked the velocity of the wave can be calculated. The velocity between

one source and receiver pair represents an average velocity along that raypath. By conducting a tomographic survey where multiple raypaths are measured at different orientations across the sample, many velocities along the different raypaths can be found. These velocities are then inverted to produce a velocity profile along the plane being measured.

The algorithms used for ultrasonic tomography have improved since the first application of geophysical tomography by Dines and Lytle. Two common algorithms used for tomographic inversion are the algebraic reconstructive technique (ART) and the simultaneous iterative reconstructive technique (SIRT). The ART method is used for linear models. This method inverts all of the data at once to form a tomographic representation of the data. This method is simpler than the SIRT method, however if a large data set is used it requires large amounts of computer memory and processing time to conduct the transformation. The SIRT method iteratively inverts rows of data that improve the initial inversion, the iterations continue until all data has been processed. This method is useful for large data sets because the amount of computer memory required is significantly less than the amount required when using the ART method. A comprehensive review of both methods is found in the literature [5,7].

2.4.1 APPLICATIONS OF TOMOGRAPHY

Tomography has been used widely for geophysical applications such as earthquake tomography, three dimensional structural imaging, geologic hazard identification, and stress identification. For large structures seismic tomography is commonly used because seismic waves can travel longer distances than an ultrasonic waves. The theory behind seismic tomography is comparable to that of ultrasonic tomography. Field studies using seismic tomography have been conducted in mines to characterize underground rock masses [12] and map underground structures [13, 14]. Tomography has also been used in mining to monitor for roof or pillar failure, identify regions of relatively higher stress, and strata identification. The use of these mine-wide monitoring systems can increase miner safety and also help maintain production by preventing potential roof failure.

Hazard detection is one way in which ultrasonic tomography can increase miner safety. In active mining sections, structural analysis can be done by observing the roof, rib, and floor surfaces. Further geologic characterization and hazard recognition efforts are not undertaken due to cost constraints [24]. If further geologic characterization is undertaken it usually requires boreholes to be drilled from the surface to intersect the ore deposit. To reduce characterization costs ultrasonic tomography can be employed to detect hazards ahead of mining or within the mine workings. Some hazards that can be detected are old mine workings, structural changes in geology, or high stress zones [24]. To detect old mine workings reflection tomography can be employed. Structural changes in geology are detected by measuring anisotropy [12], high resolution 3D tomography [13], or by noting velocity characteristic changes across a rock mass [14, 20]. Using these methods faults, strata changes, and in some cases water content can be defined within a rock mass. This information is very valuable in mine planning. High stress detection is also an important application of ultrasonic tomography. Field studies have been conducted successfully while excavating tunnels [19], excavating longwall panels [15], identifying burst prone faces [22, 25], and measuring mining induced geological changes [16]. Coupling tomography with other imaging techniques such as ground penetrating radar (GPR) can give an indication where surfaces are located in addition to knowing the stress at these interfaces [23]. Another combination combines acoustic emission detection with ultrasonic tomography to monitor faulting or failure [27]. This testing method has been used in mines but is mainly being studied on the laboratory scale. An overview of other engineering applications and equipment design for ultrasonic investigations can be found in the literature [17, 18, 21, and 26].

Ultrasonic tomography has been conducted in the laboratory to better understand the implications of this monitoring method. By analyzing sample behavior in the laboratory many experiments with different loading conditions and sample characteristics can be conducted rapidly. The design of a tomographic data acquisition system for the laboratory would be advantageous to allow these experiments to be conducted. Laboratory tomographic systems have been developed in past experiments [6, 29]. These

systems were not designed to accommodate new technologies such as faster acquisition computers and higher resolution A/D converters. Experiments that have been investigated involve the stress distribution from indentation [28], stress distribution and acoustic emission location in hydraulically loaded samples [30, 31].

CHAPTER 3: ULTRASONIC DATA ACQUISITION SYSTEM: HARDWARE DESIGN

The accuracy and precision of a tomographic imaging system is determined by the quality of the acquisition system used. The data acquisition system for this study was designed to be used in a laboratory setting. Samples for this system can have a cross sectional area between 20 cm^2 – 100 cm^2. Sensors with smaller diameters should be used to improve the contact between the sensor and rock; additionally the small diameter increases the number of sensors that can be attached to the sample. The selection of the proper couplant is important to increase the signal to noise ratio (SNR) of the received signal. A high SNR will increase the accuracy of arrival time picking. The sensors must be capable of transmitting an ultrasonic pulse or receiving the pulse. The ultrasonic pulser that is used with this system should have adjustable output frequency and output amplitude. This will allow for more precise matching of the resonant frequency of the transmitted signal to that of the rock. Once the signal is received, the signal is digitized using an analog to digital (A/D) converter. The resolution of this device must be fine enough to resolve the first break of the received waveform to accurately calculate the velocity of the wave. The resolution of the A/D converter is determined by the number of quantization steps (vertical resolution) and also by the acquisition speed (horizontal resolution). The flowchart in Figure 3.1 shows the relationship of the instruments selected for the ultrasonic data acquisition system.

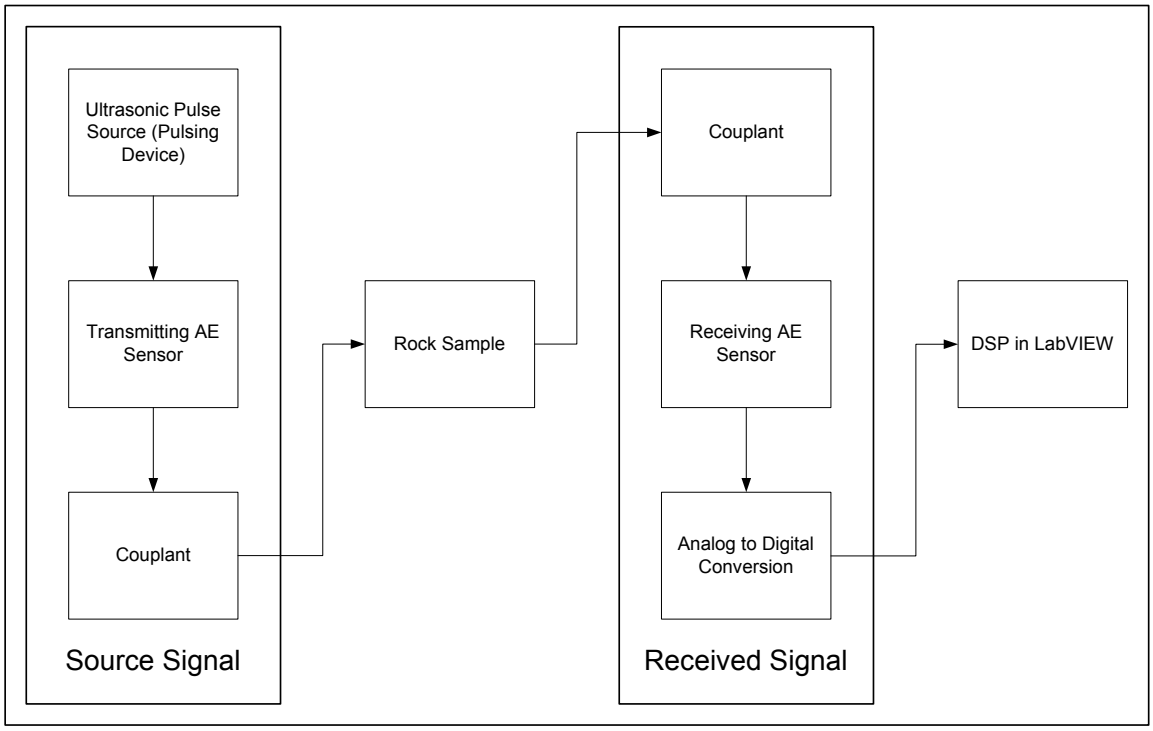

FIGURE 3.1: ULTRASONIC DATA ACQUISITION SYSTEM HARDWARE FLOWCHART

All of the devices within the system should be capable of being controlled by the user at one location. This chapter outlines the selection and design process for the ultrasonic tomographic data acquisition system.

3.1 SENSOR SELECTION

The most sensitive components of the ultrasonic data acquisition system are the sensors. Piezoelectric transducers (PZT) are often used for ultrasonic testing to translate vibration into an electrical signal. Damping is used to tune a PZT sensor to a specific resonant frequency where the sensor would be most sensitive and would be excited more by a wave that had a matching resonant frequency. The advantage of a damped PZT sensor is that it can effectively filter out unwanted frequencies. Undamped sensors can be excited by a wider range of frequencies. The energy received by an undamped sensor is not as great as a damped sensor, but the wider bandwidth allows for more data to be collected. For this study undamped sensors were selected due to their wide bandwidth.

The sensors are the point of contact between the acquisition system and the rock specimen. Improper frequency matching of the sensor to the testing material will result in a reduction of transmitted energy into the rock. A perfect match between the resonant frequency of the sensor and the rock would result in the maximum energy transfer of the ultrasonic signal through the rock specimen. The other consideration at the interface of the sensor and the rock involves acoustic impedance. Acoustic impedance is the opposition to the flow of sound through a material [40]. The effect of acoustic impedance can be minimized by using a couplant that has impedance close to the impedance of the rock. The typical frequency range for ultrasonic testing in rock is 100 kHz to 1MHz. The sensors used in this acquisition system were selected based on the criteria above.

3.2 Sensor Mounting

A couplant is required to mount sensors to rock core samples, because ultrasonic contact acoustic emission sensors were selected. The sensors will not collect ultrasonic signals through the air, so any air pockets between the sensor and the material must be eliminated by using a couplant. Common couplants used for ultrasonic testing consist of viscous oils or epoxy adhesives. These couplants are very effective on flat surfaces but on curved surfaces gaps between the sensor and the rock surface can exist. Therefore, beeswax was used to mount sensors to cylindrical samples. This material is appropriate because it molds to the curved surface of the rock core and also fills in any gap between the sensor and the sample due to the curved surface. The effective use of beeswax to fill gaps formed by incompatible geometries can be seen in Figure 3.2.

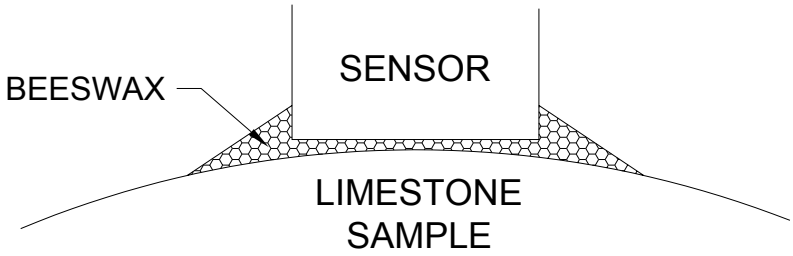

Figure 3.2: Beeswax couplant application

When the beeswax is heated it becomes soft and pliable, and when it cools it hardens. The hardening of the wax ensures that the sensors are held in a rigid position, not sliding when the sample is moved or loaded. A disadvantage to using wax is that the sample and sensors must be kept warm or the wax becomes brittle, pulling away from the sample under high loads. A cynoacrylate adhesive was used to mount sensors to flat non-reactive surfaces. This adhesive becomes very rigid when dry and can be released by a debonding agent.

The sensors selected for this system are Physical Acoustics Corporation Micro-80 miniature acoustic emission sensors. Properties for these sensors are listed in Table 3.1.

Table 3.1: Physical Acoustics Micro-80 AE Sensor Properties

Micro 80 Specifications	
DIMENSION DIAxHT (mm [Inch])	10x12 [.4x.5]
WEIGHT (gm)	5
OPERATING TEMP (ºC)	-65 to 177
SHOCK LIMIT (g)	10,000
CASE MATERIAL	Stainless Steel
FACE MATERIAL	Ceramic
CONNECTOR TYPE	Microdot
CONNECTION LOCATION	SIDE
PEAK SENSITIVITY dB 1V/(m/s)[1V/µbar]	57 [-65]
OPERATING FREQ. RANGE (kHz)	175-1000
RESONANT FREQUENCY (kHz)	250
DIRECTIONALITY (dB)	[325] ±1.5
GROUNDING	B
SEAL TYPE	EPOXY

The sensors have a wide bandwidth, allowing for a wide range of frequency matching to different rock types. The small diameter (10 mm) allows for a reduction in energy loss through the couplant from mounting the flat sensor face to the curved rock surface.

3.3 Ultrasonic Pulser

The ultrasonic pulse that passes through the sensors and into the rock originates at a pulsing device. The pulsing device selected for this data acquisition system was a Panametrics 5077PR. This is an ultrasonic square wave pulser/receiver unit. The pulser can operate in two modes, pulse-echo or thru transmission. The thru transmission mode was used for this system and the receiving capability of the unit was not utilized. A picture of this unit is shown in Figure 3.3.

Figure 3.3: Panametrics 5077PR Ultrasonic Square Wave Pulser

The pulser features adjustable output voltage, output frequency, and repetition rate. Table 3.2 shows a summary of these features.

TABLE 3.2: PANAMETRICS 5077PR ULTRASONIC SQUARE WAVE PULSER SPECIFICATIONS

Panametrics 5077PR Specifications	
Pulse Type (Main Bang)	Negative Square Wave, adjustible duration & amplitude
Maximum Pulse Amplitude	400V (no external load)
Pulse Width	10 preset fixed widths for the following transducer frequencies/ranges: 15 - 20MHz, 10MHz, 7.5MHz, 5.0 - 6.0MHz, 3.5 - 4.0MHz, 1.0MHz, 0.5MHz, 0.25MHz, and 0.1MHz. Each width can be fine tuned by at least 25%
Repetition Rate (internal and external trigger)	100, 200, 500, 1000, 2000, 5000Hz for all transducers, except that maximum PRF is limited to: 2000Hz for 0.5MHz transducers, 1000Hz for 0.25MHz transducers, and 500Hz for 0.1 MHz transducers.
Pulse Rise and Fall Time (minimum pulse voltage and no load)	20ηS max (10% - 90%), Typically 10ηS
Available Pulse Voltage (no load)	100, 200, 300, and 400 Volts (selectable)
Sync Signal Output	3.0V into 50 ohms. Pulse duration 0.5-10ηS. Capable of driving up to 26 standard TTL Loads @2.4V. Sync Out precedes leading edge of Main Bang by 30-60ηS
External Trigger	Positive edge, 2.4V minimum. Min pulse duration 50ηS. Input is AC coupled through 1000pF into 10K ohms. Internal delay between External Trigger and leading edge of Main Bang is approx. 2ηS
Mode	Pulse-echo or Thru Transmission (selectable)
Operating Temperature	0 to 50°C

The ultrasonic pulser is a versatile device that has adjustable pulse width and amplitude in addition to different triggering options. The triggering features were not utilized for this system but are useful for other ultrasonic testing applications.

3.4 ULTRASONIC SWITCHBOX

To move the source pulse from one location to another an ultrasonic switchbox was used. The ultrasonic switchbox pulser device was manufactured by Engineering Seismology Group (ESG) Solutions (Figure 3.4).

FIGURE 3.4: ESG ULTRASONIC SWITCHBOX PULSER

This device has 16 relay channels with high voltage and trigger inputs. An ISA control card was included with this device which utilized Visual Basic programming to control the relay function of the switchbox. This card was not used because the control computer did not have an ISA slot to accommodate the factory control card. A National Instruments PCI-6503 digital input/output data acquisition card was used as a digital control for the relay box (Figure 3.5b).

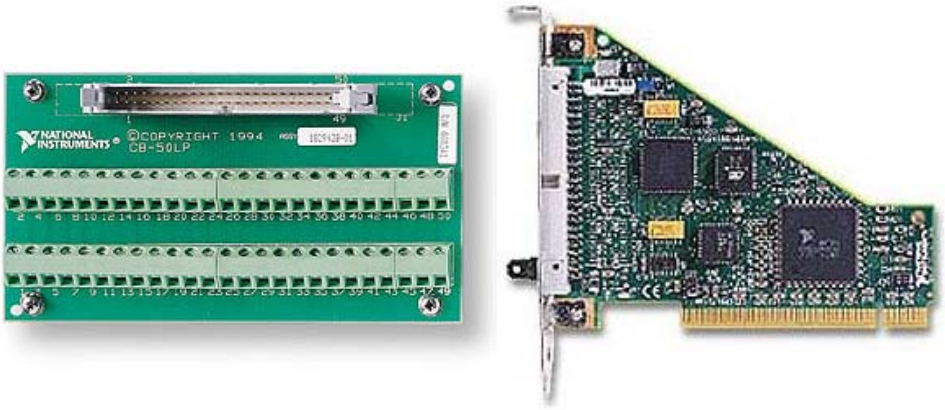

(a) (b)

FIGURE 3.5: (A) DIGITAL INPUT/OUTPUT CONNECTOR BLOCK, (B) NI PCI-6503 DIGITAL INPUT/OUTPUT DATA ACQUISITION CARD

Wires from the digital I/O connector block (Figure 3.5a) were connected to a 25 pin dongle. A dongle was made to plug into a 25 pin serial cable and was wired according to the pin-out diagram shown below:

1	CH1 - DQ0	14	CH9 - DQ0
2	CH2 - DQ1	15	CH10 - DQ1
3	CH3 - DQ2	16	CH11 - DQ2
4	CH4 - DQ3	17	CH12 - DQ3
5	CH5 - DQ4	18	CH13 - DQ4
6	CH6 - DQ5	19	CH14 - DQ5
7	CH7 - DQ6	20	CH15 - DQ6
8	CH8 - DQ7	21	CH16 - DQ7
9	N/C	22	N/C
10	Vcc (9V)	23	Vcc (9V)
11	GND	24	GND
12	N/C	25	TTL pulse out
13	N/C		

Power for the box was supplied by an Agilent power supply running at a constant output voltage of 10V. The complete switchbox controller is shown in Figure 3.6.

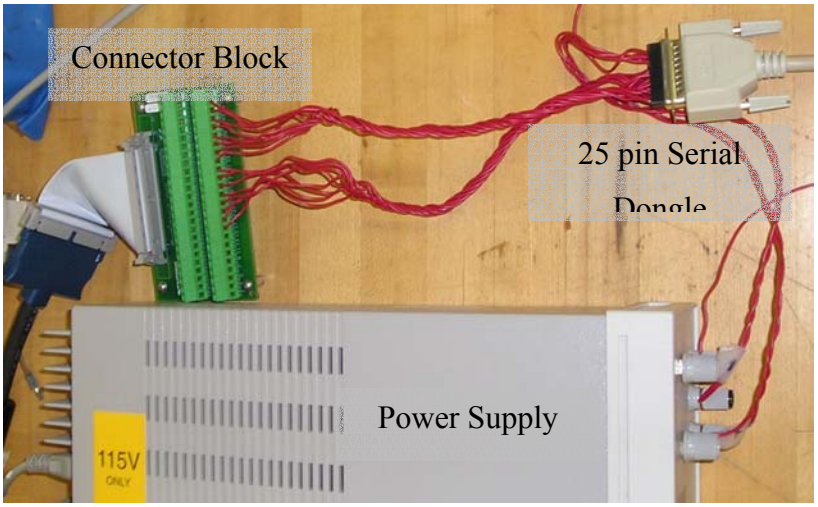

FIGURE 3.6: ULTRASONIC SWITCHBOX CONTROLLER HARDWARE CONNECTIONS

The setup shown in Figure 3.6 allows for the relay of the ESG ultrasonic switchbox to be controlled in a LabVIEW environment along with the rest of the system. This is favorable because it allows for the user to manipulate one program instead of two or more.

3.5 Data Acquisition Instrumentation

After the sensors had been mounted to the sample using a couplant the ultrasonic pulse could pass through the rock to a reception location. The receiving sensor collected the analog waveform and passed it into the analog to digital converters (ADC). National Instruments PXI-5102 Digital Oscilloscopes were used as the ADC for this system. These cards were mounted into a National Instruments PXI 1006 (PCI Extension Interface) Chassis (Figure 3.7).

Figure 3.7: PXI 1006 Chassis with PXI 5102 Digital Oscilloscopes

This chassis has advanced timing and synchronization capabilities through the Real Time Signal Interface (RTSI) bus that connects all the instrument slots in the chassis. The chassis is connected to the control computer using National Instruments MXI-3 technology. The MXI-3 control consists of a PCI card that is installed on the control computer. A similar control card is connected to the control slot in the PXI 1006 chassis. A fiber optic cable connects the two control cards. The use of fiber optics to transfer data allows for high data transfer rates without delaying acquisition on any of the instrument cards in the PXI chassis. The PXI-5102 Digital Oscilloscopes (Figure 3.8) were chosen as the ADC for this system because of their high sample rate and relatively lower cost. The specifications for this card can be seen in Table 3.3.

FIGURE 3.8: PXI 5102 DIGITAL OSCILLOSCOPE

TABLE 3.3: PXI 5102 SPECIFICATIONS

PXI-5102 Specifications	
Resolution	8 bits
Bandwidth	15 MHz
No. of channels	2 simultaneously sampled
Maximum sample rate	1 GS/s repetitive, 20MS/s single shot
Onboard sample memory	663,000 samples
Max waveform buffer	Up to 16 MMS/channel
Vertical ranges	±50 mV to ±5 V
DC accuracy	±2.5% of full scale at all gains
Input coupling	DC or AC
Input impedance	1MΩ ±1% in parallel with 25 pF ±10 pF
Input protection	±42V

The cards have a vertical resolution of 8 bits which correlates to 256 quantization steps. If the minimum vertical range of ±50 mV is used then the smallest quantization step is 0.4 mV. The horizontal resolution of the cards is 20MS/s which corresponds to 0.5 μs. The vertical and horizontal resolutions are acceptable to capture the arrival time of the

waveform provided the waveform does not attenuate to a value less than 0.4 mV. There exists a tradeoff between vertical and horizontal resolution for A/D converters. At higher acquisition speeds the vertical resolution is less than at lower acquisition speeds. To improve the vertical resolution the vertical range can be reduced, which reduces the quantization step, increasing the resolution. However, amplitude data might be lost due to clipping of the signal. Clipping occurs when the vertical range of the acquisition window is less than the actual vertical range of the analog signal being captured. The top of the waveform appears to be cut off and the data outside of the digitizing range is lost. Therefore the vertical range that is used for acquisition must be set so that the arrival time of the waveform can be acquired with minimal clipping of the waveform. LabVIEW programming allows for the vertical range to be adjusted easily, minimizing any loss of data due to clipping.

Precise triggering of the digital oscilloscopes reduces timing errors and improves the overall precision of the acquisition system. To achieve this, the output signal of the pulser was wired into one of the digital oscilloscopes using a voltage divider circuit. The input voltage was dropped from -400V to -4V by using the circuit shown in Figure 3.9.

(a) (b)

FIGURE 3.9: (A) BREADBOARD VOLTAGE DIVIDER CIRCUIT, (B) VOLTAGE DIVIDER CIRCUIT SCHEMATIC

The equation used to calculate the resistances and the final voltage is shown in Equation 3.1.

$$V_o = \frac{R_2}{R_1 + R_2} V_{in} \qquad (3.1)$$

Where: V_o = Output voltage

$R_{1,2}$ = Resistance

V_{in} = Input voltage

The input voltage value was -400 V, originating from the Panametrics ultrasonic pulser. The resistance for R1 was calculated as 100 kΩ, and for R2 as 1 kΩ, resulting in an output voltage to the digital oscilloscope of 3.96 V. Using this signal as a trigger for the acquisition, the arrival time was able to be referenced from the transmitted pulse of the pulser instead of a logic signal that might need to have timing corrections.

3.6 LabVIEW Processing

After the waveforms had been digitized by the PXI 5102 A/D cards digital signal processing (DSP) of the waveforms was done in LabVIEW. The processing that needed to be conducted was the automated picking of the arrival times. This was done by direct correlation. To correlate the correct arrival time a LabVIEW program was written to compare a reference waveform to the actual waveform. The reference waveform was compared to a piece of the total waveform and the correlation between the two was calculated. At the point of highest correlation the arrival time was picked. This method worked well for waveforms with a high signal to noise ratio (SNR), however all of the picks were double checked manually to ensure accurate picking. The accuracy of the picks is very important due to the small scale that is used; therefore great care was taken to ensure the picks were correct.

3.7 LabVIEW Program for Ultrasonic Data Acquisition

Tomographic data was acquired from ultrasonic sensors attached to the sample and was processed by a data acquisition system. A simplified flowchart of the data acquisition system is shown in Figure 3.10.

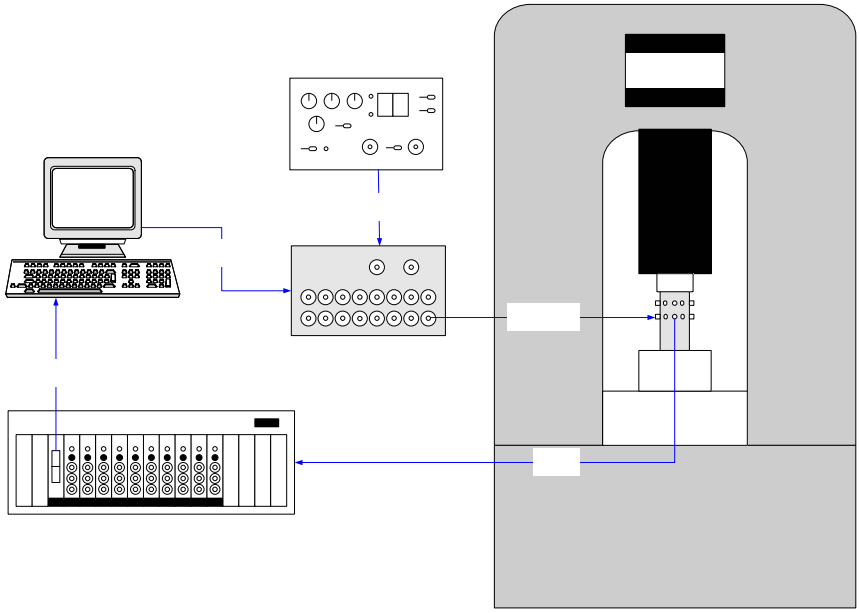

FIGURE 3.10: HARDWARE FLOWCHART

The data acquisition system is controlled by a personal computer. An ultrasonic pulse originates from a Panametrics 5077PR Ultrasonic Square Wave Pulser. The pulser transmits an ultrasonic frequency that matches that of the material being measured at a repetition rate of 100 Hz. This signal is relayed to one sensor on the sample through an ESG Ultrasonic Switchbox Pulser. The switchbox relays are controlled digitally by a LabVIEW program. The computer multiplexes the pulse through each of the predetermined source locations, switching after the signal has been received by every receiving sensor. Once the signal is relayed it enters a transmitting sensor on the rock sample inside of the load frame. This signal is received by the reception sensors which are passively waiting for the ultrasonic signal. The received data passes from the sensors into National Instruments 5102 Digital Oscilloscopes. These analog to digital converters collect the analog signal at 20 MS/second. The digitized waveforms are then passed back into the personal computer for post processing.

Control PC

Acquired Waveforms

LabVIEW programs were created to acquire and process ultrasonic signals from the UDAQ system. A flowchart of the structure of the control program is shown in Figure 3.11.

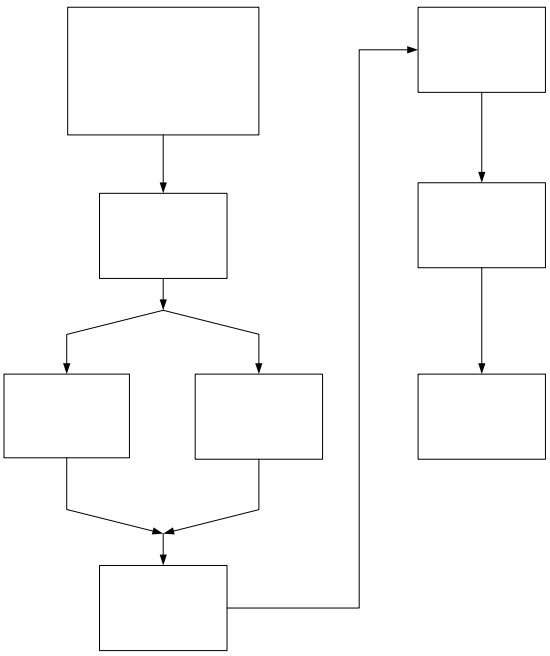

FIGURE 3.11: LABVIEW PROGRAM FLOWCHART

The hierarchy of the program can be seen in Figure 3.11. When the program is first called a main application control menu is opened. In this main panel there are four options. The first is to set the source and receiver locations by calling a setup program. The number of sources and receivers ultimately determines the pixel size of the final tomogram. The pixel size is related to the number of raypaths going between source and receiver locations. The optimum pixel size would be the same length as the wavelength of the ultrasonic waveform. The program has a simple calculation to determine the number of sensors based on the estimated wavelength of the ultrasonic waveform. The source/receiver location program will then output the X, Y, Z location of each sensor in two tables, one for receiver locations and one for source locations. The saved location data is then passed back into the main panel program so the location data can then be called by the acquisition programs. The next two options are acquisition options. The first acquisition option is to acquire pairs. Choosing this option opens up a program that allows the user to acquire tomographic data from unbalanced source/receiver combinations (the number of sources ≠ the number of receivers). This program matches each source with a receiver and then collects the waveform between the pair before moving to the next pair. The other option of acquisition is for simultaneous acquisition.

This option opens up a program that will simultaneously collect waveforms from 16 reception locations from a single source at one time. This acquisition is a little faster and introduces less timing errors because it simultaneously acquires instead of individually acquiring the waveforms. After the waveforms are acquired they are saved. The last option in the main panel is to pick the arrival times. When this option is selected a program opens that cross correlates the acquired waveforms with a reference waveform to determine the arrival time. The correlated arrival times can then be cycled through to manually adjust any necessary picks. A plot of time versus distance is plotted to help determine the fit of the correlation. The final step of processing the data in LabVIEW is to format the data into the correct format for input into the third party tomogram program. This program adjusts the fit of the data so that the general linear trend of the time versus distance plot passes through the origin. An offset was created in the acquisition program to ensure that all ultrasonic data is collected before and after the trigger pulse.

The validation of the data acquisition system for tomographic data collection was achieved by using acoustic emission sensors on three different materials, Plexiglas, Berea Sandstone and Five Oaks Limestone. The sensor locations and assignments (source or receiver) were entered into the LabVIEW program to determine X, Y, Z locations. The acquisition was done using the simultaneous option to eliminate some of the timing error that might be introduced by multiplexing through the sensor array. The arrival times were then picked using the direct correlation program and the times were adjusted to fit a linear trend passing through the origin.

Tomographs were created in GeoTomCG. This software was developed by GeoTom,LLC for creating tomograms from geophysical data. This program uses simultaneous iterative reconstruction technique (SIRT) to perform tomographic inversions. To create a tomogram in GeoTomCG a model is generated in the program. This model then undergoes an iterative inversion using SIRT. The inverted model is then displayed showing a pixilated cross section of the model. Each pixel represents a point velocity at raypath intersections. It is important to have at least one intersection for each pixel, so each pixel represents an average velocity.

CHAPTER 4: ULTRASONIC DATA ACQUISITION SYSTEM: CALIBRATION AND TESTING

Ultrasonic data acquisition was conducted on three different materials to test the system for velocity calibration, void identification, and stress identification. Velocity calibration and void identification was done by testing Polymethylmethacrylate (PMMA or Plexiglas) material of known velocity in the ultrasonic data acquisition system (UDAQ). Stress measurements were done using Five Oaks Limestone and Berea Sandstone. Index properties for the limestone were obtained experimentally in this study; the index properties for the sandstone had been previously tested. This chapter describes the process of preparing and testing samples for index property values as well as the procedure for using the UDAQ system.

The reliability of velocity measurements from the UDAQ system was tested to calibrate and validate the system for velocity measurements. The calibration of the velocity measurement in the UDAQ system was done using Plexiglas plates and initial application tests were conducted to image a void within a Plexiglas plate. Final application testing was to image an indentation load in rock. Two indentation tests were conducted on two different materials, Five Oaks Limestone, and Berea Sandstone. The index properties for the rock were needed to design the tomographic test. The procedure for capturing the index properties for the Five Oaks Limestone is discussed in detail below. The same procedure was done to assess the index properties for the Berea Sandstone.

4.1 CALIBRATION TESTING

In polymer classification testing, PMMA is used as a reference for calibration of ultrasonic transducers [37, 38]. The material exhibits an acoustoelastic effect when subject to a load [37]. This material was used for calibration and initial application testing of the UDAQ system. A test was conducted on two Plexiglas plates to calibrate the ultrasonic test system and to verify tomograms created from the ultrasonic data. One plate was solid and a second plate had a hole drilled in the lower left quadrant of the

plate. Both plates had the same dimensions in length, width and height of 10 x 10 x 2 cm. Figure 4.1 shows a scale picture of the plate with a hole (plate 2).

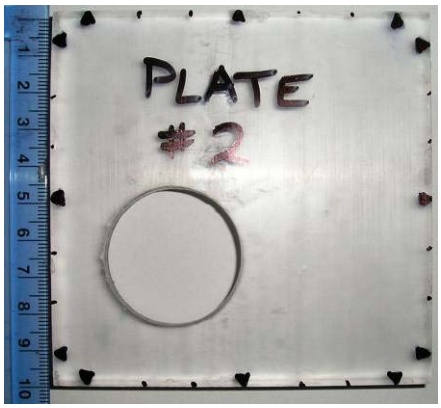

FIGURE 4.1: SCALED IMAGE OF THE PLEXIGLAS PLATE WITH A HOLE (PLATE 2)

A total of twelve sources and sixteen receivers were evenly placed around each plate. The drawing in Figure 4.2 shows the source and receiver locations as well as the ultrasonic raypaths between source and receiver pairs.

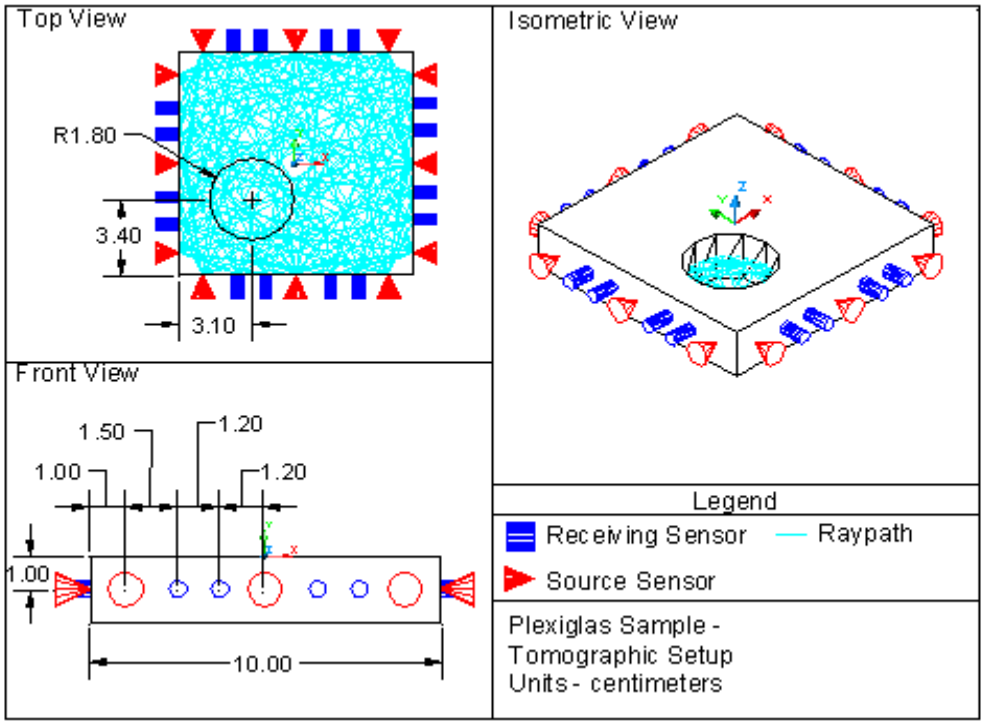

FIGURE 4.2: PLEXIGLAS PLATE TOMOGRAPHIC SETUP

To mount the sensors beeswax was used. The wax was warmed and placed around the perimeter of the plate. The sensors were then placed into the wax (Figure 4.3).

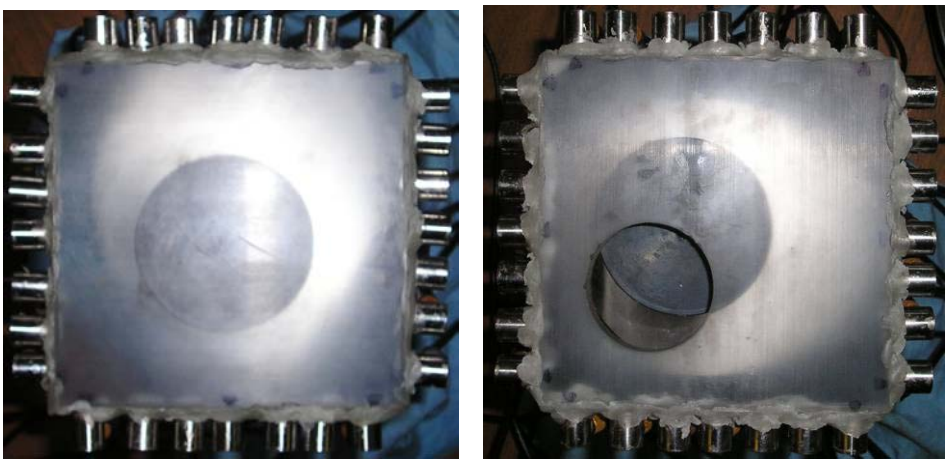

(a) (b)

FIGURE 4.3: SENSORS MOUNTED TO PLEXIGLAS (A) SOLID PLATE 1 AND (B) PLATE 2 WITH A HOLE USING BEESWAX

After acquiring the all of the waveforms, the arrival times were picked using the Correlation program in LabVIEW. The arrival time was then plotted with distance to produce a linear plot of time vs. distance (Figures 4.4 and 4.5).

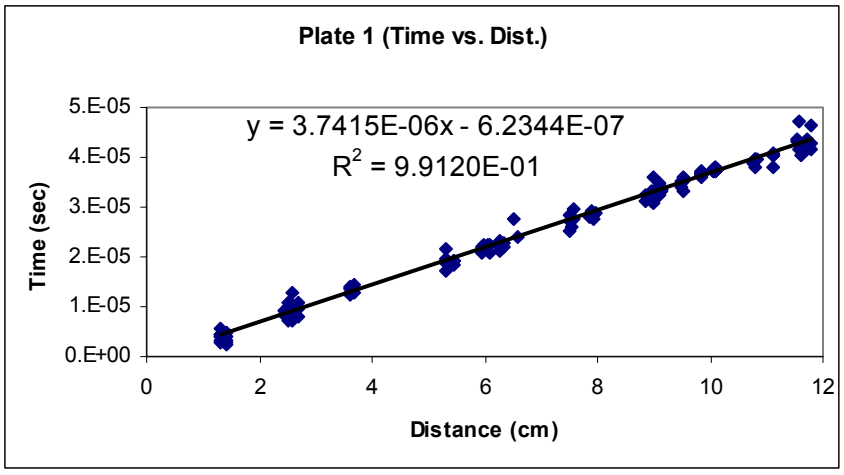

FIGURE 4.4: PLATE 1 TIME VS. DISTANCE PLOT

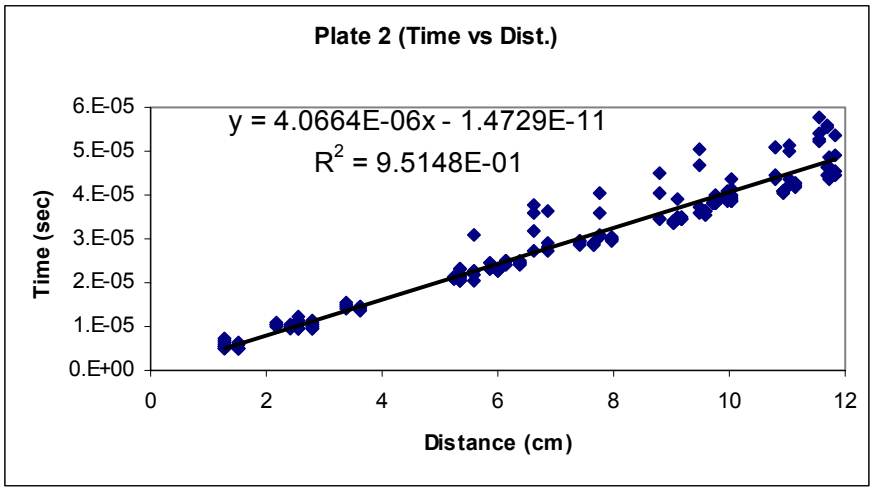

FIGURE 4.5: PLATE 2 TIME VS. DISTANCE PLOT

The calibration of the system was done by comparing the average velocity of all raypaths through the solid plate to average velocity measurements obtained from the ultrasonic P-wave measurement device from the Virginia Tech Rock Mechanics Laboratory and to an average of reported velocity measurements from the literature ([36-39]). The apparatus used to find the ultrasonic velocities is shown in Figure 4.6.

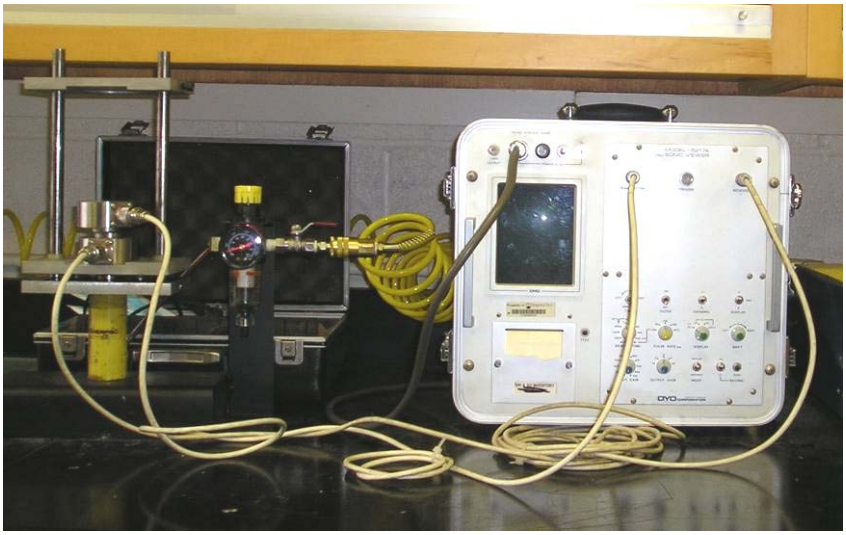

FIGURE 4.6: VIRGINIA TECH ROCK MECHANICS LABORATORY ULTRASONIC VELOCITY VIEWER

Using the Virginia Tech Rock Mechanics Laboratory Ultrasonic Velocity Viewer, 10 velocity measurements were made on Plexiglas samples of varying length to calculate

an average ultrasonic velocity. The transducer frequency used on the ultrasonic velocity viewer was 1MHz. The same test frequency was used in Plexiglas testing using the UDAQ system. Table 4.1 shows the average velocity values, the standard deviation and the comparable error of the measurements.

TABLE 4.1: ULTRASONIC DATA ACQUISITION SYSTEM VELOCITY CALIBRATION MEASUREMENTS

	Velocity		Standard Deviation		Error	
	in/sec	m/s	in/sec	m/s	Rock Lab	Table
Table	106,800	2,700	84	21.3	--	--
Rock Lab	110,500	2,810	18,183	4,620	--	--
DAQ	111,000	2,820	16,226	4,120	0.47%	3.84%

* Table velocity represents an average from [36-39]

From Table 4.1 it can be seen that the velocity measurements from ultrasonic tomographic data collection system (in grey) are accurate. Knowing that the velocity measurements from the system are accurate, some observations of the measurements shown in Figures 4.4 and 4.5 can be made. The two plots of time vs. distance are not the same. Figure 4.4 shows the plot for Plate 1. This plot shows a tight linear trend with a high statistical correlation to the linear trend ($R^2 = 0.99$). It is expected that the tomogram for this data set will be fairly uniform due to the tight linear trend. The plot in Figure 4.5 shows the linear fit for Plate 2. The trend in this plot is linear like Plate 1, but the fit is not as tight ($R^2 = 0.95$). The variation in fit is most likely due to the presence of the hole in Plate 2.

Using GeotomCG, velocity tomograms were made. The smallest structure that can be viewed in the tomograms is dependant on the wavelength of the ultrasonic wave that is received through the Plexiglas. The calculation for wavelength is shown in Equation 4.1.

$$\lambda = \frac{V}{f} \qquad (4.1)$$

Where: λ = Wavelength

V = Material Velocity

f = Frequency

The ultrasonic frequency used for testing the Plexiglas was 1MHz and the ultrasonic velocity was found experimentally to be 2,820 m/s. Using equation 4.1 the resulting wavelength was 0.28 cm. Tomograms were made from the ultrasonic data using GeoTomCG (Shown in Appendix A). The resulting tomographic data was smoothed using the Nearest Neighbor interpolation method. The smoothing did not add erroneous data points and made the visual interpretation of the tomograms easier. The tomograms in Figure 4.7 show that the hole in Plate 2 was clearly imaged and the solid plate (Plate 1) has uniform velocity across the tomogram.

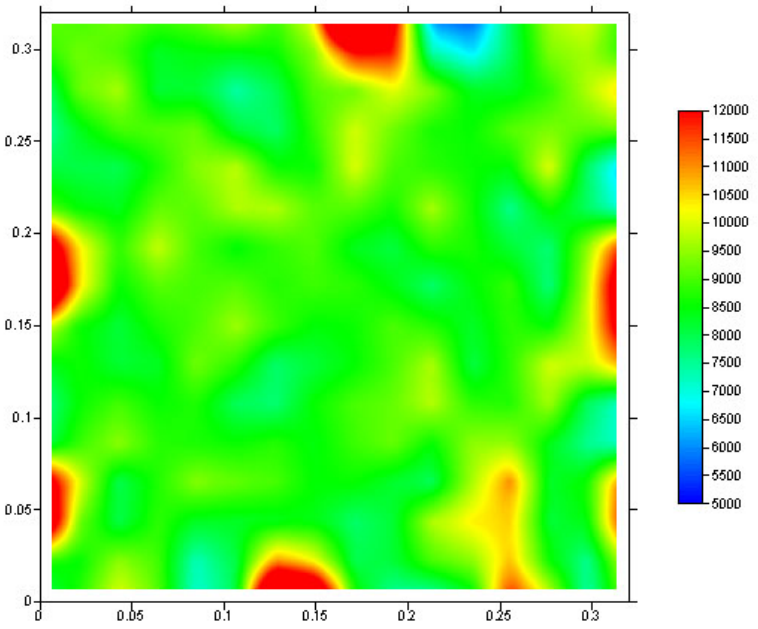

FIGURE 4.7A: TOMOGRAM OF THE SOLID PLEXIGLAS CALIBRATION PLATE

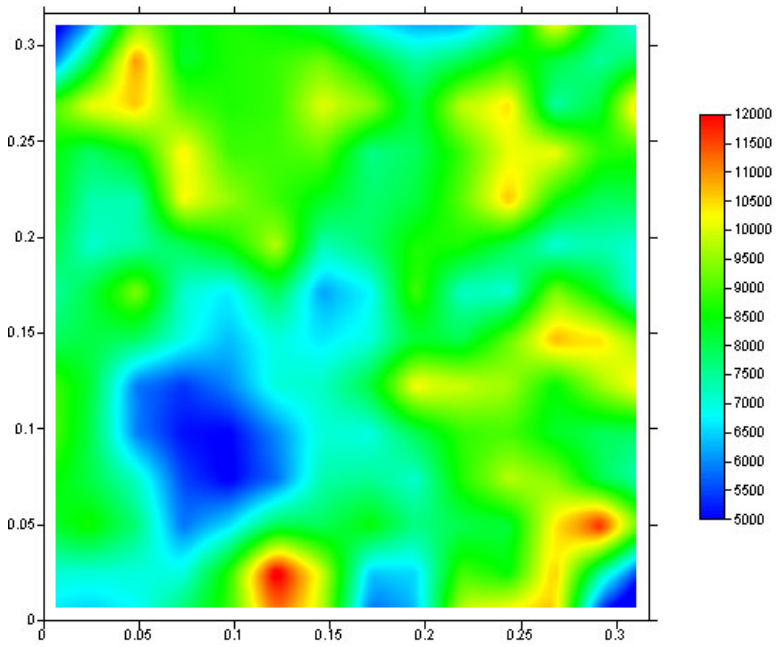

FIGURE 4.7B: TOMOGRAM OF THE PLEXIGLAS CALIBRATION PLATE WITH A HOLE

The velocity scale shown in Figure 4.7 is in feet per second. The background velocity for both plates is the same at around 9000 ft/sec (2743 m/s). The background velocity from this experiment matches the Plexiglas acoustic velocity value of 2700 m/s (9058 ft/sec) reported by ndt-ed.org [36]. The most significant finding in this experiment is the presence of the hole in the tomogram for Plate 2 (Figure 4.7b). The hole is not only clearly shown, but it is accurately placed in the tomogram. In addition to the presence of the hole, artifacts are seen around the perimeter of the tomogram. The cause of these artifacts is most likely due to the beeswax couplant. The artifacts correlate closely to source and receiver locations. By comparing the source locations (Figure 4.2) to the red artifacts (Figure 4.7) around the perimeter of the tomograms a close match is made. The same trend can be seen when the receiver locations (Figure 4.2) are compared to the blue artifacts (Figure 4.7).

4.2 APPLICATION TESTING

Testing in rock was conducted to verify the application of the UDAQ system for stress redistribution tomography. The application testing was conducted in Berea Sandstone and in Five Oaks Limestone. An indentation test was selected to test the

system for tomographic imaging of stress. The purpose of the indentation test was to create a large stress contrast within a rock sample and capture the stress zone at different stress levels. To be able to know the levels at which to acquire ultrasonic data, index testing was conducted to find the average compressive strength, ultrasonic velocity, and elastic modulus for the rock being tested. Two rock types, sandstone and limestone, were used to observe the ability of the UDAQ system to image the indentation stress and stress redistribution patterns for the rock samples.

Index properties for each rock type were found experimentally in the Virginia Tech Rock Mechanics Laboratory. The properties tested were porosity, density, compressive strength, and ultrasonic velocity. Standard testing procedure was followed for these tests [33, 34]. Porosity was measured to determine the percentage of pore space within the rock. A high porosity was favorable because it allowed for the coalescing processes to be potentially imaged. Compressive strength was tested to determine the stress states at which tomographic imaging would be conducted. Ultrasonic pressure and shear waves were passed through a sample to obtain the ultrasonic pressure (p) wave and shear (s) wave velocities. This was done to be able to calculate the theoretical dynamic constants such as the Young's Modulus of Elasticity, Poisson's Ratio, and the Bulk Modulus using ultrasonic velocity and density values.

4.2.1 Berea Sandstone Experiment

Berea Sandstone is commonly used for laboratory testing because the variance between samples is smaller than that for other rock types. The sandstone used in this experiment was obtained from Cleveland Quarries in Amhurst, Ohio. The index properties were tested in the Virginia Tech Rock Mechanics Laboratory by Dr. Karfakis prior to this study (1993 and 1994). A summary of index properties for this Berea Sandstone is shown in Table 4.2.

TABLE 4.2: BEREA SANDSTONE INDEX PROPERTIES

	Porosity,n (%)		Density, γ (g/cm^3)[lb/ft^3]		Specific Gravity, G		Tensile Str (MPa)[psi}		Compressive Str (MPa)[psi]		Compressive Vel (m/s)]ft/sec]	
	Avg.	St. Dev.	Avg.	St. Dev.	Avg.	St. Dev.	Avg.	St. Dev.	Avg.	St. Dev.	Avg.	St. Dev.
(Metric)	19.5	0.81	2.35	0.06	2.92	0.10	3.57	0.37	6.26	0.36	2,200	191
(English)	19.5	0.81	147	4.00	2.92	0.10	518	53.7	907	51.6	7,220	626

A testing frequency of 300 kHz was used to image the 10.16 x 2.54 cm (4 x 1 in, diameter x height) cylindrical sample. The effective wavelength through the sample was estimated to be 0.73 cm (0.29 in). The cylindrical platen with a diameter of 5.08 cm (2 in) used in the limestone experiment was used to apply an indentation load to the sandstone sample. Thirty-two sensors were equally spaced around the sandstone sample. The drawing in Figure 4.8 shows the location of the load platen, the sensor spacing, and the ultrasonic raypaths between each source and receiver pair.

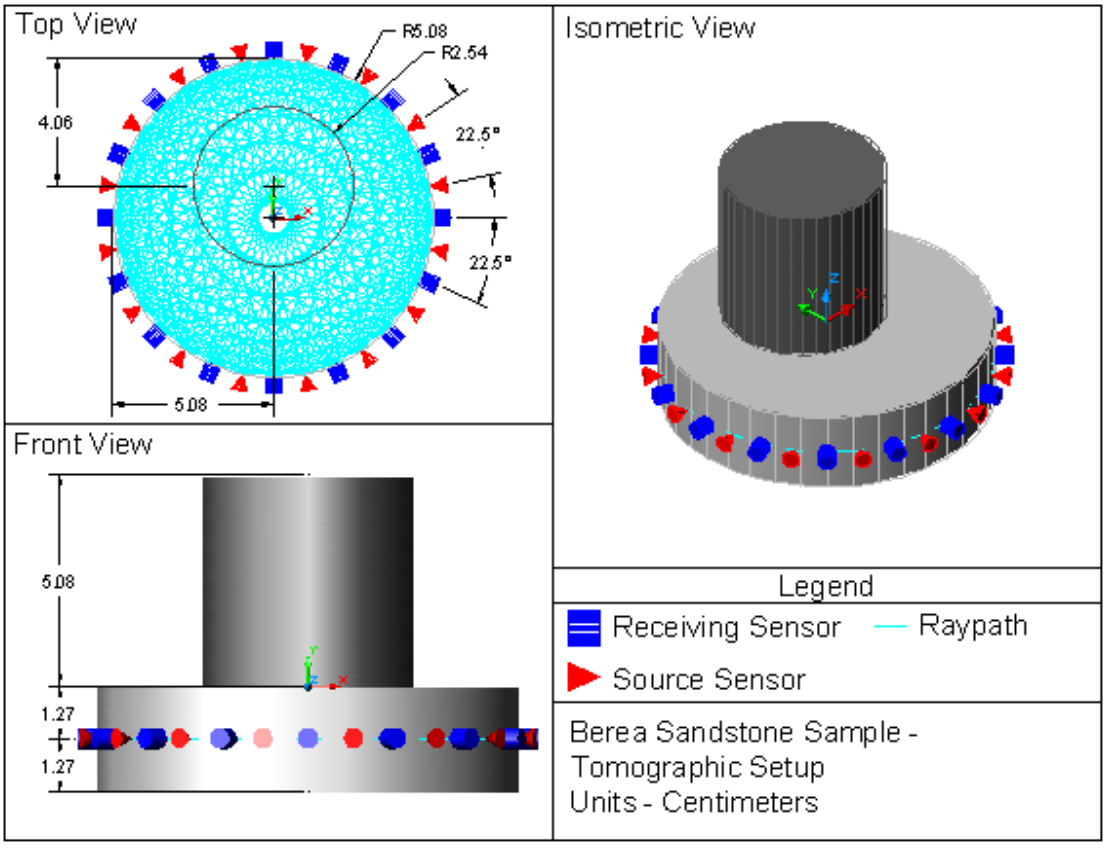

FIGURE 4.8: BEREA SANDSTONE TOMOGRAPHIC SETUP

The sensors were attached using beeswax. Figure 4.9 shows the sample before and after failure.

(a) (b)

FIGURE 4.9: BEREA SANDSTONE TEST SAMPLE (A) PRIOR AND (B) POST FAILURE

Tomographic data were collected as the sample was loaded. The loading was paused to collect data at 0, 17.24, 24.82, 34.47, 46.54 MPa using the *Acq_16.vi* in LabVIEW. The arrival times for each load were then picked using the *Correlation.vi* LabVIEW program. Arrival times were plotted against distance to observe how well the arrival times were picked. Figure 4.10 shows plots of arrival time vs. distance for all different load conditions.

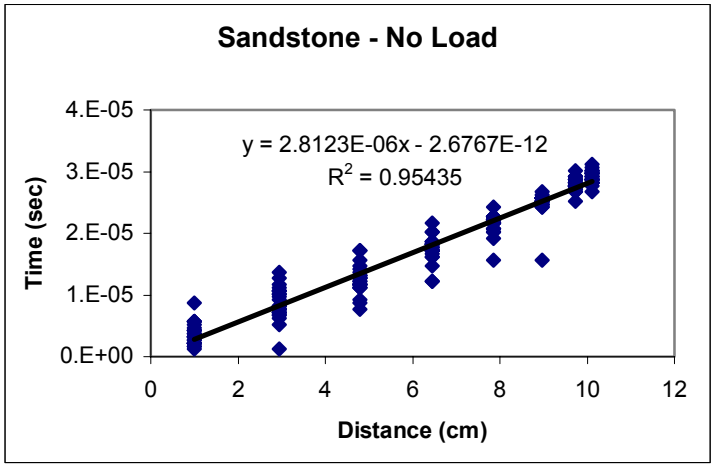

FIGURE 4.10A: BEREA SANDSTONE TIME VS. DISTANCE PLOT AT LOAD 1, 0 MPA LOAD

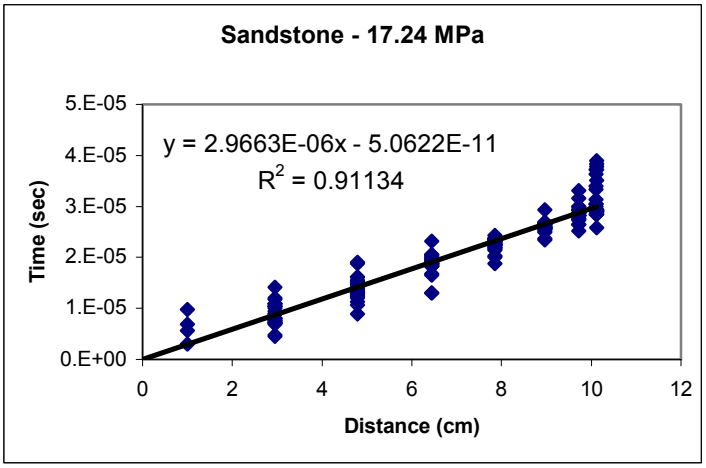

FIGURE 4.10B: BEREA SANDSTONE TIME VS. DISTANCE PLOT AT LOAD 2, 17.24 MPA LOAD

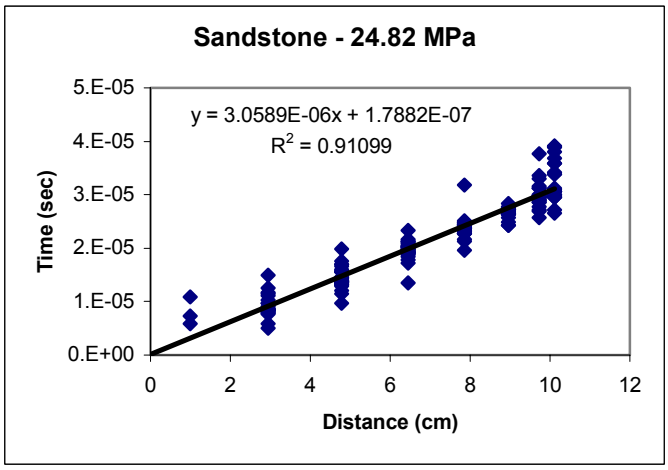

FIGURE 4.10C: BEREA SANDSTONE TIME VS. DISTANCE PLOT AT LOAD 3, 24.82 MPA LOAD

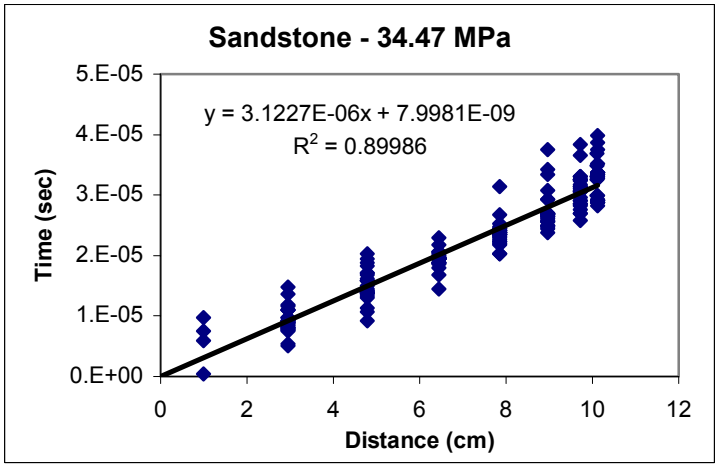

FIGURE 4.10D: BEREA SANDSTONE TIME VS. DISTANCE PLOT AT LOAD 4, 34.47 MPA LOAD

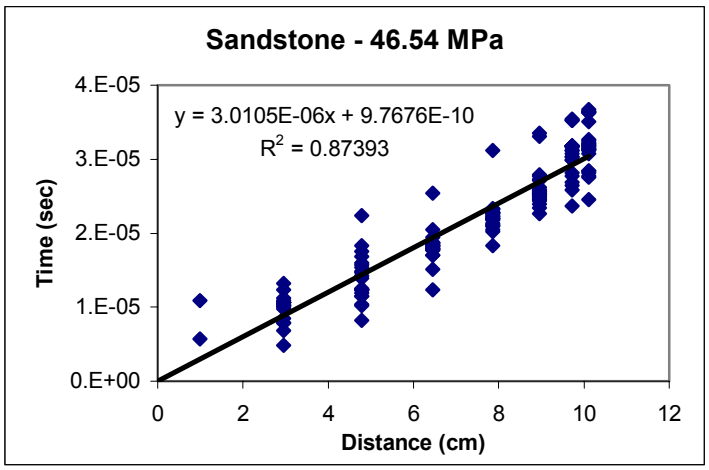

FIGURE 4.10E: BEREA SANDSTONE TIME VS. DISTANCE PLOT AT LOAD 5, 46.54 MPA LOAD

The sample failed at a load of 65.16 MPa (9450 psi). The slope of the plots in Figure 4.10 is important to note. The slope tends to increases with increasing stress. The scatter in the plot also increases with increasing stress. The increasing slope indicates that the average velocity across the sample is decreasing as the stress increases. Table 4.3 shows a summary of average velocity at different stress levels.

TABLE 4.3: SANDSTONE VELOCITY SUMMARY

Stress Level		Average Velocity	
(psi)	(MPa)	(ft/sec)	(m/s)
0	0.00	13,439	4,096
2500	17.24	11,874	3,619
3600	24.82	10,971	3,344
5000	34.47	11,309	3,447
6750	46.54	12,732	3,881

The average velocity represents the average velocity along each raypath on which an arrival time was picked. The tomograms in Figure 4.11 show the velocity levels across the sample for different stress levels. The scale of the velocity for the tomograms is the same for all tomograms and the units are in ft/sec. The background velocity for the different stress levels seems to stay the same. A transition in stress state can be seen at a load of 34 MPa. At this level the stress distribution is more scattered than in the previous

two tomograms (17 and 25 MPa). The previous tomograms show an anomalous presence which corresponds to the indentation load applied to the sample. The tomogram at 34 MPa shows a wider scatter of stress and an increase in velocity in the indentation area which could correspond to the pore spaces being completely closed and the rock beginning to be elastically loaded. The final tomogram shows an additional increase in velocity directly under the indentation area. The sample failed after the last tomogram and no other data were collected.

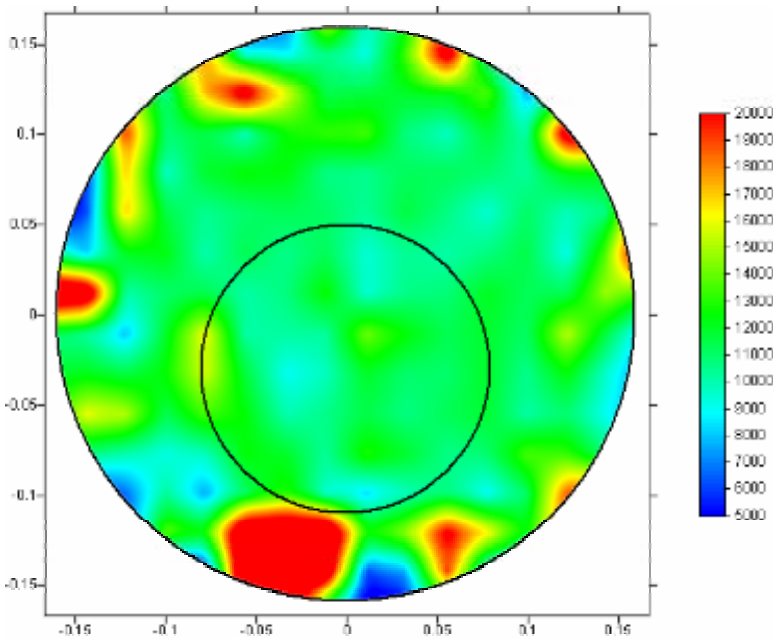

FIGURE 4.11A: BEREA SANDSTONE TOMOGRAM AT INITIAL STATE, 0 MPA

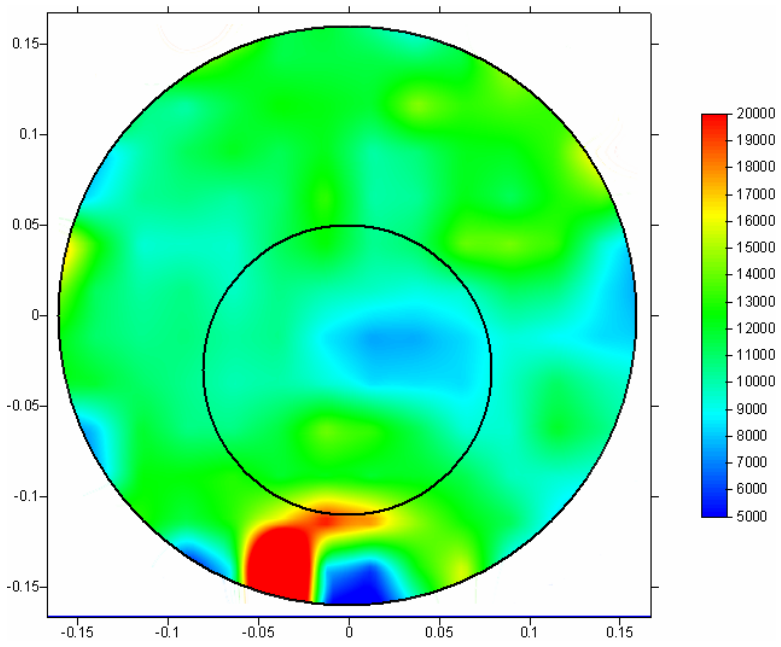

FIGURE 4.11B: BEREA SANDSTONE TOMOGRAM AT LOAD 1, 17.24 MPA

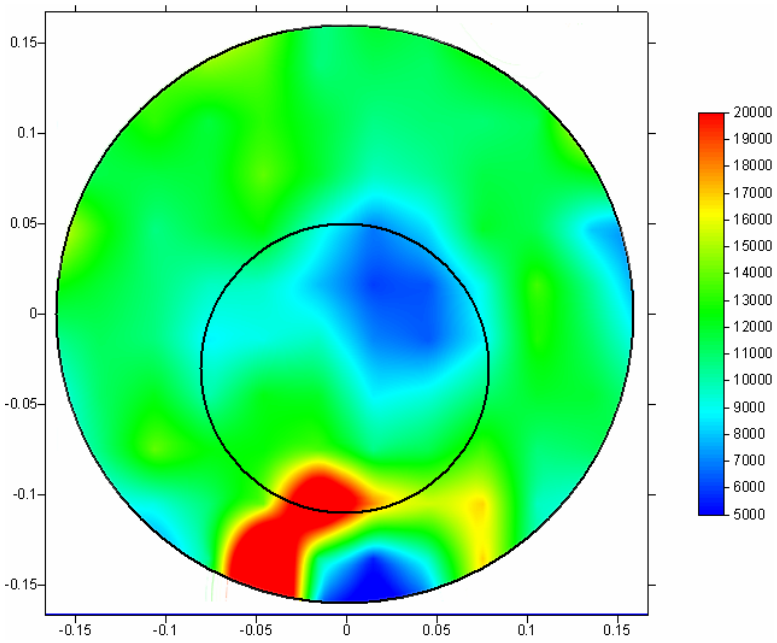

FIGURE 4.11C: BEREA SANDSTONE TOMOGRAM AT LOAD 2, 24.82 MPA

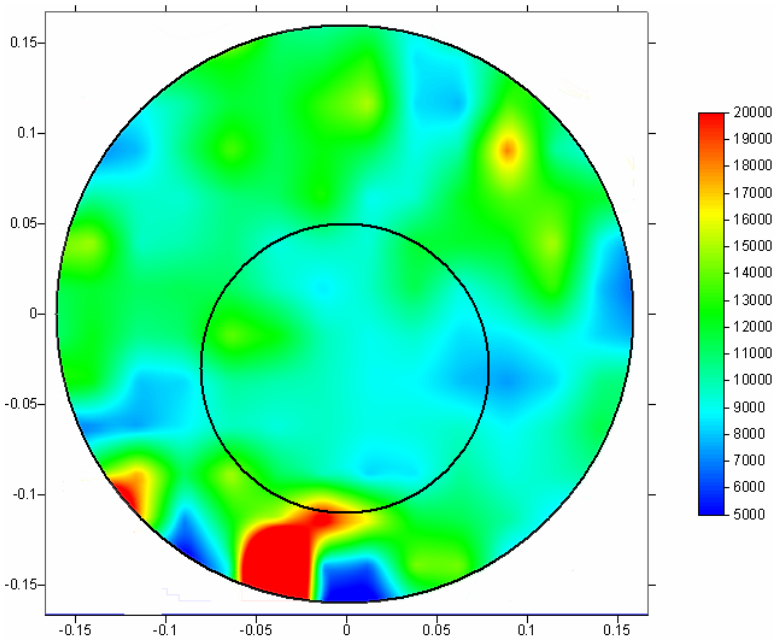

FIGURE 4.11D: BEREA SANDSTONE TOMOGRAM AT LOAD 3, 34 MPA

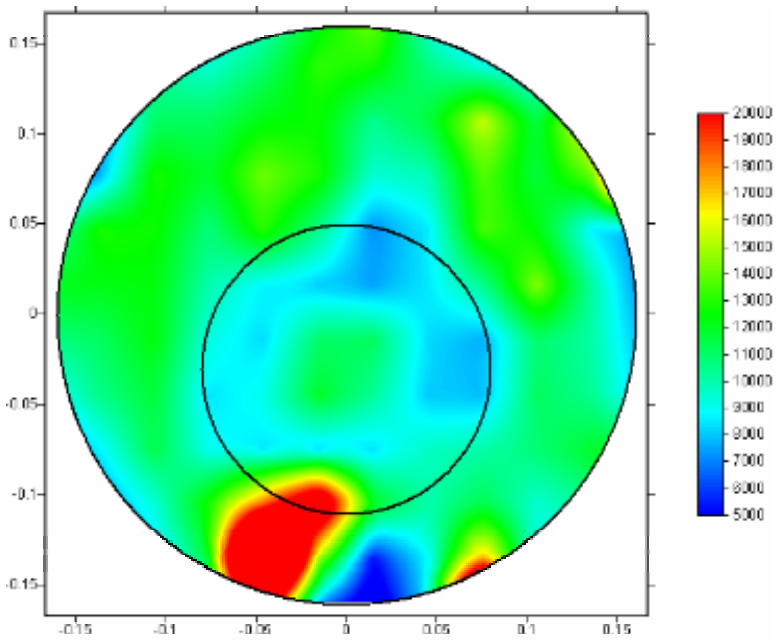

FIGURE 4.11E: BEREA SANDSTONE TOMOGRAM AT LOAD 4, 46 MPA

4.2.2 Five Oaks Limestone Experiment

Limestone samples were obtained from the Kimballton Mine in Ripplemeade, VA, which is located in the Five Oaks Limestone seam. This rock was chosen for testing because it is a high quality limestone with few imperfections. It was also readily available at the time of this study. The index properties for this rock were not known prior to testing. The index tests preformed on the limestone were done to classify the rock prior to ultrasonic tomographic imaging. Limestone blocks were collected from pillars near the working section. Blocks with rough dimensions of 3' x 2' x 1' were pried from the rib. An arrow was painted on each block to indicate the direction of the roof so that samples cut from these blocks could be oriented with respect to the rib they were pulled from. The blocks were pulled from pillars in the 12 East mains at a depth of 2200ft. The mineralogy of the limestone deposit is 99.7% pure calcium carbonate ($CaCO_3$) with some impurities (Mg, SiO_2).

When the blocks were collected in the mine the vertical direction of the blocks was marked in paint. This orientation was important to note so that each block could have core samples cut in the same vertical orientation as the pillars. This ensured that the

samples in the laboratory were tested in the same orientation as in the mine. A summary of the index properties are shown in Table 4.4.

TABLE 4.4: FIVE OAKS LIMESTONE INDEX PROPERTIES

	Metric Units		English Units	
Property	Avg.	St. Dev.	Avg.	St. Dev.
P Velocity m/s (ft/sec)	6.65E+03	2.88E+02	2.18E+04	9.43E+02
S Velocity m/s (ft/sec)	2.75E+03	1.31E+02	9.01E+03	4.30E+02
Effective Porosity (%)	0	0	0	0
Density g/cm3 (lb/in3)	2.70E+00	9.21E-03	1.68E+02	9.21E-03
Tensile Strength MPa (psi)	9.79E+00	*	1.42E+03	*
Compressive Strength MPa (psi)	1.64E+02	4.35E+01	2.38E+04	6.31E+03
Elastic Modulus MPa (psi)	3.51E+04	4.43E+03	5.09E+06	6.42E+05

* Not enough samples to calculate the standard deviation

From Table 4.4 the P-Wave velocity was found to be 6,650 m/s. From testing the frequency of a test waveform, the average value of transmission frequency through the limestone was found to be 250 kHz. These properties result in an ultrasonic wavelength of 2.66 cm. This wavelength is longer than the radius of the uniaxial compression samples that were prepared for index testing. The smallest structure that was expected to be resolved was 2.66 cm in length. Knowing this restriction for tomographic reconstruction, a limestone block was prepared for tomographic testing. The dimensions of the block, the placement and size of the load, and the sensor locations are shown in Figure 4.12.

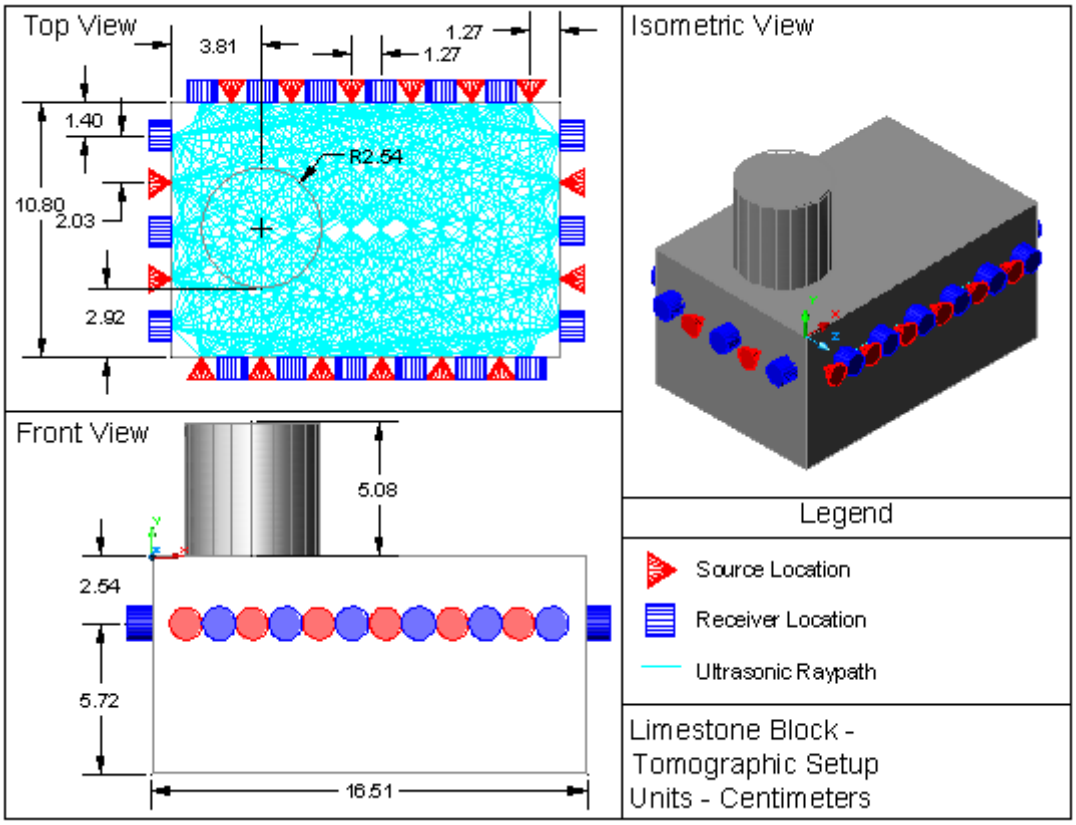

FIGURE 4.12: FIVE OAKS LIMESTONE TOMOGRAPHIC SETUP

The indentation load was used to apply a concentrated stress state on the limestone sample. This stress state would create a large stress contrast that should be able to be acquired by the UDAQ system. Ultrasonic data were acquired at the points shown in Table 4.5.

TABLE 4.5: LOAD CONDITIONS FOR TOMOGRAPHIC DATA COLLECTION

Load	MPa	PSI
1	0	0
2	17	2,500
3	34	5,000
4	52	7,500
5	69	10,000
6	86	12,500
7	103	15,000
8	0	0

At each load point 288 ultrasonic waveforms were collected, one waveform for each source and receiver pair. From these waveforms the arrival time was correlated and checked. To improve the picking accuracy of the program two correlations were done at each load and the arrival times that were not found in both files were removed as outliers. The arrival times were plotted against distance to observe the linearity of the picks. These plots are shown in Figures 4.13a – 4.13h.

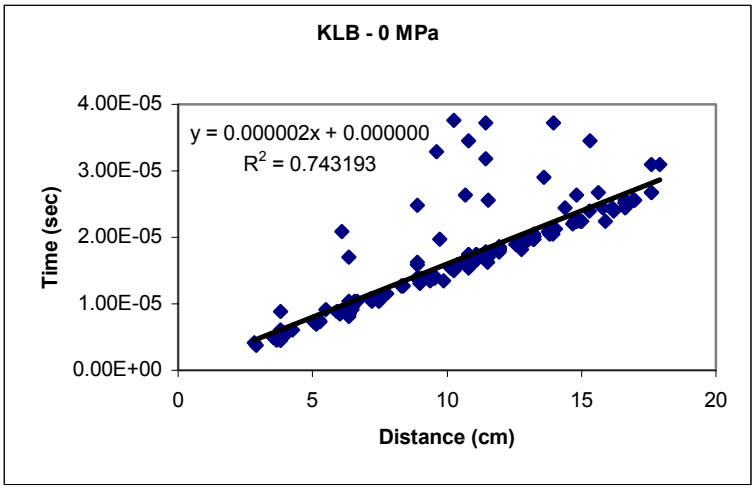

FIGURE 4.13A: FIVE OAKS LIMESTONE TIME VS. DISTANCE PLOT AT INITIAL STATE, 0 MPA

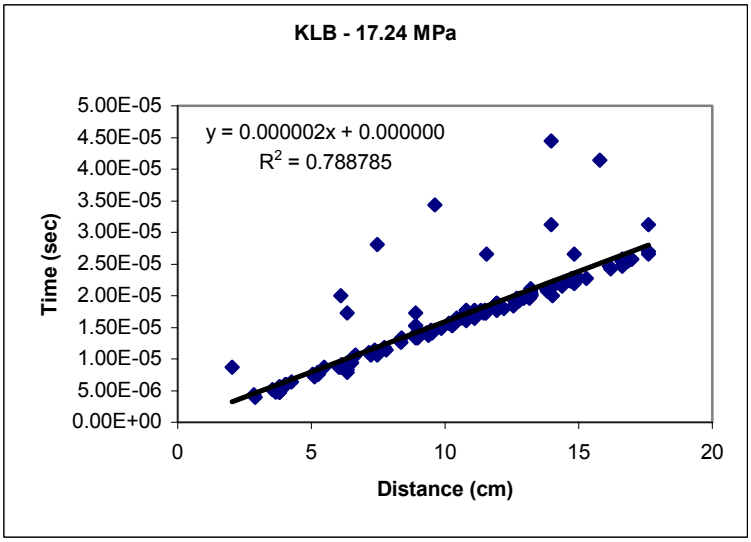

FIGURE 4.13B: FIVE OAKS LIMESTONE TIME VS. DISTANCE PLOT AT LOAD 1, 17.24 MPA

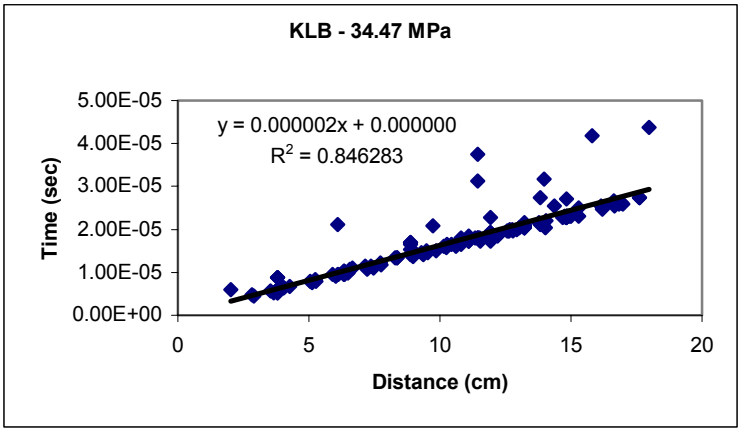

FIGURE 4.13C: FIVE OAKS LIMESTONE TIME VS. DISTANCE PLOT AT LOAD 2, 34.47 MPA

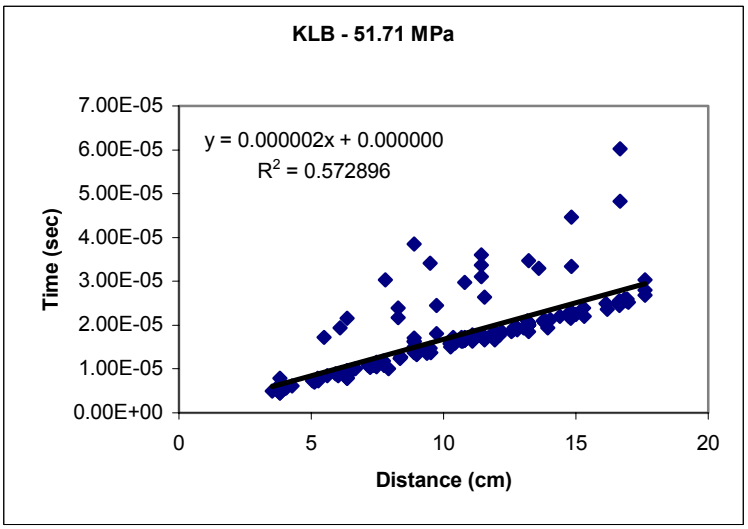

FIGURE 4.13D: FIVE OAKS LIMESTONE TIME VS. DISTANCE PLOT AT LOAD 3, 51.71 MPA

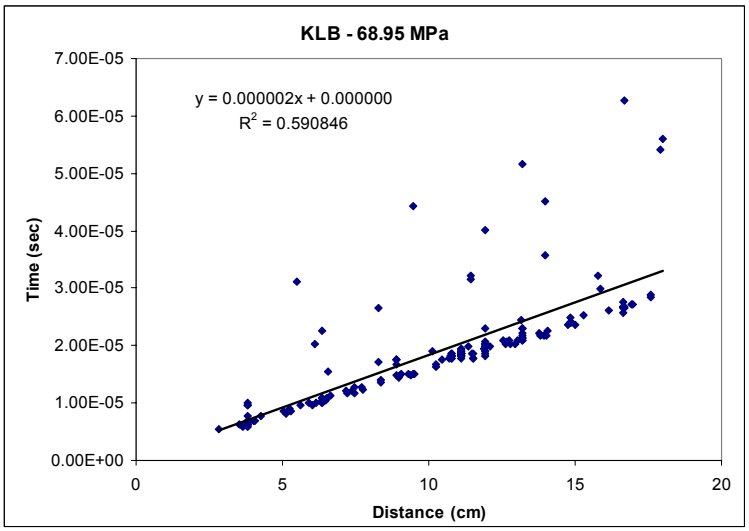

FIGURE 4.13E: FIVE OAKS LIMESTONE TIME VS. DISTANCE PLOT AT LOAD 4, 68.95 MPA

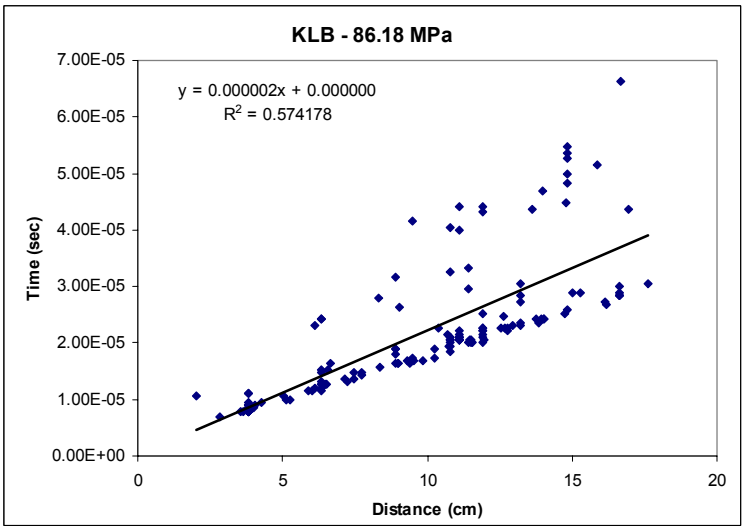

FIGURE 4.13F: FIVE OAKS LIMESTONE TIME VS. DISTANCE PLOT AT LOAD 5, 86.18 MPA

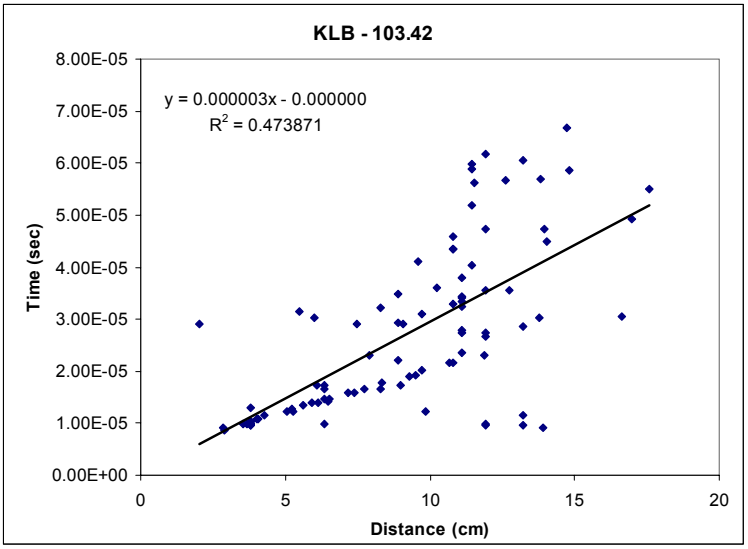

FIGURE 4.13G: FIVE OAKS LIMESTONE TIME VS. DISTANCE PLOT AT LOAD 6, 103.42 MPA

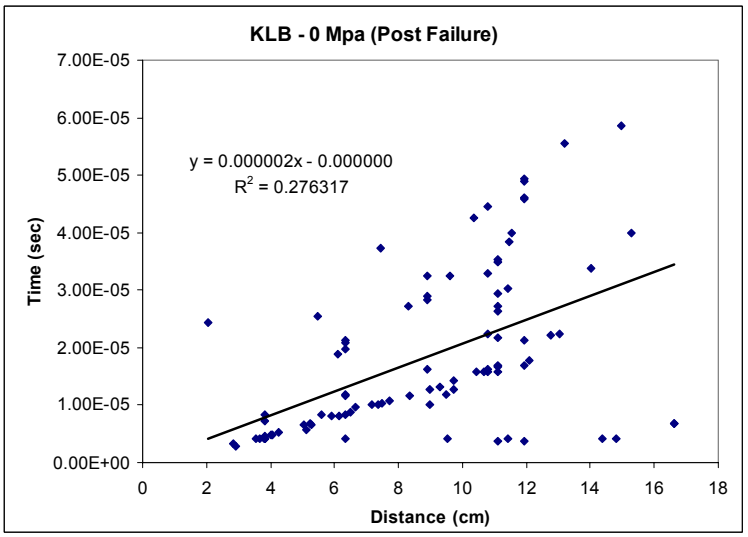

FIGURE 4.13H: FIVE OAKS LIMESTONE TIME VS. DISTANCE PLOT AT POST FAILURE, 0 MPA

The trend to note in Figure 4.13 is that the scatter in the plots increases as the load increases. This scatter is most likely due to fractures within the sample as it approaches failure. The fracturing of the block from the indentation load can be clearly seen in Figure 4.14.

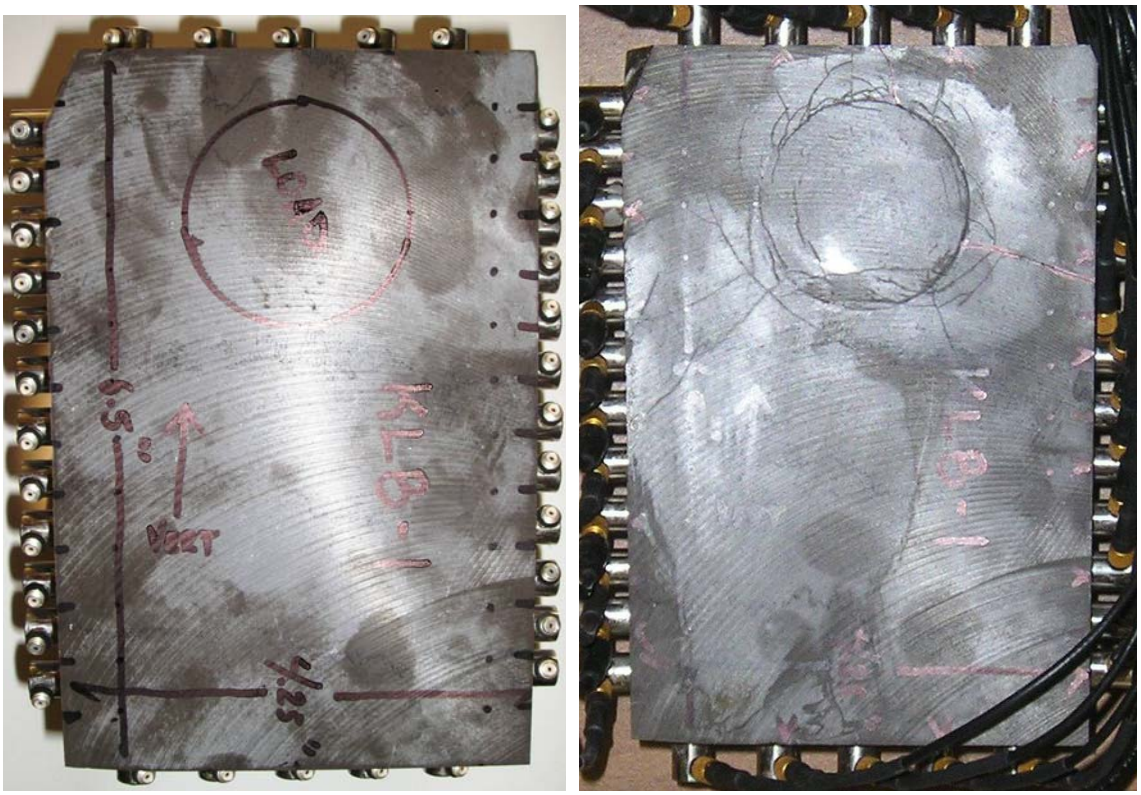

(a) (b)

FIGURE 4.14: FIVE OAKS LIMESTONE TEST BLOCK (A) PRIOR AND (B) POST FAILURE

The sensors were attached to the limestone using a cynoacrylate adhesive. The flat surfaces allowed for this application method of the sensors. Tomograms were calculated from the arrival time data using GeoTomCG to get a clear picture of what was happening inside of the limestone as stress increased. The tomograms for this sample are shown in Figures 4.15a – 4.15h.

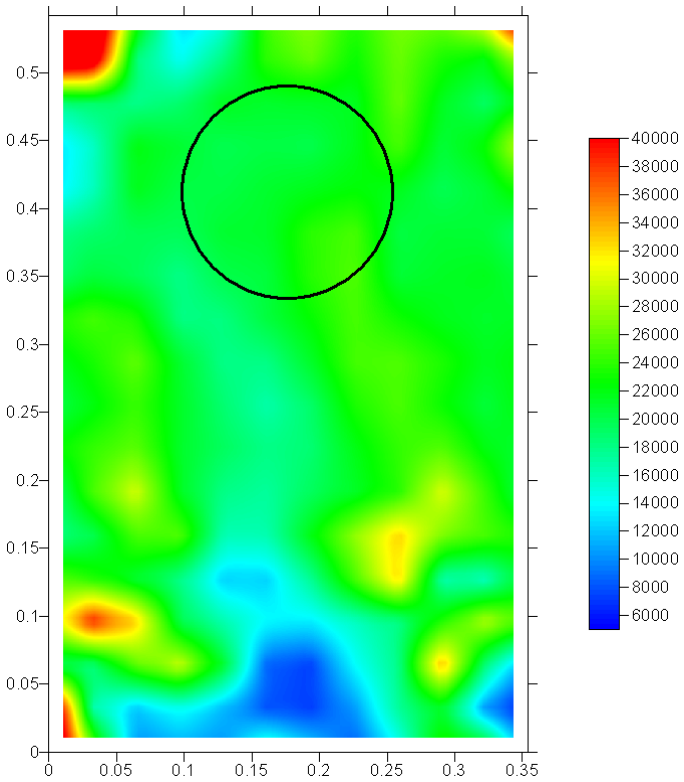

FIGURE 4.15A: FIVE OAKS LIMESTONE TOMOGRAM PRIOR TO LOADING, 0 MPA (UNITS – FT/SEC)

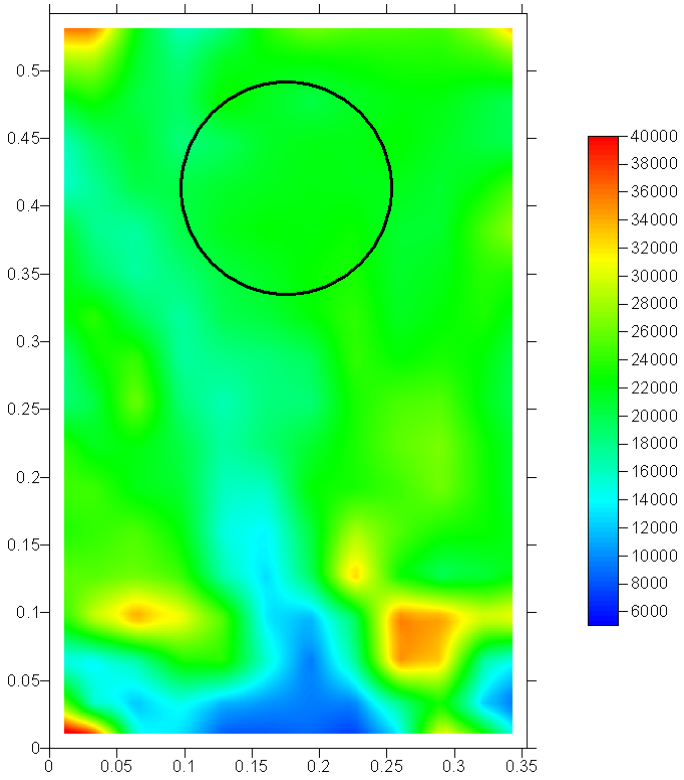

FIGURE 4.15B: FIVE OAKS LIMESTONE TOMOGRAM AT 17.24 MPA (UNITS – FT/SEC)

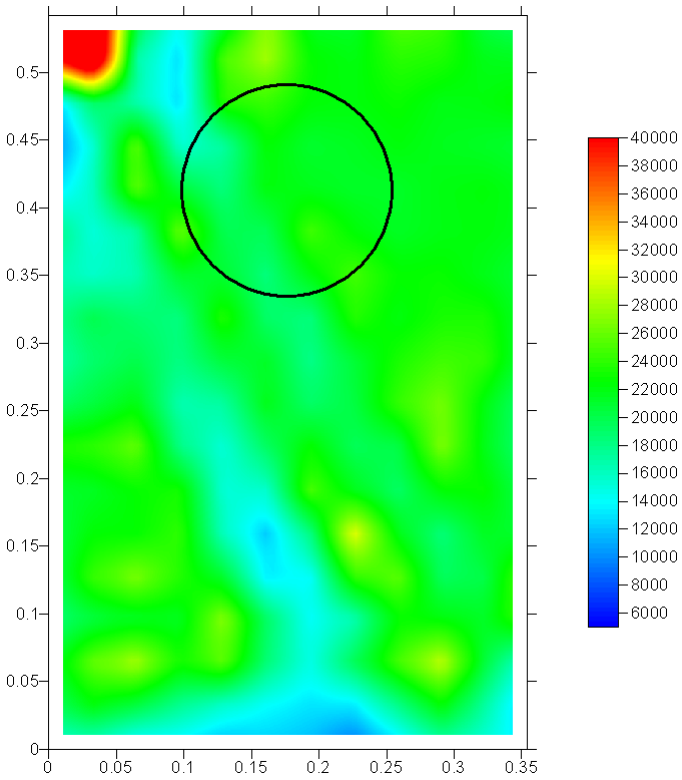

FIGURE 4.15C: FIVE OAKS LIMESTONE TOMOGRAM AT 34.47 MPA (UNITS – FT/SEC)

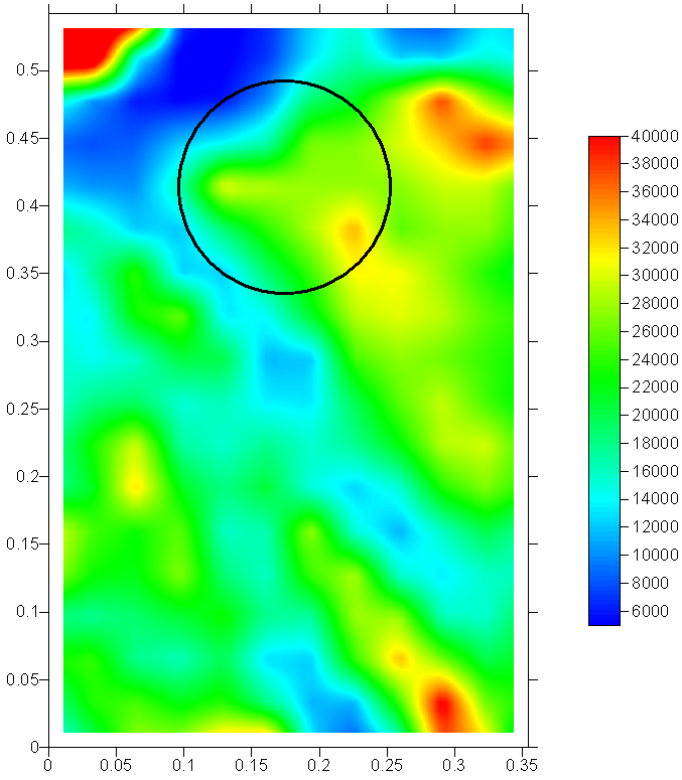

FIGURE 4.15D: FIVE OAKS LIMESTONE TOMOGRAM AT 51.71 MPA (UNITS – FT/SEC)

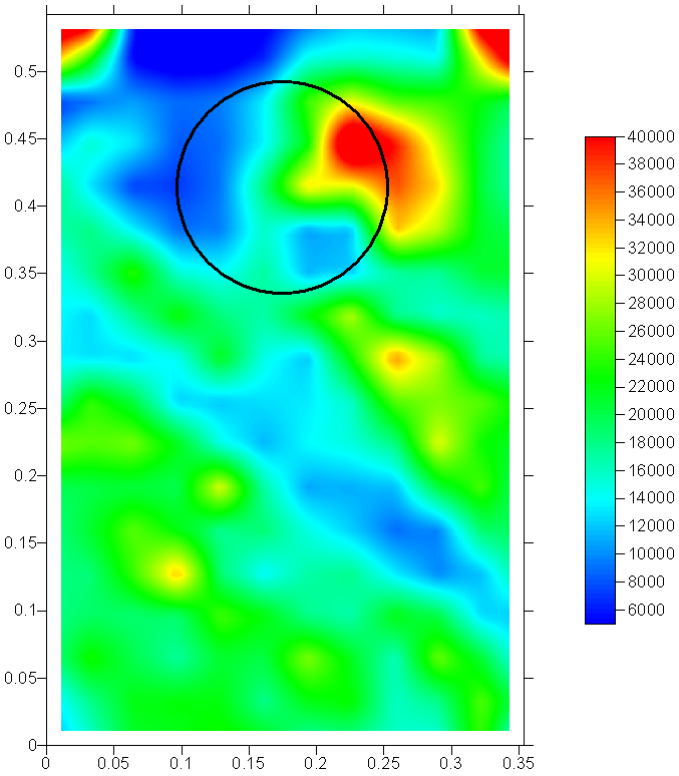

FIGURE 4.15E: FIVE OAKS LIMESTONE TOMOGRAM AT 68.95 MPA (UNITS – FT/SEC)

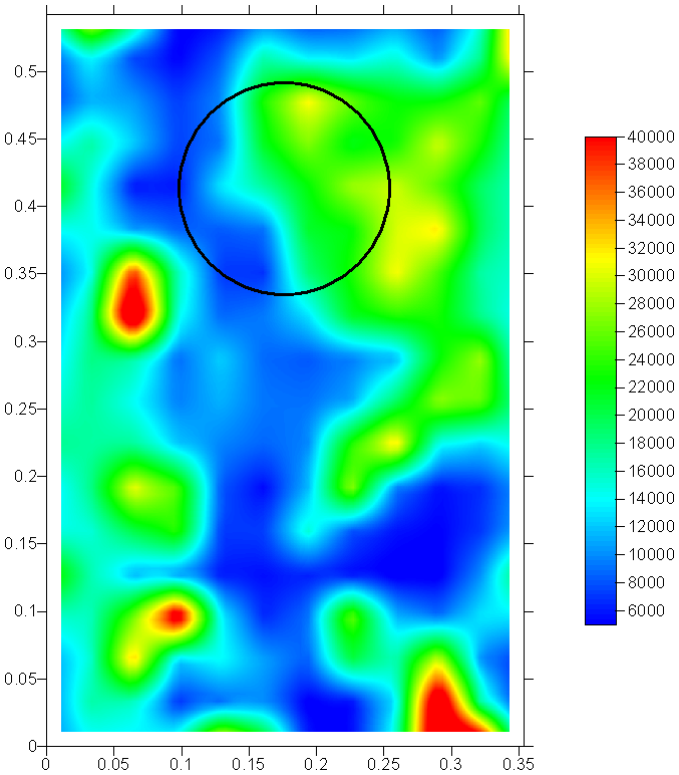

FIGURE 4.15F: FIVE OAKS LIMESTONE TOMOGRAM AT 86.18 MPA (UNITS – FT/SEC)

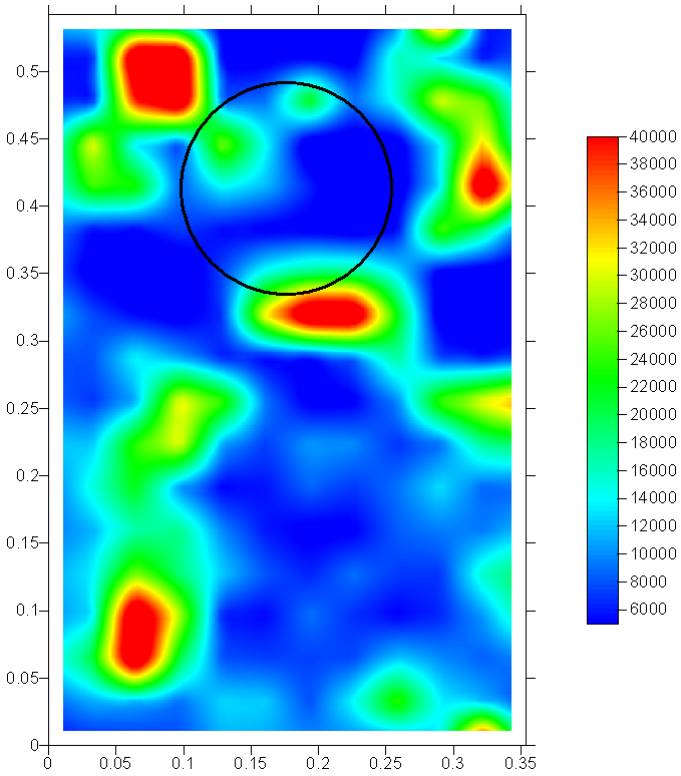

FIGURE 4.15G: FIVE OAKS LIMESTONE TOMOGRAM AT 103.42 MPA (UNITS – FT/SEC)

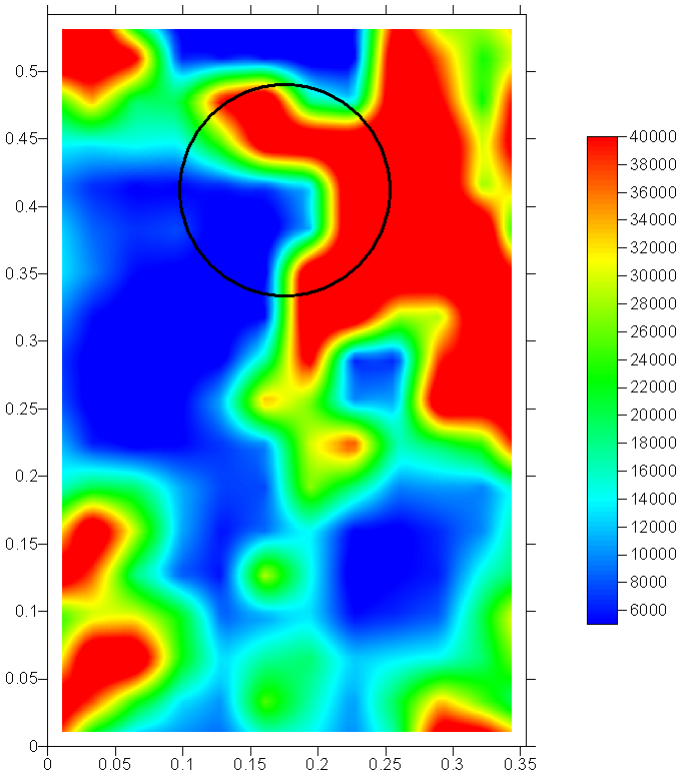

FIGURE 4.15H: FIVE OAKS LIMESTONE TOMOGRAM POST FAILURE, 0 MPA (UNITS – FT/SEC)

The presence of the stress can be seen in Figure 4.15. From the initial state (Figure 4.15a), a void or low velocity zone can be seen at the bottom of the tomogram. In addition to this structure there also seems to be a thin low velocity zone running from the upper left to the lower right The low velocity zones observed in the initial condition are known (from pre- and post-failure inspections of the sample) to be pre-existing fractures within the sample. The indentation load (warm color at the top of the figure) is clearly seen in Figures 4.15e – 4.15f. The location of the indentation does not appear to be in the position shown in Figure 4.12. The reason for the discrepancy is from eccentric loading of the indentation platen. The loading of one side of the platen more than the other results in the stress condition observed. The uneven loading was due to non-parallel load faces. The location of the stress appears to be in the correct location however, the large wavelength through the limestone reduces the precision in locating the stress zone.

The final tomograms (Figures 4.15g – h) show the presence of very low velocities and very high velocities. The reason for the high contrast in these final tomograms is due to the fracturing of the limestone. In Figure 4.15g, the low velocity zones follow the patterns observed in the initial tomogram. The contrast is increased because loading has dilated the existing fractures. In Figure 4.15h, the high velocities are due to reflections of the ultrasonic waves at the fracture interface. To enhance the resolution within the tomograms the wavelength should be reduced. To reduce the wavelength in the limestone a higher frequency wave should be introduced. Another option is to use the same frequency but use a sample with a lower ultrasonic velocity so that the wavelength is smaller.

CHAPTER 5: SUMMARY AND CONCLUSIONS

A tomographic data acquisition system has been presented in this study. The system was developed in a LabVIEW programming environment. The advantage of using this program is that all ultrasonic data acquisition can be done within LabVIEW as well as all signal processing. LabVIEW is an intuitive and easy to learn programming language that is geared towards engineering applications. The plug and play capabilities of LabVIEW allow for upgrades of the control computer, sensors, and acquisition cards without any new programs being written. This allows for the data acquisition system to be upgraded as technology advances with minimal reprogramming.

The precision in locating anomalies within tomograms was dependant on the number of sensors, the sensor locations, and the algorithm used to calculate the tomogram. Increasing the number of sensors used for tomographic acquisition increases the raypath coverage across the sample. The locations of the sensors are another factor in the precision of the acquisition system. Complete coverage around the body being imaged allows for an undistorted representation in the tomogram. The algorithm used is important because it determines how each pixel within a tomogram is calculated. Errors within the algorithm will result in erroneous tomograms.

The accuracy of the data acquisition system is comparable to other commercial acquisition systems. The main disadvantage of this system is the 8 bit resolution of the ADC cards. This could be improved by investing in higher resolution cards. The error of measurements was determined experimentally to be 0.5% when compared to an ultrasonic P-wave test unit in the Virginia Tech Rock Mechanics Laboratory and 3.8% when compared to ultrasonic test conducted in the literature.

The costs of the components in this system are summarized in Table 5.1.

TABLE 5.1: SYSTEM COST

Device	Vender	Units	Cost/Unit	Total
PXI5102 Digital Oscilloscopes	National Instruments	10	$1,500	$15,000
PXI 1006 Chassis	National Instruments	1	$4,500	$4,500
MXI 3 PXI Chassis Controller	National Instruments	1	$3,000	$3,000
5077PR Ultrasonic Square Wave Pulser	Panametrics	1	$2,000	$2,000
Ultrasonic Pulser Switchbox	Engineering Seismology Corp	1	$2,000	$2,000
Micro80 Acoustic Emission Sensors	Physical Acoustics Corp	36	$150	$5,400
			Total Cost	$31,900

This system is inexpensive when compared to other ultrasonic testing systems that are commercially available presently (ESG Laboratory System ~ $80,000). The cost specifications were obtained from vendor quotes at the time of ordering.

There are other ultrasonic tests that could be conducted using this system. Preliminary testing with this system shows that it is capable of acquiring acoustic emission data from a rock sample under load. The acoustic emission data could be used to construct tomograms using the acoustic emission event as the source for tomographic reconstruction. Other ultrasonic experiments include and are not limited to; void detection, pore pressure imaging, and three-dimensional imaging.

The development of this system now provides a means for stress studies within rock and other materials that have acoustoelastic properties. The experiment in sandstone shows the capability of this system for stress redistribution study. By obtaining tomographic slices at different stress states the stress within the sample can be correlated to the increase or decrease of velocity in the tomogram. Future studies will explore the phenomena of stress redistribution in different rock types using this data acquisition system along with discrete element models in two and three dimensions.

This new tool for ultrasonic imaging of rock provides a means to better understand the implications of tomographic imaging in geophysics. The greatest benefit to the mining industry is for identifying geologic hazards within mining operations. Accurate interpretations of tomographic data as well as the design of mine-wide monitoring systems will allow for geologic hazards to be correctly identified. Through further tests with this ultrasonic data acquisition system, different stress conditions relating to mine conditions and geologic hazards can be identified in the laboratory providing the mining industry a means to correctly interpret stress redistribution readings using current mine-wide monitoring systems.

REFERENCES

[1] Halliday, D., R. Resnick, and J. Walker. Fundamentals of Physics. 6th ed. New York: John Wiley & Sons, Inc., 2001.

[2] NDT Resource Center. 1996. Iowa State University. Sept. 2004 <http://www.ndt-ed.org>.

[3] Lempriere, B.M., Ultrasound and Elastic Waves: Frequently Asked Questions. New York: Academic Press, 2002.

[4] Bishop, R., Learning with LabVIEW 6i. Upper Saddle River, NJ: Prentice Hall, 2001.

[5] Nolet, G. (Ed.) Seismic Tomography: With Applications in Global Seismology and Exploration Geophysics. Boston, MA: D. Reidel Publishing Co., 1987.

[6] Terada, M., and T. Yanagidani. *Application of Ultrasonic Computer Tomography to Rock Mechanics*. Ultrasonic Spectroscopy and its applications to material science (1986): pp. 205-210.

[7] Trampert, J., and J.-J. Leveque. *Simultaneous Iterative Reconstruction Technique: Physical Interpretation Based on the Generalized Least Squares Solution*. Journal of Geophysical Research, Vol. 95, No. B8: pp. 12,553-12,559, 1990.

[8] Daily, W., and E. Owen, *Cross Borehole resistivity tomography*, Geophysics, Vol. 56, No. 8: 1228-1235, 1990.

[9] Dines, K.A., and R.J. Lytle, *Computerized Geophysical Tomography*, Proceedings of the IEEE, Vol. 67, No. 7: pp. 1065-1073, 1979.

[10] Beard, M.D., and M.J.S. Lowe, *Non-destructive testing of rock bolts using guided ultrasonic waves*, International Journal of Rock Mechanics and Mining Sciences, 40: pp. 527-536, 2003.

[11] Molyneux, J.B., and D.R. Schmitt, *First-break timing: Arrival onset by direct correlation*, Geophysics, Vol. 64, No. 5: pp. 1492-1501, 1999.

[12] Song, L., H. Liu, S. Chun, Z. Song, and S. Zhang, *Mapping an underground rock mass by anisotropic acoustical transmission tomography*, Ultrasonics, 52: pp. 1009-1012, 1998.

[13] Marti, D., R. Carbonell, A. Tryggvason, J. Escuder, and A. Pérez-Estaún, *Calibrating 3D tomograms of a granitic pluton*, Geophysical Research Letters, 29, No. 17: pp. 15-1 – 15-4, 2002.

[14] Blaha, P., *Selected Examples of Seismic Tomography Usage in Mining and Geotechnics*, Institute of Gephysics, Polish Academy of Science, M-24 (340): pp. 215-225, 2002.

[15] Friedel, M.J., M.J. Jackson, E.M. Williams, M.S. Olsen, and E. Westman, *Tomographic Imaging of Coal Pillar Conditions: Observations and Implications*, International Journal of Rock Mechanics and Mining Sciences and Geomechanical Abstracts, Vol. 33, No. 3: pp. 279-290, 1996.

[16] Cheng, J., L. Li, S. Yu, Y. Song, X. Wen, *Assessing changes in the mechanical condition of rock masses using P-wave computerized tomography*, International Journal of Rock Mechanics and Mining Sciences, 38: pp. 1065-1070, 2001.

[17] Malinský, K., *Ultrasonic investigations in a coal mine*, Ultrasonics, 34: pp. 421-423, 1996.

[18] Plocek, J. *Equipment for ultrasonic investigation in mines*, Ultrasonics, 34: pp. 425-430, 1996.

[19] Falls, S.D., and R.P. Young, *Acoustic emission and ultrasonic-velocity methods used to characterize the excavation disturbance associated with deep tunnels in hard rock*, Tectonophysics, 289: pp. 1-15, 1998.

[20] Seebold, I., B. Lehmann, A. Arribas, C. Ruiz, T.J. Shepherd, and K.L. Ashworth, *Development of tomographic systems for mining, mineral exploration, and environmental purposes*, Trasnacions of the Institution of Mining and Metallurgy, Section B: Applied Earth Science, 108: pp. B105-B118, 1999.

[21] Goulty, N.R., *Controlled-source tomography for mining and engineering applications*, Seismic Tomography: Theory and Practice. London: Chapman and Hall, 1993.

[22] Semandeni, Calder, P.N., *High frequency microseismic monitoring applied to the determination of stress levels in hard rock mines*, Rockbursts and Seismicity in Mines, Fairhurst (ed.), 1990.

[23] Dérobert, X., O. Abraham, *GPR and seismic imaging in a gypsum quarry*, Journal of Applied Geophysics, 45: pp. 157-169, 2000.

[24] Hanson, D.R., T.L. Vandergrift, M.J. DeMarco, and K. Hanna, *Advanced techniques in site characterization and mining hazard detection for the underground coal industry*, International Journal of Coal Geology, 50: pp. 275-301, 2002.

[25] Friedel, M.J., D.F. Scott, M.J. Jackson, T.J. Williams, and S.M. Killen, *3D tomographic imaging of mechanical conditions in a deep US gold mine*, Mechanics of Jointed and Faulted Rock, Rossmanith (ed.), pp. 689-695, 1995.

[26] Scott, D.F., T.J. Williams, D.K. Denton, and M.J. Friedel, *Seismic tomography as a tool for measuring stress in mines*, Mining Engineering, pp. 77-80, January 1999.

[27] Itakura, K., K. Sato, and A. Ogasawara, *Monitoring of AE Clustering Activity Prior to Main Faulting of Stressed Rock by Acoustic Tomography Technique*, Fifth Conference on Acoustic Emission/Microseismic Activity in Geologic Structures and Materials, Penn State University, June 11-13, 1991, Clausthal-Zellerfeld, Germany: Trans Tech Publications, pp.1-17, 1995.

[28] Scott, T.E., Q. Ma, J.C. Roegiers, and Z. Reches, *Dynamic stress mapping utilizing ultrasonic tomography*, Rock Mechanics, Nelson and Laubach (eds.), Balkema, Rotterdam, pp. 427-434, 1994.

[29] Couvreur, J.F., A. Vervoort, M.S. King, E. Lousberg, and J.F. Thimus, *Successive cracking steps of a limestone highlighted by ultrasonic wave propagation*, Geophysical Prospecting, 49: pp. 71-78, 2001.

[30] Falls, S.D., R.P. Young, S.R. Carlson, and T. Chow, *Ultrasonic tomography and acoustic emission in hydraulically fractured Lac du Bonnet grey granite*, Journal of Geophysical Research, Vol. 97, No. B5, pp. 6867-6884, 1992.

[31] Villaescusa, E., M. Seto, and G. Baird, *Stress measurements from oriented core*, International Journal of Rock Mechanics and Mining Sciences, 39, pp. 603-615, 2002.

[32] Analog Devices, Analog-Digital Conversion Handbook. N.p.: Prentice Hall, 1994.

[33] Goodman, Introduction to Rock Mechanics. 2nd ed. New York: Wiley, 1989.

[34] Lama, R.D., and V.S. Vutukuri, Handbook on Mechanical Properties of Rocks. Vol. II, Clausthal, Germany: Trans Tech Publications, 1978.

[35] Karfakis, M., Lecture Notes, Rock Mechanics, 2002.

[36] UT Material Properties Tables. 1996. NDT-ED.org. 3 Nov. 2004 <http://www.ndt-ed.org>.

[37] Bloomfield, Philip E., Wei-Jung Lo, and Peter A. Lewin. "Experimental Study of the Acoustical Properties of Polymers Utilized to Construct PVDF Ultrasonic Transducers and the Acousto-Electric Properties of PVDF and P(VDF/TrFE) Films." IEEE transactions on ultrasonics, ferroelectrics, and frequency control, 2000.

[38] Lee, Yung-Chun and Shi Hoa Kuo. "A New Point Contact Surface Acoustic Wave

Transducer for Measurement of Acoustoelastic Effect of Polymethylmethacrylate." IEEE transactions on ultrasonics, ferroelectrics, and frequency control, Vol. 51, No. 1, p. 114 – 120, 2004.

[39] Onda Corporation - References. 2002. Onda Corporation. 3 Nov. 2004 <http://www.ondacorp.com>.

[40] Stein, J. (ed.), The Random House College Dictionary, 1980, Random House, Inc.

APPENDIX: A

GEOTOMCG TOMOGRAPHIC OUTPUT

A.1 PLEXIGLAS TOMOGRAMS

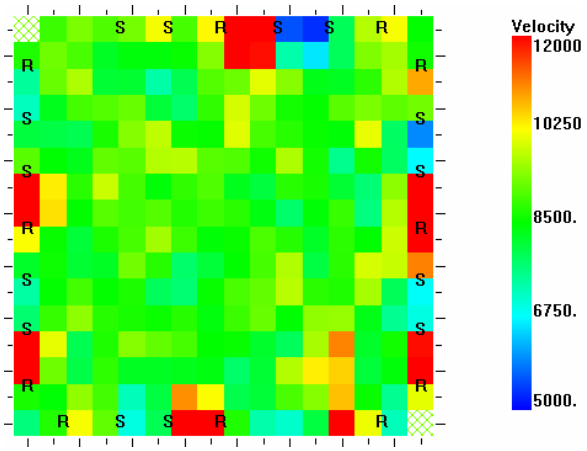

FIGURE A.1A: TOMOGRAM OF THE SOLID PLEXIGLAS CALIBRATION PLATE

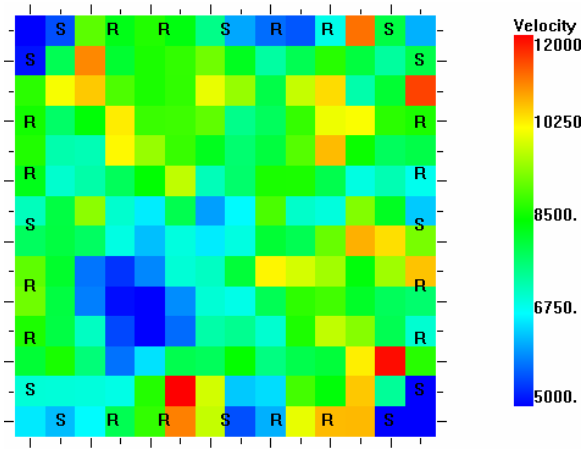

FIGURE A.1B: TOMOGRAM OF THE PLEXIGLAS CALIBRATION PLATE WITH A HOLE

A.2 BEREA SANDSTONE TOMOGRAMS

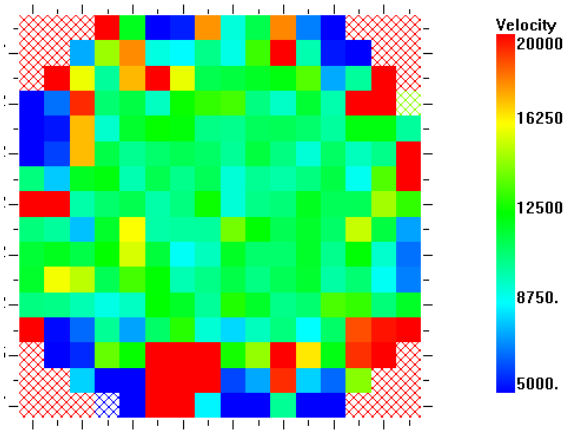

FIGURE A.2A: BEREA SANDSTONE TOMOGRAM AT INITIAL STATE, 0 MPA

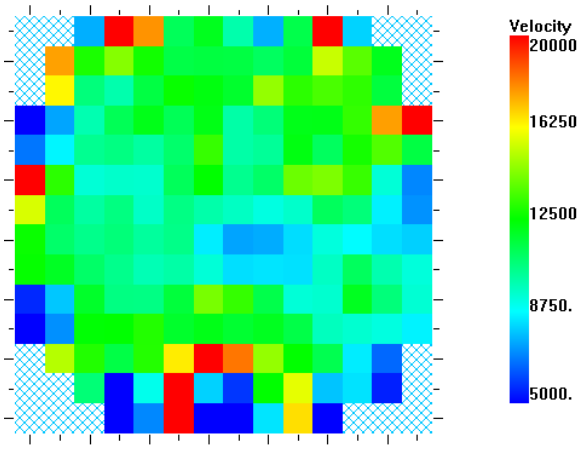

FIGURE A.2B: BEREA SANDSTONE TOMOGRAM AT LOAD 1, 17.24 MPA

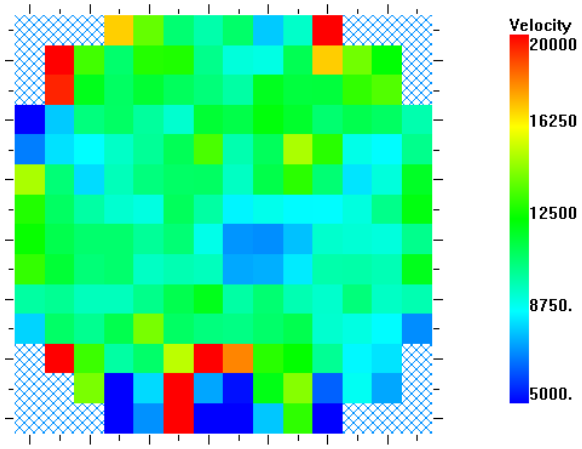

FIGURE A.2C: BEREA SANDSTONE TOMOGRAM AT LOAD 2, 24.82 MPA

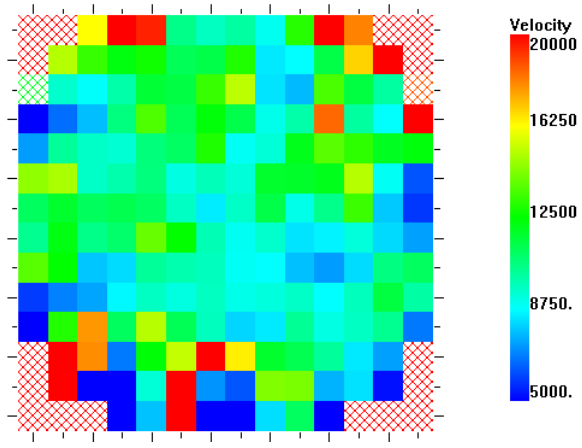

FIGURE A.2D: BEREA SANDSTONE TOMOGRAM AT LOAD 3, 34 MPA

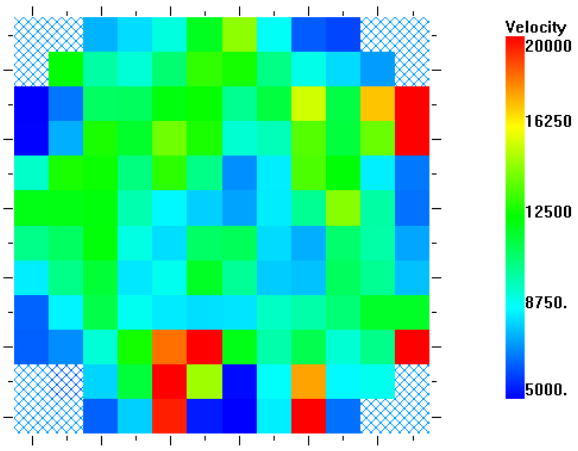

FIGURE A.2E: BEREA SANDSTONE TOMOGRAM AT LOAD 4, 46 MPA

A.3 FIVE OAKS LIMESTONE TOMOGRAMS

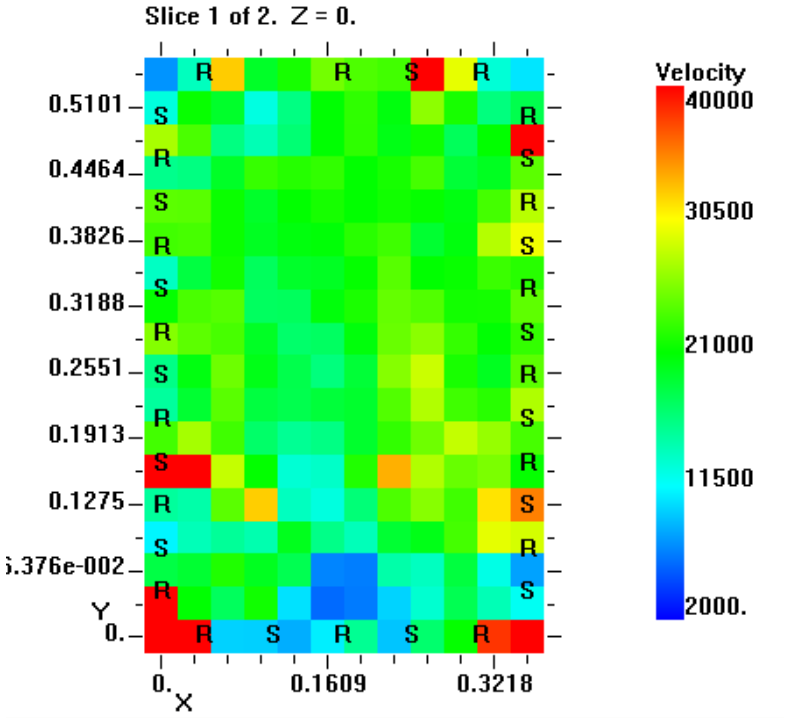

FIGURE A.3A: FIVE OAKS LIMESTONE TOMOGRAM PRIOR TO LOADING, 0 MPA (UNITS – FT/SEC)

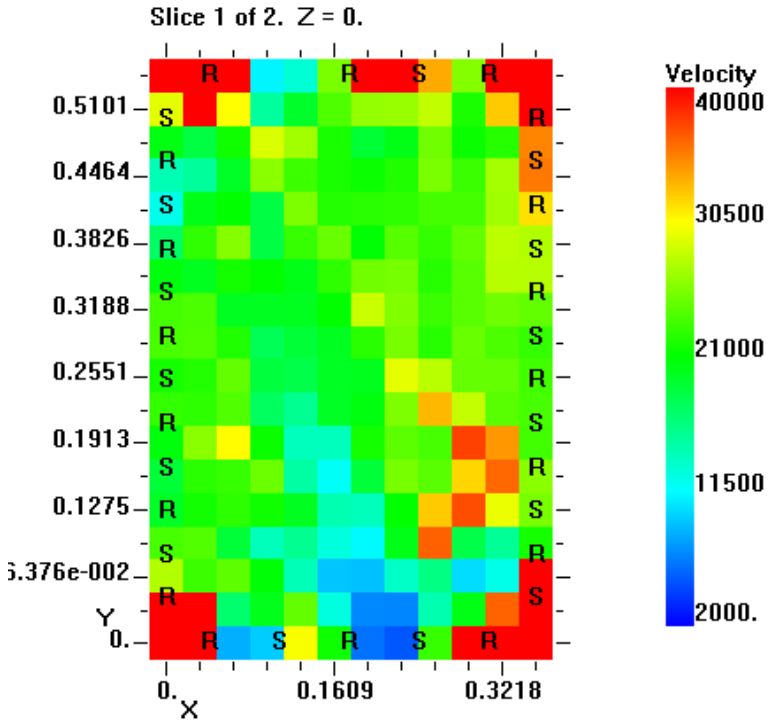

FIGURE A.3B: FIVE OAKS LIMESTONE TOMOGRAM AT 17.24 MPA (UNITS – FT/SEC)

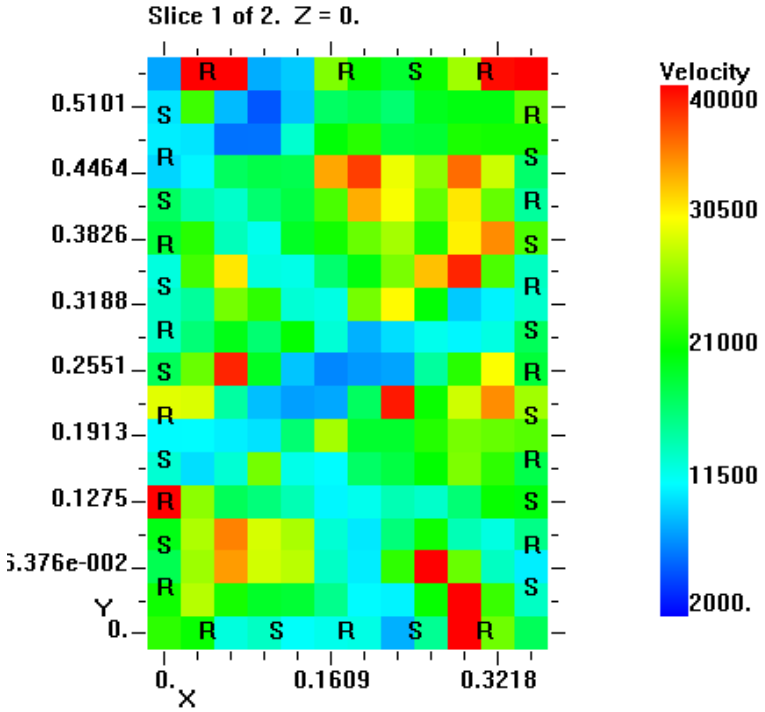

FIGURE A.3C: FIVE OAKS LIMESTONE TOMOGRAM AT 34.47 MPA (UNITS – FT/SEC)

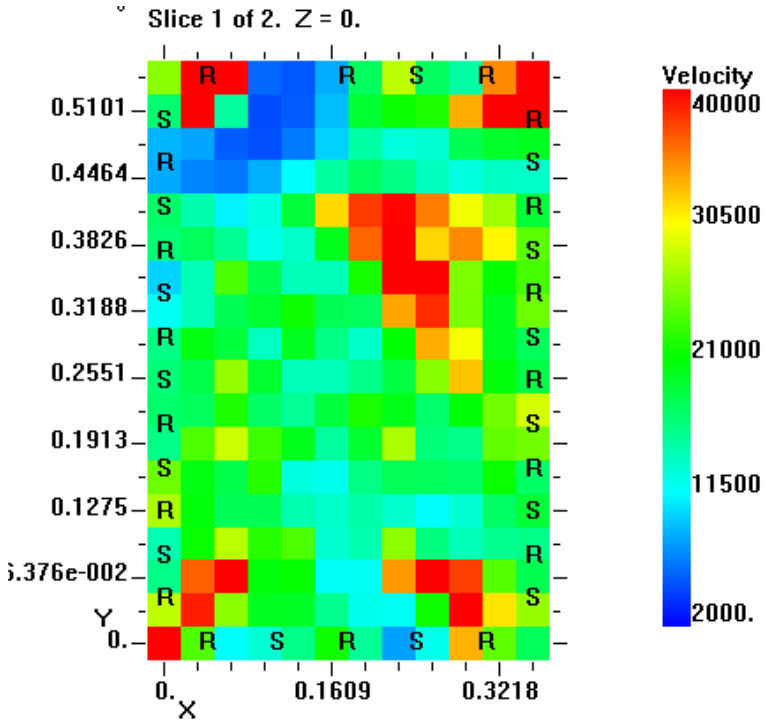

FIGURE A.3D: FIVE OAKS LIMESTONE TOMOGRAM AT 51.71 MPA (UNITS – FT/SEC)

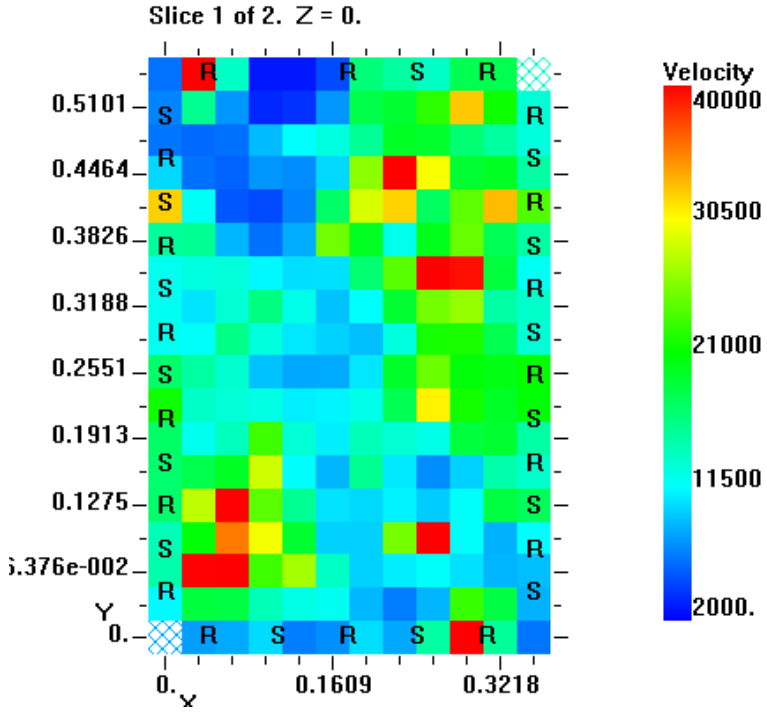

FIGURE A.3E: FIVE OAKS LIMESTONE TOMOGRAM AT 68.95 MPA (UNITS – FT/SEC)

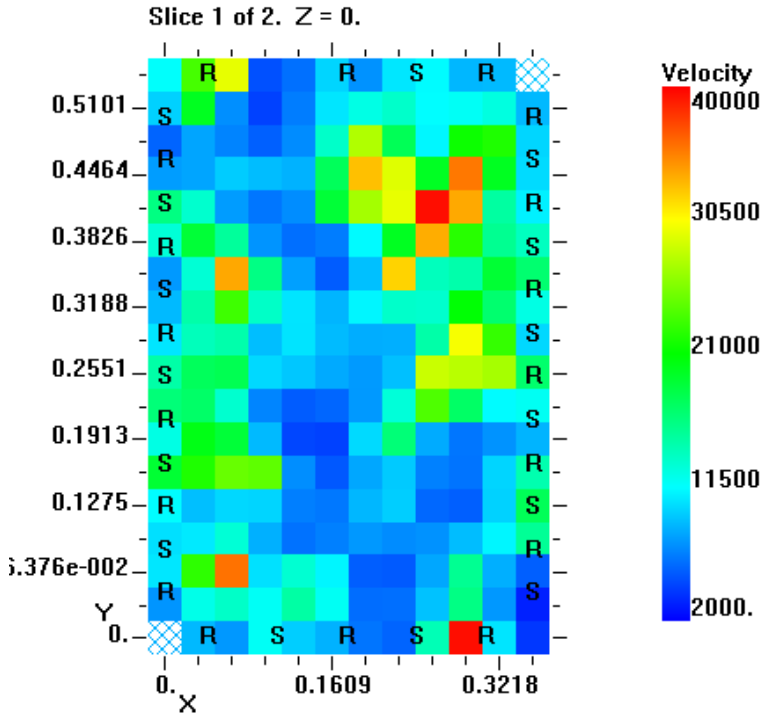

FIGURE A.3F: FIVE OAKS LIMESTONE TOMOGRAM AT 86.18 MPA (UNITS – FT/SEC)

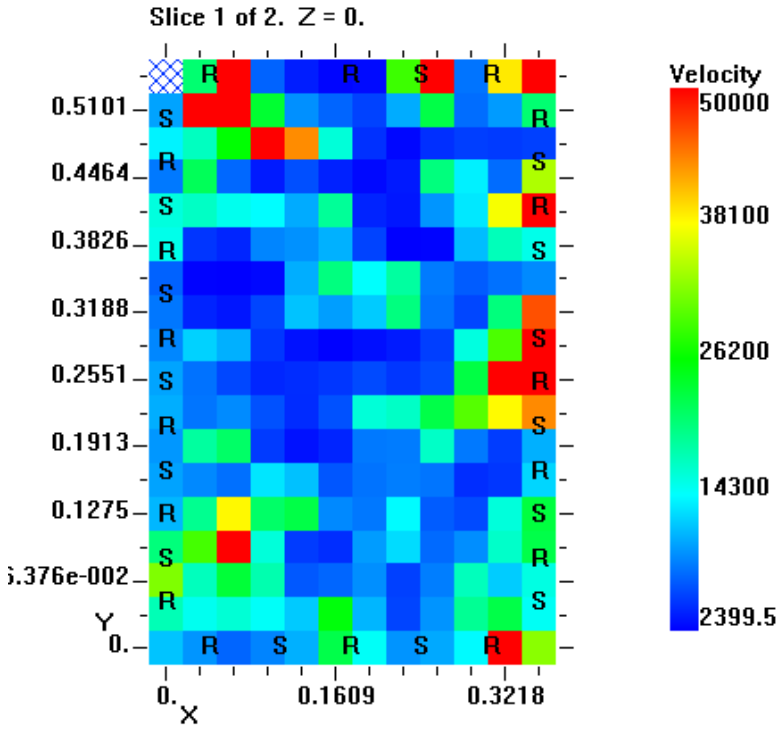

FIGURE A.3G: FIVE OAKS LIMESTONE TOMOGRAM AT 103.42 MPA (UNITS – FT/SEC)

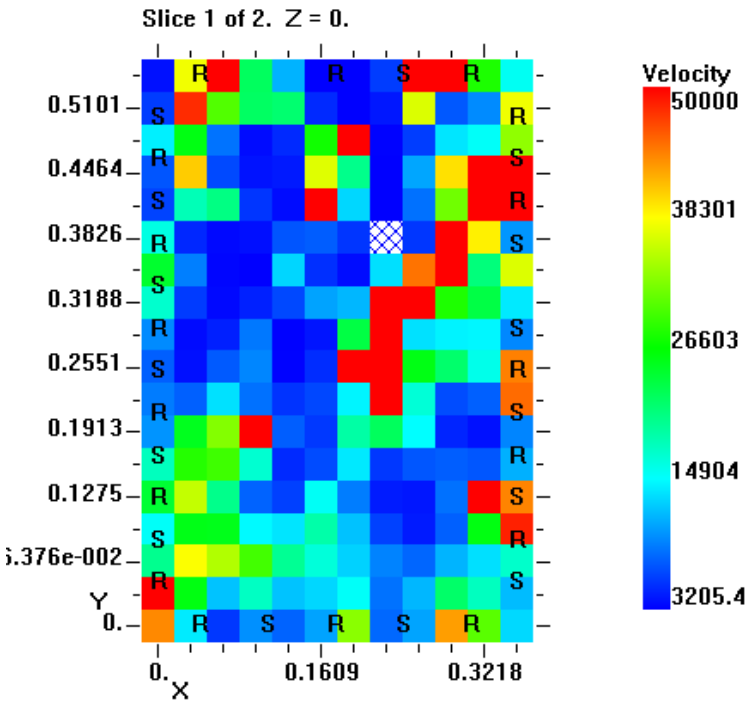

FIGURE A.3H: FIVE OAKS LIMESTONE TOMOGRAM POST FAILURE, 0 MPA (UNITS – FT/SEC)

APPENDIX: B

ULTRASONIC DATA ACQUISITION SYSTEM

LABVIEW PROGRAM MANUAL FOR TOMOGRAPHIC DATA COLLECTION

USER'S MANUAL FOR ULTRASONIC DATA ACQUISITION USING LABVIEW

Laboratory Virtual Instrumentation Engineering Workbench or LabVIEW is a graphical programming language developed for testing and research engineers. This intuitive programming language was developed by National Instruments to help engineers collect data from Data Acquisition (DAQ) equipment without having to learn programming syntax. Within LabVIEW Virtual Instruments (VIs) are developed to control instruments, read and process data, and present data.

Within in a VI there are two windows to be familiar with, the front panel and the block diagram. The front panel is the testing interface used when data is being collected, analyzed, or displayed. The block diagram is the graphical user interface where the front panel items (such as buttons, graphs, and user inputs) are 'wired' together to conduct an operation. The block diagram is programmed graphically where function nodes are wired together by connecting terminals. The wires pass data from one node to another, so that the path of computation can be followed by tracing a wire, similar to following current flow in an electrical schematic. Groups of functions can be combined within a VI to form a subVI. This subVI is an embedded program within the parent VI. The subVI can be called in different ways, it can be called to open and ask for user input, or it can run in the background. SubVIs are useful for repetitive actions within a VI, they also clean up the block diagram making it easier to read the block diagram.

This appendix is intended to be used as a guide to better understand the programming of the control applications developed for the ultrasonic data acquisition system. The programs discussed are used for ultrasonic acquisition for the purpose of creating tomograms.

B.1 MAIN APPLICATION CONTROL

The tomographic data acquisition system programs, written in LabVIEW, are used to acquire, process, and format data for tomographic inversion. The tomographic

inversion is done using a third party program, GeoTomCG. The different applications for this system were tied together under one main control. Each program can be run independently but are designed to be run together. The program architecture is shown in Figure B.1.

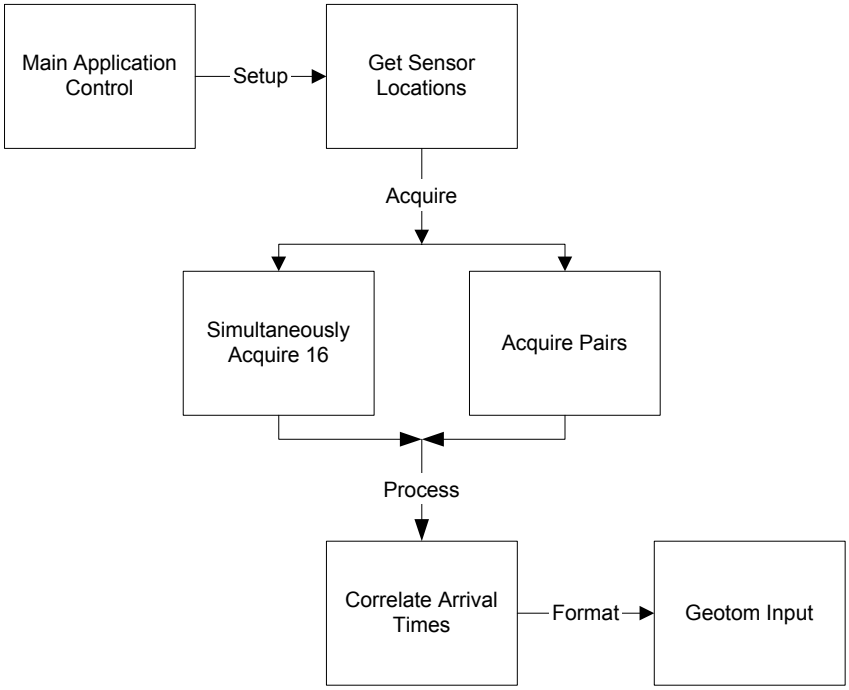

FIGURE B.1: UDAQ LABVIEW PROGRAM ARCHITECTURE

The options within the main control are to setup, acquire, and to process ultrasonic signals. The setup command uses the physical dimensions of a cylindrical sample to calculate the wavelength, and the sensor locations around the sample. The ultrasonic raypaths (the straight line estimation of where the ultrasonic signal travels) can be drawn between source and receiver locations showing the raypath coverage across the sample. This drawing will show the user areas of low raypath coverage and by using different combinations of sources and receivers the raypath coverage can be optimized. Once the sensor locations are determined the ultrasonic waveforms are collected simultaneously or by matching pairs of sources and receivers. The acquired waveforms are processed by a correlation program, which determines the time of arrival for each waveform. A tomogram is made by inputting the sensor location information with the arrival times into

GeoTom. A utility was created to format the data for direct input into GeoTom. A screen capture of the front panel of the main control program is shown in Figure B.2.

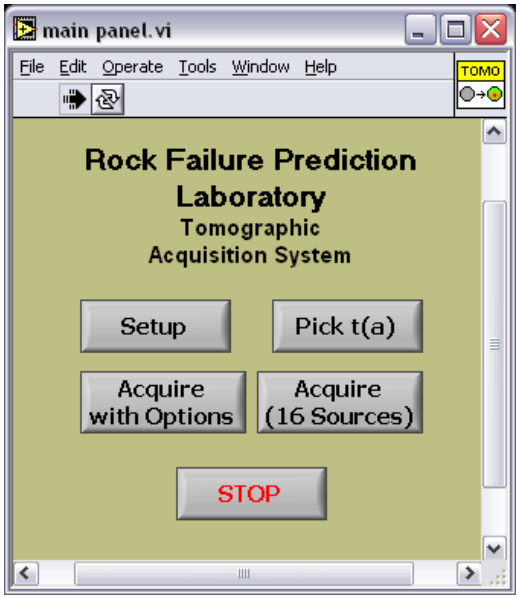

FIGURE B.2: MAIN APPLICATION CONTROL FRONT PANEL

B.2 SETUP PROGRAM

The setup application for the ultrasonic data acquisition system determines the coordinates of the transmitting and receiving sensors around the sample. A VI was developed to calculate these locations as well as to visualize the raypaths between ultrasonic sources and receivers as an estimate of the resolution within a tomogram. The user inputs sample and sensor geometry and the VI draws a cross section of the sample. If the number of sensors is not known, a utility is included to calculate the number of sensors to use based on the wavelength within the material. After entering the required input, the user selects the source locations and can output the sensor coordinates, view the raypaths, or reinitialize the drawing to start over. The front panel of this VI is shown in Figure B.3.

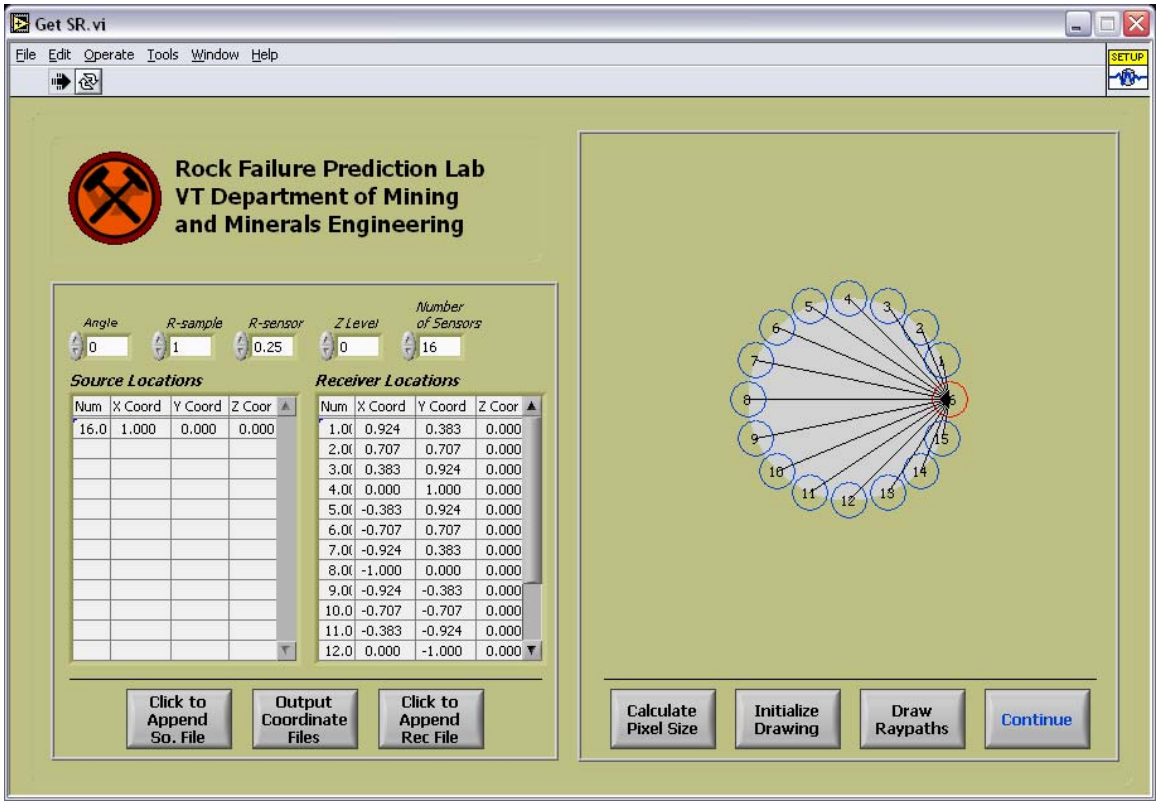

FIGURE B.3: GET SR FRONT PANEL

This VI is called by its parent VI, Main Panel.vi. To draw the sample and sensors the radius of the sample is input into *R-sample*, and the radius of the sensor is input into *R-sensor*. The control *Z Level* refers to the vertical location of the plane that is being modeled. The control *Angle* refers to a constant angle that should be added to offset the sensor array angularly. Lastly the number of sensors is input into *Number of Sensors*. Once these inputs are satisfied the model can be drawn by clicking the button Initialize Drawing. This will draw a picture of the sample surrounded by the number of sensors specified equally spaced around the sample. The table showing Receiver Locations will then fill up with all of the sensor coordinates. The Source Locations table will remain empty until a sensor is selected to be a source. To select a sensor to become a source click on the desired sensor and the color of that sensor will change from blue to red indicating the change. The coordinate for this sensor will then move from the Receiver Locations table to the Source Locations table. To output these coordinates click on

Output Coordinate Files. This action will save both tables to a text file specified by the user.

To add another plane to the coordinate files previously saved reinitialize the drawing with a new *Z Level* value. Once this is done select the sensors that are to be sources. Click on the *Click to Append So. File*, and *Click to Append Rec. File* buttons to append both the source and receiver files that were previously saved. If this is not done then the files will be rewritten with whatever data is in the tables for Source Locations and Receiver Locations. To stop this VI and return to the Main Panel click on the Continue button.

To determine the number of sensors to use in creating a tomogram a utility has been incorporated into this VI. The utility is called by clicking the *Calculate Pixel Size* button. This calls a program that calculates the pixel size of a 2D tomogram or the voxel size of a 3D tomogram based on the acoustic wavelength through the material. The largest pixel size or voxel size (depending on the number of dimensions selected) is equal to the wavelength. The front panel of this program is shown in Figure B.4.

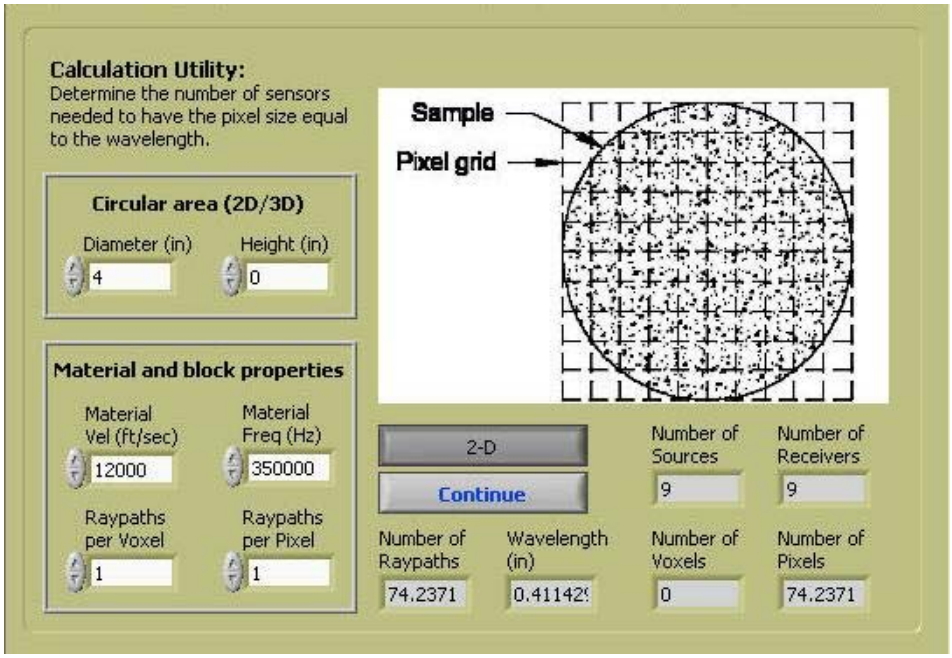

FIGURE B.4: SENSOR CALCULATION UTILITY FRONT PANEL

The output of the utility shows the number of pixels/voxels and the number of sources and receivers needed to have that number of pixels/voxels in the final tomogram. The number of sources and receivers are always equal but could be changed to adjust the raypath coverage as long as the total number of sensors remains the same.

The setup VI uses 'events' to control the flow of data through the program. Events are handled in LabVIEW through an event structure. This structure is programmed to execute when a specific event occurs while the program is running. For instance, if a Boolean button is pressed on the front panel it will change the state of that button from false to true. The change in the Boolean value can be programmed into an event structure so when that button is depressed an action such as the execution of a loop takes place in the block diagram. The VI is contained in a while loop that waits for events to happen, this loop terminates and the VI will close when 'Continue' is pressed on the front panel of the VI. The button activates the stop event in the block diagram and the value from the continue control button is passed to the stop function of the while loop.

The event call when the 'Initialize Drawing' button is pressed is shown in Figure B.5.

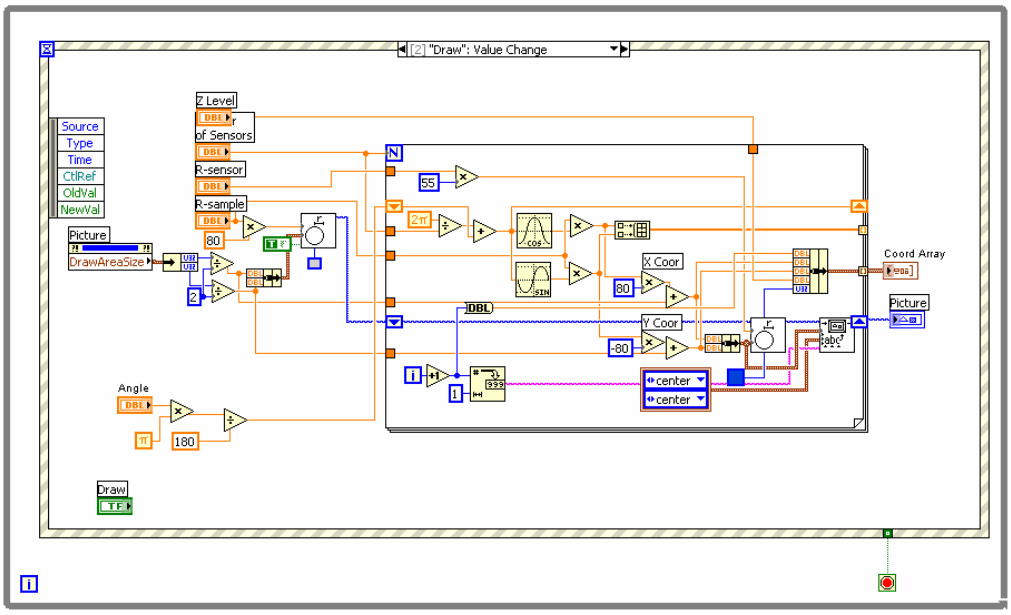

FIGURE B.5: GET SR:BLOCK DIAGRAM – DRAW EVENT

This event takes the user input values for Z Level, Number of Sensors, R-Sensor, R-Sample, and Angle and uses them to draw a picture of the sample. This VI will only create geometry and sensor locations for cylindrical samples. The geometry is calculated inside a for loop. Equation 1 shows how to calculate a point.

$$x = \cos\left(\frac{2\pi}{NumberofSensors} + Angle\right) * R - Sample \qquad \text{(eq.1)}$$

The calculated points are used as a center point to draw the sensors on the picture. A cluster array (*Coord Array*) of the x and y coordinates and the color (default is blue) is output for each sensor by the for loop to be used in other events.

When a sensor is selected in the picture an event structure (Figure B.6) determines the point where the mouse button was depressed and whether or not the user selected a sensor.

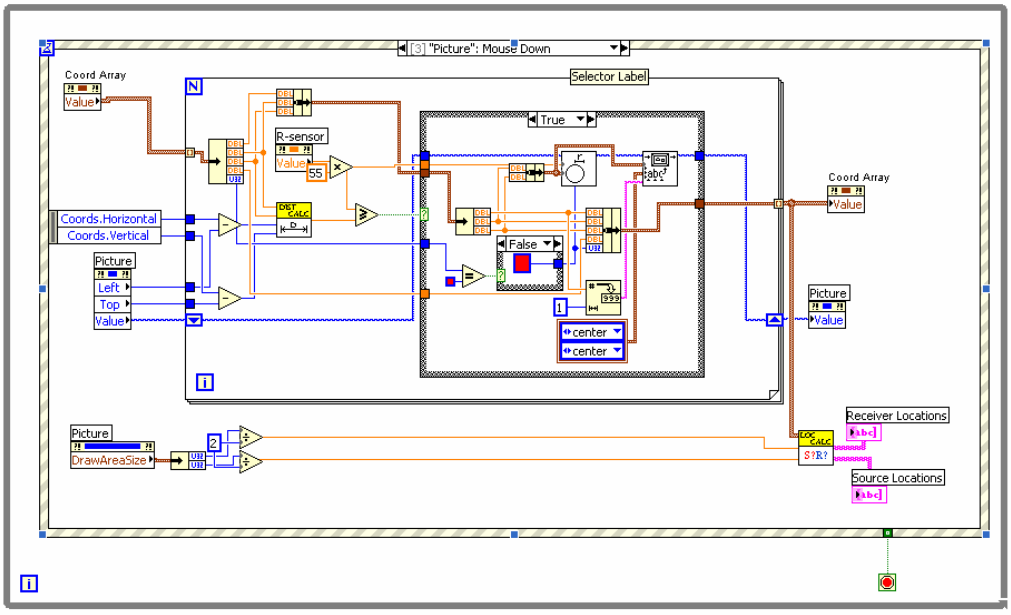

FIGURE B.6: GET SR:BLOCK DIAGRAM – PICTURE EVENT

The 'picture' event uses property nodes to collect information from the previous initialize event. Property nodes contain values that are specific to the front panel object that they refer to. A property node for an array would contain properties such as the values in the array, whether the control is visible or not visible, the position of the control on the front panel, etc. The coordinates from the coordinate array calculated in the initialize event are subtracted from the point at which the mouse button was depressed. If this value is less than the radius of the sensor then the data passes into the true case in a case structure, if it is greater than the radius then the data passes to the false case. If the case is true this indicates that a sensor was selected in the picture. The function inside of the true case changes the color of the sensor from the default of blue to red to indicate the change from receiver to source or vise versa. If the case is false then nothing is done. After comparisons have been made of distance of the mouse relative to the radius of each sensor the coordinate array is compiled and updated. This data is also sent to a subVI to fill in the receiver and source tables with the corresponding coordinates.

Another event is used to handle saving the coordinate data in the tables to a file. This event is called when the Output Coordinates button is pressed on the front panel. The event call is shown in Figure B.7.

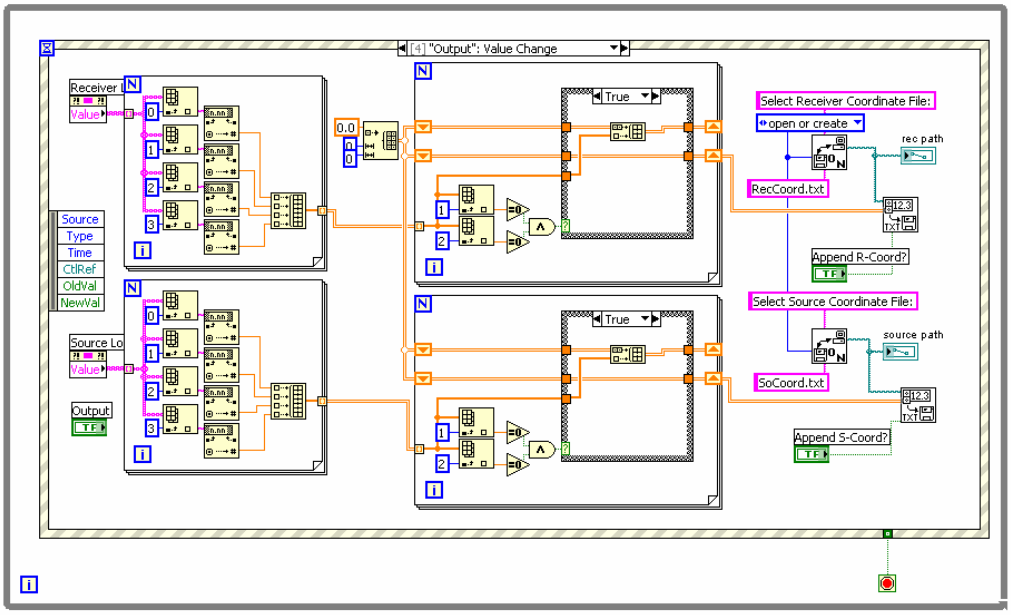

FIGURE B.7: GET SR:BLOCK DIAGRAM – OUTPUT EVENT

When the event is called it takes the coordinates stored in the tables and converts the data type to a double precision integer. The numerical arrays for the source and receiver coordinates are then passed into a loop that erases any null data. The data are then passed to a user specified file. This file can be appended with more data points if the append buttons are pressed on the front panel.

When the Draw Raypaths button is pressed an event occurs that draws lines from the user specified source locations to the receiver locations. This event is shown in Figure B.8.

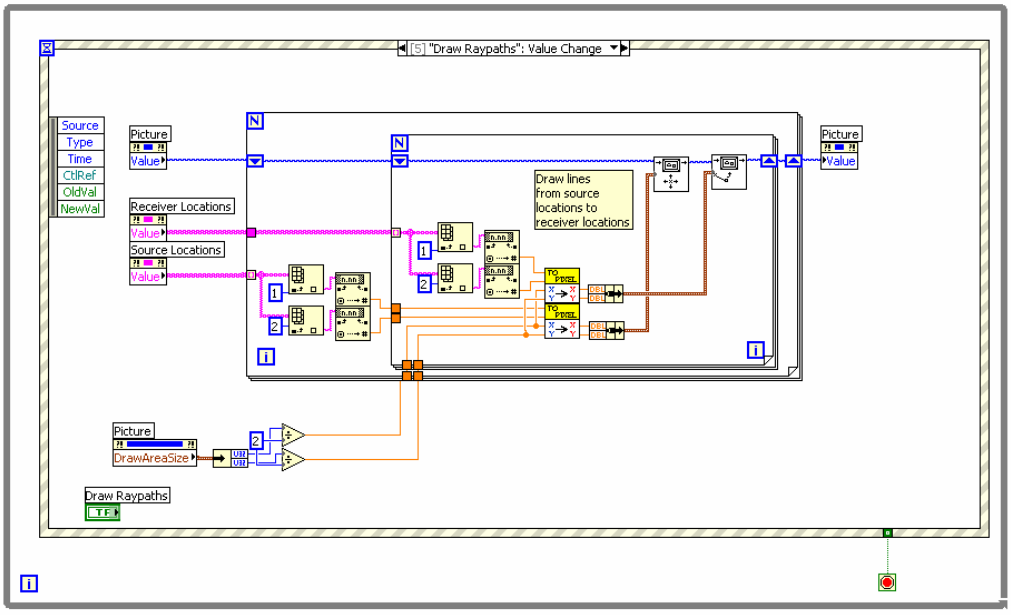

FIGURE B.8: GET SR:BLOCK DIAGRAM – DRAW RAYPATHS EVENT

This event uses the location data to update the picture with raypaths between source and receiver locations. The event calls the *to_pixel.vi* to convert the rectangular coordinates from inches to pixels so that they can be drawn in the picture.

B.3 SIMULTANEOUS ACQUISITION PROGRAM

Once the setup has been conducted, acquisition of the ultrasonic waveforms can be done. One option for this is to simultaneously acquire ultrasonic waveforms from 16 channels on the PXI chassis. This VI could be easily modified to handle more or less acquisition channels. This program was written to acquire ultrasonic waveforms from 8 PXI-5102 digital oscilloscopes. The oscilloscopes were setup in a master/slave configuration. A total of 9 oscilloscopes are used with this program. The first oscilloscope reads a trigger signal from the square wave pulse. The triggering pulse then triggers simultaneous acquisition on the other 8 oscilloscopes. The front panel of this VI is shown in Figure B.9.

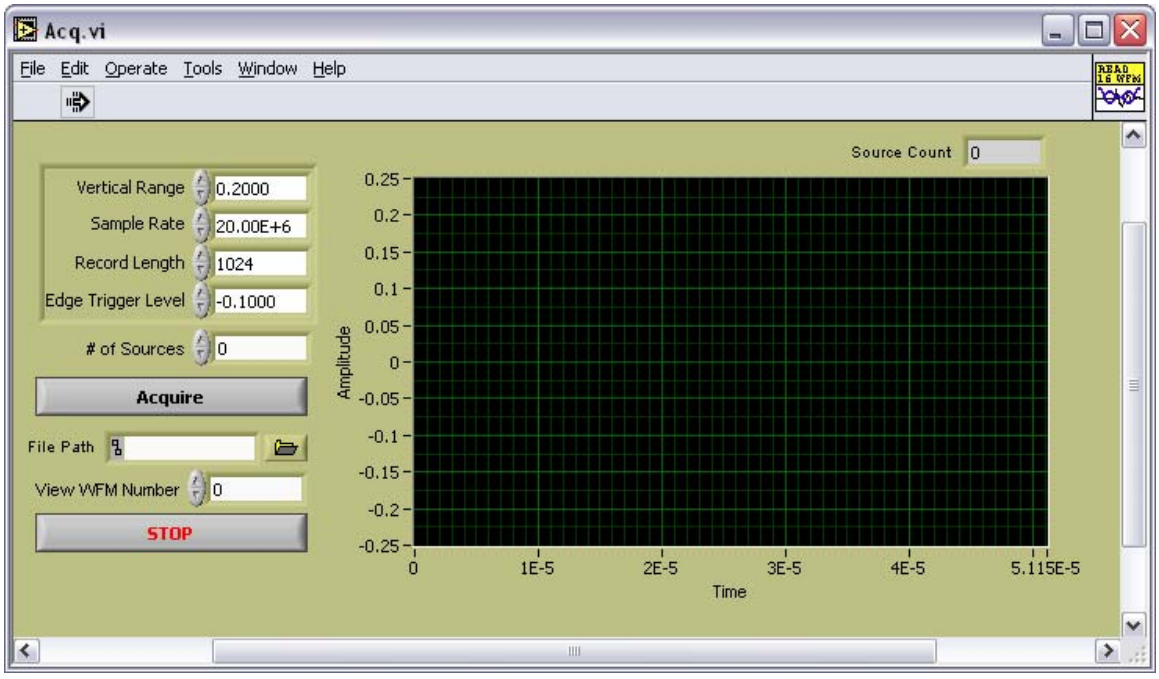

FIGURE B.9: SIMULTANEOUS ACQUISITION FRONT PANEL

The user inputs the scope properties in the upper left portion of the Front Panel. The inputs include the vertical range, sample rate, record length, and the trigger level. The user then inputs the number of source channels being acquired and a file path to save acquired ultrasonic waveforms. Once these inputs have been satisfied, the acquire button can be pressed to begin acquisition. When this button is depressed the counter in the upper left will count up to the number of sources specified. The acquired waveforms can be viewed by changing the value in the numerical control. The waveform numbering begins at zero and counts up to the number of sources x 16. To stop the program, press the stop button.

The block diagram programming for this VI is simple as well. The same event structure programming used in the previous programming is used again here. This programming allows for simple control of operations by the user and also makes the program easier to read. The main function in this program is the acquisition call. Figure B.10 shows the acquisition call to the block diagram.

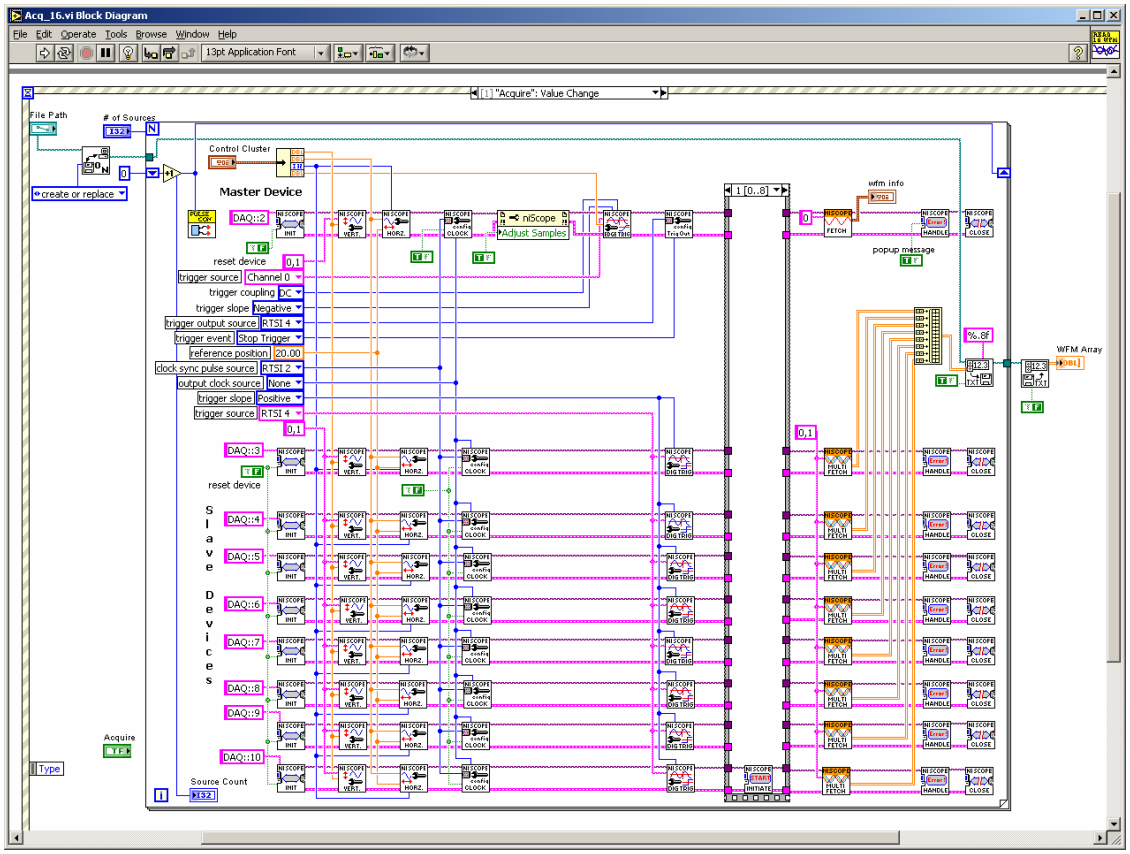

FIGURE B.10: SIMULTANEOUS ACQUISITION BLOCK DIAGRAM

The acquisition call shows the master device initialization and setup in addition to the subsequent slave device calls. The master device sets up the timing and triggering for the acquisition. Once the program senses a trigger even it waits for the last slave device to get the trigger. In the sequence structure the start acquisition call goes to each device in turn, starting with the last device to receive the trigger. The synchronization of the acquisition is handled by these programs automatically so no timing adjustments need to be made. Once the waveforms have been acquired they are placed in to an array and saved to the file. The program then activates the next source channel and continues acquisition until it runs out of source locations to activate.

B.4 PAIRED ACQUISITION PROGRAM

There are circumstances where simultaneous acquisition might not be possible, or not appropriate. For these circumstances a program was made to acquire data based on source and receiver locations. Each receiver is paired with a source in turn and the

ultrasonic waveform between the two sensors is acquired. Figure B.11 shows the Front Panel of this VI.

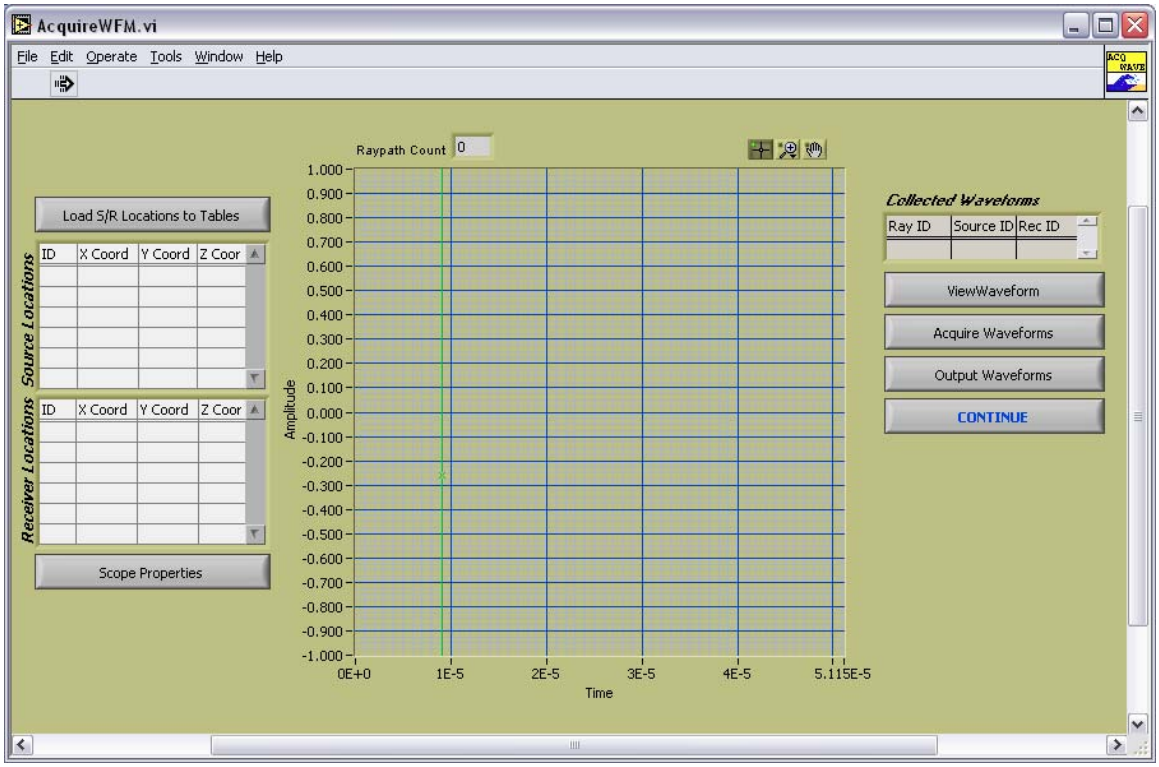

FIGURE B.11: PAIRED ACQUISITION FRONT PANEL

The operation of this program is similar to the previous program. The first step is to load in the source and receiver location files by clicking on the Load S/R Locations to Tables button. This activates a file dialog to open the files. The user then sets the properties for the scope by clicking on the Scope Properties button. This brings up a dialog where the scope parameters can be set. The final step in acquisition is to click the acquire waveforms button. This will start the acquisition of ultrasonic waveforms for every combination of source and receiver sensors. The waveforms can be viewed by scrolling through the collected waveforms table in the upper right corner and then clicking the view waveform button. To save the ultrasonic waveforms, click on the output waveforms button. This will open a save file dialog. The program is stopped by clicking on the continue button.

The block diagram for this VI is very similar to the previous acquisition program. The program again uses event structure program to divide the functions in the program and make reading the block diagram easier.

B.5 Arrival Time Correlation Program

The final step in ultrasonic data acquisition for tomographic imaging is to pick the arrival times for the acquired waveforms. The waveform file created in the acquisition step is used here to determine the ultrasonic arrival time. This data processing step is the most important step in tomographic acquisition. The accuracy of the arrival time picking determines the accuracy of the tomograms. The Front Panel of this program is shown in Figure B.12.

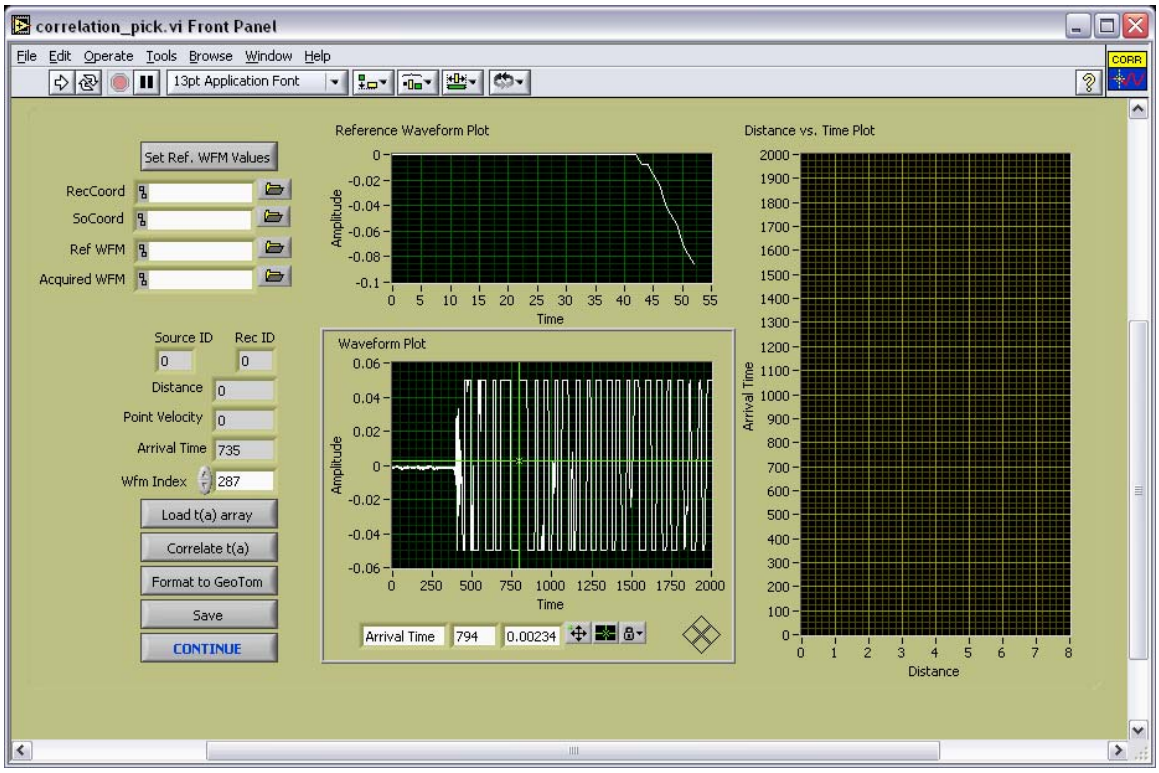

FIGURE B.12: ARRIVAL TIME FRONT PANEL

This program uses direct correlation to assist in the arrival time picking procedure. Direct correlation allows for a comparison of a reference arrival time to the actual waveforms. The correlation function picks the point where the waveform best fits the

reference arrival time. To use this program the user first needs to input the source location, receiver location, reference waveform, and acquired waveform files. This being done, the reference waveform properties can be adjusted by clicking on the Set Ref. WFM Values. The default reference waveform properties should be acceptable for most applications. Having entered in the file locations and the reference waveform values, the arrival times can be correlated by clicking on the Correlate t(a) button. This will call the direct correlation function to pick the arrival times on each waveform. After the correlation is finished the user then needs to cycle through each waveform to check the fit. To cycle through the waveforms click on the WFM Index numerical control. Changing the value in this numerical control will produce a plot of arrival times versus distance in the right hand graph window. The linearity of this curve is dependant on the quality of picking. Once all arrival times have been picked for each waveform, the arrival times need to be formatted into the acceptable GeoTom format. This is done by clicking on the Format to Geotom button. The popup window from this call is shown in Figure B.13.

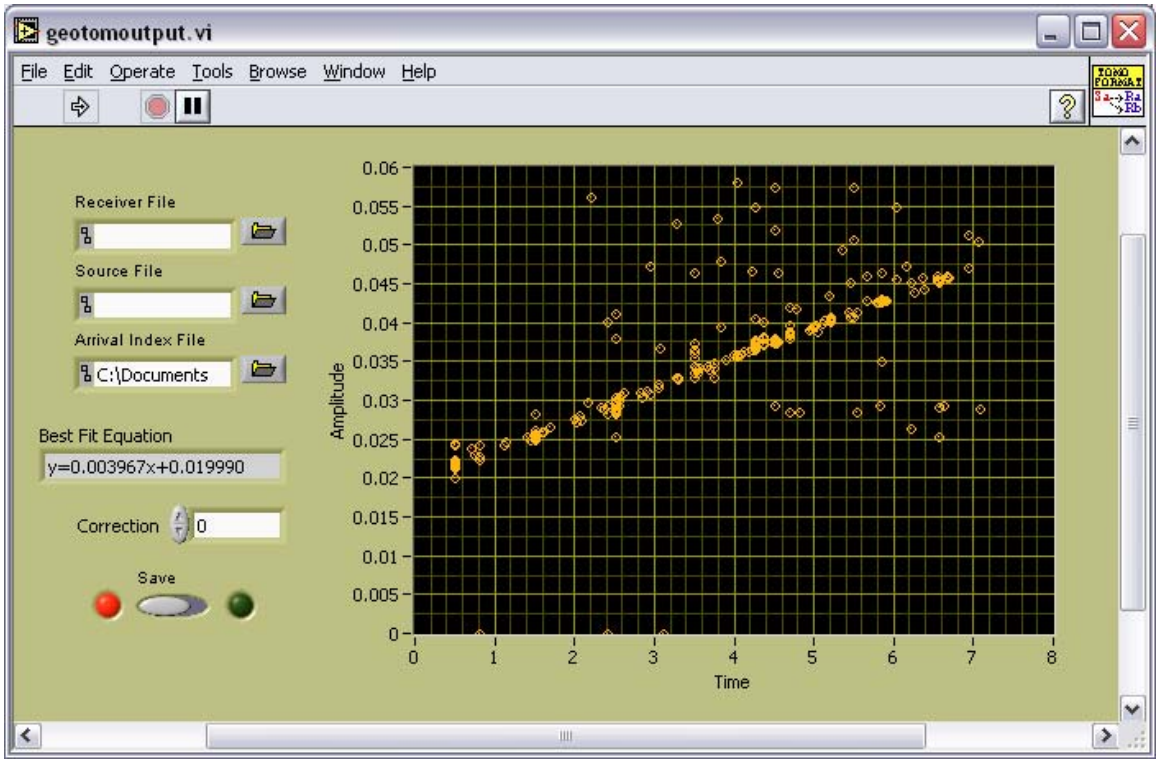

FIGURE B.13: GEOTOM FORMAT FRONT PANEL

The input into Geotom assumes that the linear curve passes through the origin. To have this done the intercept must be corrected to pass through the origin. Enter in the correction into the correction numerical control. The play button must be pressed to make changes within this VI. Once the curve is acceptable change the Save slide control towards the green indicator. Click the play button and save the file in Geotom format (*.3dd). To create a tomogram, simply open the saved *.3dd file in Geotom and follow the instructions in the Geotom manual to create a tomogram.

APPENDIX: C

HARDWARE WIRING INSTRUCTIONS

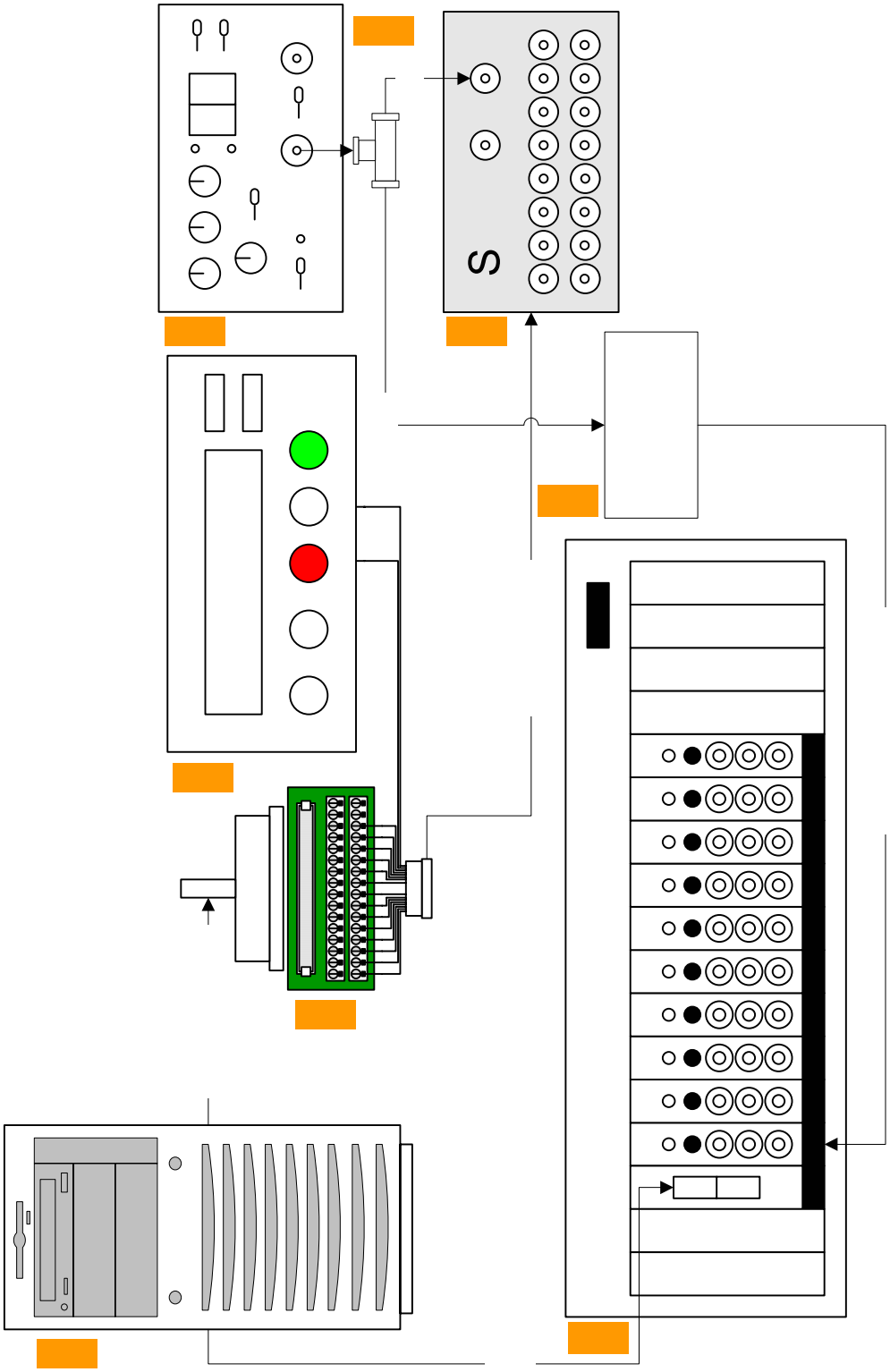

FIGURE C.1: ULTRASONIC DATA ACQUISITION SYSTEM HARDWARE WIRING FLOWCHART

The wiring of the instrumentation components are shown in Figure C.1, this figure is used as a reference for the wiring descriptions given in this appendix. The components are numbered 1 – 8. The description of each component is given in Table C.1.

TABLE C.1: HARDWARE DESCRIPTIONS

Number	Description
1	Computer Control – Contains a PCI Control card for the PXI Chassis and a PCI Digital I/O ACQ card for the Ultrasonic Switchbox Pulser Control
2	Digital I/O Connector Block with 25 pin serial dongle – for connection to the Ultrasonic Switchbox Pulser
3	Aglient Technologies Power Supply – provides power for the Ultrasonic Switchbox Pulser
4	Panametrics 5077PR Ultrasonic Square Wave Pulser – generates the ultrasonic source pulse
5	BNC T Connector – splits the output pulse from the 5077PR
6	ESG Ultrasonic Switchbox Pulser – relays the ultrasonic pulse to different sensors
7	Voltage Divider Breadboard Circuit – drops the high voltage pulse to a level that can be input into a PXI 5102 acquisition card
8	PXI 1006 Chassis – contains PXI 5102 digital oscilloscopes for acquiring ultrasonic signals

To use the Ultrasonic Data Acquisition System all the components must be connected correctly. The personal computer (1) controls the acquisition of the ultrasonic signals from the PXI 1006 chassis (8) and also controls the ESG Ultrasonic Switchbox Pulser (6). A fiber optic cable connects the PXI chassis to the computer. The Ultrasonic Switchbox Pulser (6) is connected through a Digital Input/Output Acquisition Card. The card is connected via a cable to a screw terminal connector block (2). The wires from the connector block are connected to a 25 pin serial dongle. The dongle is wired according

to the channel specifications of the Switchbox (6) and the power requirements for the switchbox. The power for the switchbox is provided by an Aglient Technologies Power Supply (3). The voltage requirement for the switchbox is 9V. The wired dongle with the channel relay and power requirements is connected to a serial cable that connects to the Switchbox (6). The ultrasonic pulse is supplied by a Panametrics 5077PR Ultrasonic Square Wave Pulser (4). This device outputs a -400V pulse that is relayed to source locations via the Switchbox (6). A BNC "T" (5) connector is used to split the output signal from the 5077PR (4). One side of the T (5) is connected to the input terminal of the Switchbox (6) and the other is connected to the input of the Voltage Divider Circuit (7). The voltage divider circuit (7) drops the voltage from the 5077PR (4) to a level that can be input into the PXI Chassis (8). The output of the voltage divider circuit (7) is input into channel 0 of device 1 in the PXI Chassis (8). This input is the trigger input for the UDAQ system. The last step in wiring this system is to connect the acoustic emission sensors to the respective source relay terminal or acquisition terminal via a BNC/Microdot connecting cable.